Thesis for the degree of Doctor of Technology
Sundsvall 2007

Characterisation and application of photon counting X-ray detector systems

Börje Norlin

Supervisors: Docent Christer Fröjdh
Professor Hans-Erik Nilsson

Electronics Design Division, in the
Department of Information Technology and Media
Mid Sweden University, SE-851 70 Sundsvall, Sweden

ISSN 1652-893X
Mid Sweden University Doctoral Thesis 26

ISBN 978-91-85317-55-4

ELECTRONICS
Design Division

Mittuniversitetet
MID SWEDEN UNIVERSITY

Akademisk avhandling som med tillstånd av Mittuniversitetet i Sundsvall framläggs till offentlig granskning för avläggande av teknologie doktorsexamen i elektronik ***fredagen den 1 juni 2007***, klockan ***10.15*** i sal ***O102***, Mittuniversitetet Sundsvall. Seminariet kommer att hållas på engelska.

Characterisation and application of photon counting X-ray detector systems

Börje Norlin

Electronics Design Division, in the
Department of Information Technology and Media
Mid Sweden University, SE-851 70 Sundsvall
Sweden

Telephone: +46 (0)60 148594

Printed by Kopieringen Mittuniversitetet, Sundsvall, Sweden, 2007

To my sons, Johan and William, and to my wonderful wife Monica

ABSTRACT

This thesis concerns the development and characterisation of X-ray imaging systems based on single photon processing. “Colour” X-ray imaging opens up new perspectives within the fields of medical X-ray diagnosis and also in industrial X-ray quality control. The difference in absorption for different “colours” can be used to discern materials in the object. For instance, this information might be used to identify diseases such as brittle-bone disease. The “colour” of the X-rays can be identified if the detector system can process each X-ray photon individually. Such a detector system is called a “single photon processing” system or, less precise, a “photon counting system”.

With modern technology it is possible to construct photon counting detector systems that can resolve details to a level of approximately 50 µm. However with such small pixels a problem will occur. In a semiconductor detector each absorbed X-ray photon creates a cloud of charge which contributes to the image. For high photon energies the size of the charge cloud is comparable to 50 µm and might be distributed between several pixels in the image. Charge sharing is a key problem since, not only is the resolution degenerated, but it also destroys the “colour” information in the image.

This thesis presents characterisation and simulations to provide a detailed understanding of the physical processes concerning charge sharing in detectors from the MEDIPIX collaboration. Charge summing schemes utilising pixel to pixel communications are proposed. Charge sharing can also be suppressed by introducing 3D-detector structures. In the next generation of the MEDIPIX system, Medipix3, charge summing will be implemented. This system, equipped with a 3D-silicon detector, or a thin planar high-Z detector of good quality, has the potential to become a commercial product for medical imaging. This would be beneficial to the public health within the entire European Union.

SAMMANDRAG

Denna avhandling berör utveckling och karaktärisering av fotonräknande röntgensystem. ”Färgröntgen” öppnar nya perspektiv för medicinsk röntgendiagnostik och även för materialröntgen inom industrin. Skillnaden i absorption av olika ”färger” kan användas för att särskilja olika material i ett objekt. Färginformationen kan till exempel användas i sjukvården för att identifiera benskörhet. Färgen på röntgenfotonen kan identifieras om detektorsystemet kan detektera varje foton individuellt. Sådana detektorsystem kallas ”fotonräknande” system.

Med modern teknik är det möjligt att konstruera fotonräknande detektorsystem som kan urskilja detaljer ner till en upplösning på circa 50 µm. Med så små pixlar kommer ett problem att uppstå. I en halvledardetektor ger varje absorberad foton upphov till ett laddningsmoln som bidrar till den erhållna bilden. För höga fotonenergier är storleken på laddningsmolnet jämförbar med 50 µm och molnet kan därför fördelas över flera pixlar i bilden. Laddningsdelning är ett centralt problem delvis på grund av att bildens upplösning försämras, men framför allt för att färginformationen i bilden förstörs.

Denna avhandling presenterar karaktärisering och simulering för att ge en mer detaljerad förståelse för fysikaliska processer som bidrar till laddningsdelning i detektorer från MEDIPIX-projekter. Designstrategier för summering av laddning genom kommunikation från pixel till pixel föreslås. Laddningsdelning kan också begränsas genom att introducera detektorkonstruktioner i 3D-struktur. I nästa generation av MEDIPIX-systemet, Medipix3, kommer summering av laddning att vara implementerat. Detta system, utrustat med en 3D-detektor i kisel, eller en tunn plan detektor av högabsorberande material med god kvalitet, har potentialen att kunna kommersialiseras för medicinska röntgensystem. Detta skulle bidra till bättre folkhälsa inom hela Europeiska Unionen.

ACKNOWLEDGEMENTS

As a child, my parents read physics books to me, and I looked at the fascinating pictures of the Bohr model and of the solar system. At the age of 11, I became active against nuclear power and decided to work in the field of radiation in the future. After six years of accident simulations for the nuclear industry I was more comfortable with nuclear power, since I found no design error of significance in the Swedish nuclear power plants. My friend Dr. Jan-Olov Andersson persuaded me to move north to Sundsvall and to the academic world, which has made it possible for me to explore the area of X-ray imaging.

I want to express my gratitude to my supervisors. Christer Fröjdh has shown large emotional involvement in my work, I felt it especially during my hospital stay when I also learned that Christers wife Maj is one of the best nurses in the children department at Sundsvall hospital. Hans-Erik Nilsson has been deeply involved in my work when he has had the chance to develop advanced simulations. For the published work in this thesis, my co-authors are; Ervin Dubarić, Anatoliy Manuilskiy, Heinz Graafsma, Cyril Ponchut, Vedran Vonk and Lukas Tlustos.

I want to thank all the members of the Medipix collaboration for the honour to be a member of this research. I recall help and tips from Xavier Llopart, Michael Campbell, Marino Maiorino, Giovanni Mettivier, Bettina Mikulec, Daniel Niederlöhner, Jan Visschers, Stanislav Pospíšil, Jan Jakubek, Milan Siňor, Josef Uher, Tomas Holy and Daniel Vavřík.

I want to thank all my colleagues and former colleagues at the Electronics Design Division for an inspiring and friendly environment. Special thanks to Benny Thörnberg, Krister Aldén and Niklas Lepistö who never say no when I ask for help to repair equipment. Thanks to Fanny Burman, Jan Lundgren, Mattias O'Nils, Bengt Oelmann and Göran Thungström for practical help with arrangements concerning the thesis. Other sources of inspiration I want to mention are Michael Andersson, Lars Herrnsdorf (RTI Electronics AB), Ulrika Lindgren (Hospital physics, Sundsvall), Anders Nyström, Fiona Wait and Lars Wigström (Linköping University).

Mid-Sweden University, the KK-foundation and the European Commission are greatly acknowledged for their financial support.

Without the understanding from my wife Monica this thesis would probably not have been finished. Thanks to my parents in law, Anna and Tage, who stayed with the children several times during writing and research. My sons Johan (6 years) and William (3 years) also promised to be good, but only until the book is finished, as Johan expressed it. William wondered if the tooth felt pain, while Johan said he was lucky to have this book to read when he gets older.

TABLE OF CONTENTS

LIST OF FIGURES

LIST OF PAPERS

This thesis is based on the following papers, herein referred to by their Roman numerals:

Paper I **Monte Carlo simulation of the response of a pixellated 3D photo-detector in silicon**
Ervin Dubaric, Hans-Erik Nilsson, Christer Fröjdh and Börje Norlin, Nuclear Instruments and Methods in Physics Research A 487 (2002) pp. 136-141.

Paper II **Spectroscopy applications for the Medipix photon counting X-ray system**
Anatoliy Manuilskiy, Börje Norlin, Hans-Erik Nilsson and Christer Fröjdh, Nuclear Instruments and Methods in Physics Research A 531 (2004), pp. 251-257.

Paper III **Material recognition with the Medipix photon counting colour X-ray system**
Börje Norlin, Anatoliy Manuilskiy, Hans-Erik Nilsson and Christer Fröjdh, Nuclear Instruments and Methods in Physics Research A 531 (2004), pp. 265-269.

Paper IV **Energy dependence in dental imaging with Medipix2**
Börje Norlin and Christer Fröjdh, Nuclear Instruments and Methods in Physics Research A 546 (2005), pp. 19-23.

Paper V **Spectral Response of Pixellated Semiconductor X-ray Detectors**
Christer Fröjdh, Hans-Erik Nilsson and Börje Norlin, Nuclear Science Symposium Conference Record, 2005 IEEE, pp. 2967-2970.

Paper VI **Characterization of a pixellated CdTe detector with single-photon processing readout**
Christer Fröjdh, Heinz Graafsma, Börje Norlin, Hans-Erik Nilsson and Cyril Ponchut, Nuclear Instruments and Methods in Physics Research A 563 (2006), pp. 128-132. Also Erratum to “Characterization of a pixellated CdTe detector with single-photon processing readout”, Nuclear Instruments and Methods in Physics Research A (2007), doi:10.1016/j.nima.2007.01.096.

Paper VII **Characterisation of the charge sharing in pixellated Si detectors with single-photon processing readout**
Börje Norlin, Christer Fröjdh, Hans-Erik Nilsson, Heinz Graafsma, Vedran Vonk, Cyril Ponchut, Nuclear Instruments and Methods in Physics Research A 563 (2006), pp.133-136.

Paper VIII **Spectral performance of a pixellated X-ray imaging detector with suppressed charge sharing**
Börje Norlin, Christer Fröjdh and Hans-Erik Nilsson, Nuclear Instruments and Methods in Physics Research A (2007), 30 January 2007.

Paper IX **Charge sharing suppression using pixel to pixel communication in photon counting X-ray imaging systems**
Hans-Erik Nilsson, Börje Norlin, Christer Fröjdh, Lukas Tlustos, Nuclear Instruments and Methods in Physics Research A 2007), 6 February 2007.

Related papers not included in the thesis:

Monte Carlo simulation of the imaging properties of scintillator-coated X-ray pixel detectors
Mats Hjelm, Börje Norlin, Hans-Erik Nilsson, Christer Fröjdh and Xavier Badel, Nuclear Instruments and Methods in Physics Research A 509 (2003) 76-85.

Metallized and Oxidized Silicon Macropore Arrays Filled With a Scintillator for CCD-Based X-ray Imaging Detectors
X. Badel, J. Linnros, P. Kleimann, B. Norlin, E. Koskiahde, K. Balpas, S. Nenonen, C. S. Petersson and C. Fröjdh, IEEE Transactions on Nuclear Science, vol. 51 no. 3, June 2004, pp. 1001-1005.

Performance of Scintillating Waveguides for CCD-based X-ray Detectors
X. Badel, B. Norlin, P. Kleimann, L. Williams, S. Moody, G. Tyrrell, C. Fröjdh, J. Linnros, Submitted to IEEE Transactions on Nuclear Science, vol. 53, no. 1, Feb. 2006, pp. 3-8.

Evaluation of the charge-sharing effects on spot intensity in XRD setup using photon-counting pixel detectors
H.-E. Nilsson, C.G. Mattsson, B. Norlin, C. Fröjdh, K. Bethke, R. De Vries, Nuclear Instruments and Methods in Physics Research A 563 (2006) pp 182-186.

An Area Efficient Readout Architecture for Photon Counting Color Imaging
Jan Lundgren, Mattias O'Nils, Bengt Oelmann, Börje Norlin, Suliman Abdalla, Nuclear Instruments and Methods in Physics Research A (2007), 6 February 2007.

1 INTRODUCTION

1.1 THESIS OUTLINE

This thesis studies photon counting X-ray imaging systems. Photon counting, or single photon processing, is a method to improve the performance of X-ray imaging systems as compared to standard charge integrating systems. The first section offers the arguments for research in X-ray imaging and introduces some basic concepts for detector systems. Section 2 introduces the Medipix X-ray imaging system, which is used in most of the experimental work in this thesis. Section 3 is a detailed description of the charge sharing phenomenon [1]. The section presents simulations of absorption and charge transport in small pixellated detectors together with measurements on the Medipix2 system. Methods for image correction are also considered. Section 4 describes the research concerning the improvement of image quality and new possibilities for X-ray imaging applications. Tthe problem associated with charge sharing is also discussed. Section 5 summarizes the work covered by all the papers included in the appendix and section 6 contains the conclusions of this work.

1.2 THE DISCOVERY OF X-RAYS

X-rays were discovered in 1895 by W. K. Röntgen. X-rays are high-energy photons invisible to the human eye. Due to the high energy X-ray photons can penetrate through materia. Mono-energetic X-ray photons are released in the decay chain for radioactive atoms. X-rays are typically generated in an X-ray tube where electrons are accelerated by a high voltage (several thousand volts) and collide with a metal target. In the collisions "bremsstralung" is generated when the paths of the electrons are bent by the interaction with the nucleus of the metal atoms. The momentum energy lost by the electrons is emitted as X-ray photons. The process generates a spectrum with energies distributed between "low" and "maximum", where the maximum occurs when the full energy of the electron is converted to an X-ray photon, see Figure 1. It is convenient to measure the energy of the photons in electron volts (eV), for a tube voltage of 60 kV the maximum energy of the photons will be 60 keV. The majority of the photons will however receive about half this energy.

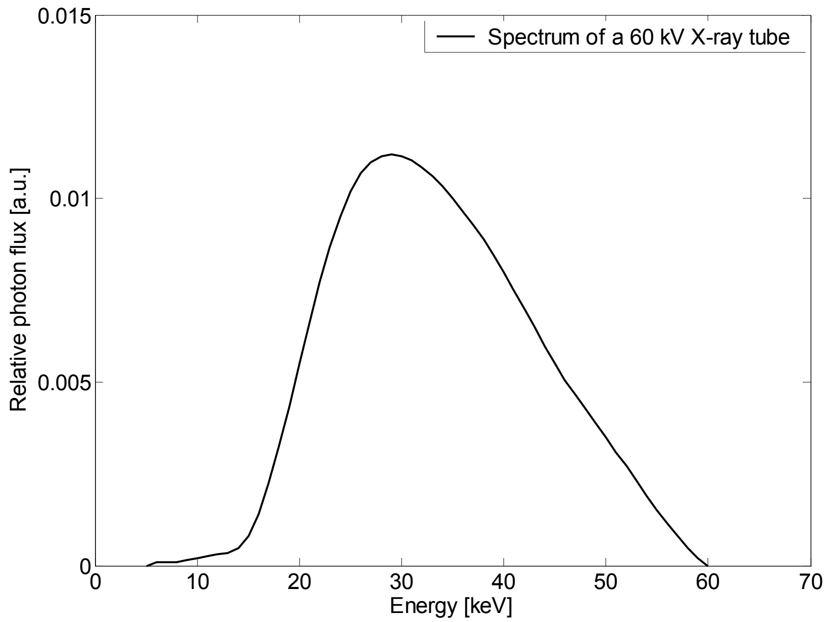

Figure 1: Measured spectrum of an X-ray tube at 60 kVp.

1.3 APPLICATIONS FOR X-RAYS

X-rays started to be used for medical diagnosis immediately after they were discovered using a photographic film as the detector. The first medical use of X-rays was to view the skeleton of a human since the X-ray absorption is much stronger in bone than in soft tissue. X-ray tubes are commonly used as sources for clinical imaging. Through means of dental X-rays imaging and mammography almost the entire population is affected by X-ray imaging today. X-rays are of course important not only in medicine but in many research areas such as astronomy, spectroscopy, and crystallography and of course in nuclear physics.

Soon after the discovery of X-rays, negative effects such as eye damage, skin damage and loss of hair were observed due to radiation exposure. Reproducing cells are more sensitive to radiation, so X-rays can be used in the treatment of growing cancer tumours. Cancer cells are more significantly damaged by radiation than are the surrounding normal cells.

1.4 NEGATIVE EFFECTS OF X-RAYS

X-rays have enough energy to ionize atoms in the material they hit and are therefore counted as ionizing radiation. This has several negative influences on the body, but the main concern is the increased risk of developing cancer. It is proven that ionizing radiation induces cancer to human tissue, and that the influence is linear.[1] For people who are exposed to radiation at work, a maximum lifetime dose and yearly dose is defined by law. This dose is considered to give a reasonable statistical reduction of the individual's lifespan, which is considered to be small relative to other negative factors such as stress, depression, lack of physical training, poor eating habits and normal consumption of poisons such as alcohol and nicotine. A statistical reduction in lifespan is a reasonable measure of the risk, since cancer generation is a slow process.

When the risk of a specific radiation exposure has to be estimated, a complication occurs. No lower level has been found for cancer induced by radiation, which is not the same as toxic influences, where a minimum level of the poison is required before the body is affected. An interesting conclusion can be drawn; a lowering of the dose will always result in less cancer development, no matter how low the risk already is. This decrease in risk might not be crucial for the individual, but when the whole population, of for example the European Union is considered, the decreased cost for society due to the cases of induced cancer which are thus avoided is significant.

1.4.1 X-ray dose and mammography

When the cancer-inducing effects of X-rays became known, ways to reduce the dose given to the patient began to be investigated. This involves both the quality of the diagnosis and ways to verify the actual radiation field exposing the patient [3]. For diagnosis, the number of images, the image size and the exposure time (connected to the image quality) can be decreased to minimize the dose.

An example of risk consideration is the discussion about the extent to which mammography examinations should be performed on a regular basis. The key to successful cancer treatment is to discover the cancer at an early stage and remove the tumour while it is still small. Thus if all females are regularly examined then, statistically, most of the breast cancers will be cured successfully. However, if the examinations are performed too often, then the examinations will themselves begin to generate breast cancers, which is unacceptable. This also affects the age at which mammography examinations should start. It is unlikely that a tumour will be found in a younger person, as the risk of developing cancer increases with age. Young females also have denser breasts, and thus a higher radiation dose is required to be able to distinguish a tumour in a young female [4]. To obtain the best outcome for the health of the whole female population, a national mammography programme must carefully consider both the regularity and the initial age for examinations. The statistical risk for some undiscovered cancers in females has to be kept at an acceptably low level.

[1] These data originates from three sources: patients irradiated for radiology treatment; studies of survivors of Hiroshima and Nagasaki 1945 and studies of workers who were accidentally exposed to radiation [2].

1.4.2 Increasing doses

The trend in clinical imaging over the past few years is that X-ray systems based on photographic film have been replaced by semiconductor detectors. There are several reasons for replacing X-ray films:

1. Digital imaging is fast, since no time for film development is needed
2. Digital imaging has positive environmental effects due to less use of raw materials (film) and less use of chemicals for film processing.
3. Image processing can be introduced to enhance image quality
4. Digital images can rapidly be distributed to other parts of the world for expert opinions.
5. Semiconductor detectors can be made more sensitive than film leading to reduced doses to the patients.

Digital images can be achieved by replacing film cassettes in existing devices by storage phosphor plates. These plates are read out by a laser scanner. This is the cheapest way for a hospital to start digital imaging.

When improvements of X-ray equipment are implemented, the choice is often to keep the old dose of the specific examination constant and, instead, gain increased image quality. If the image quality is increased the risk of missing an early tumour decreases. A rapid increase in the dose delivered to patients seems to be taking place in clinical X-ray imaging. This is mainly due to the increased use of CT (Computer tomography) to obtain correct diagnoses in cases where unclear diagnoses were previously accepted. If this trend is sustained, then the research concerning dose reduction, where image quality remains, becomes ever more important.

1.5 SOME BASICS ON SEMICONDUCTOR X-RAY DETECTORS

The first electric detectors for X-rays were gas-chambers, where the X-ray photons ionized atoms of the gas and created a discharge that could be detected. However, it is more efficient to use a solid material to absorb X-ray photons. When a photon is absorbed in a semiconductor such as silicon, a charge cloud is released. For silicon the conversion factor, or the energy necessary to create one electron hole pair, is 3.6 eV [5]. Normally the detector is designed as a diode with reversed bias applied. In this electric field the electron and the hole will move in opposite directions. When the charge cloud drifts towards the readout electrode a current pulse is generated. The size of this current pulse is proportional to the amount of energy deposited in the detector. The applied reversed bias will result in a leakage current through the diode, causing noise which limits the minimal detectable pulse.

Silicon detectors are efficient for photons in the visible range, but for X-rays the quantum efficiency is low, since the X-ray absorption in silicon is low. To improve the quantum efficiency a highly absorbing scintillator layer can be applied above the detector [6]. A scintillator is a crystal which absorbs X-rays and emits the absorbed energy as visible light. Several scintillator materials exists, but one commonly used materials is Tl-doped CsI (CsI(Tl)) [10].

1.5.1 Charge coupled devices

The CCD is the state-of-the-art imaging sensor. It consists of a matrix of small MOS capacitors. When a photon is absorbed and induces a charge cloud, the nearest capacitor will receive a charge. To retrieve the images the charge is shifted from pixel to pixel to the readout electrode.

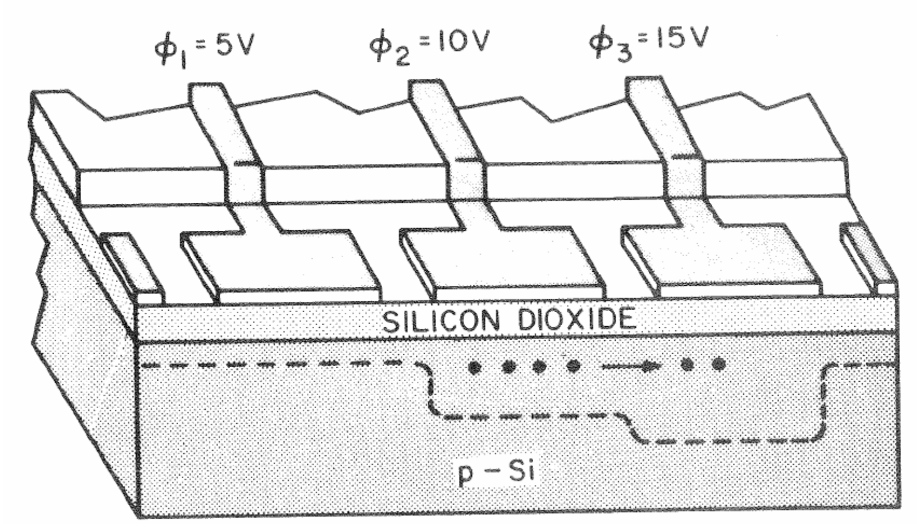

Figure 2: Illustration of the readout principle for a charge coupled device from [7].

The CCD is popular due to its simplicity. Since only three capacitors are required for each pixel, detector matrices with a small pixel size can be easily constructed. This is important since normal X-ray imaging systems do not contain any optical magnification. Relatively large-area CCD detectors can be made at a low cost.

1.5.2 Scintillator grids

CCD's are usually designed to work within the region of visible photons, the quantum efficiency for X-rays are usually considerably low. In X-ray imaging systems, the detector is usually covered with a scintillator layer. One problem with a scintillator layer is that the light emitted in the scintillator is spread laterally [8], causing the spatial resolution of the detector does deteriorate. Hence, structured scintillator films have been developed to maintain an optimal spatial resolution and sensitivity. One approach is to grow a columnar CsI(Tl) film by evaporation of CsI on a pre-patterned substrate. Light emitted from CsI(Tl) is then confined within the columns due to total internal reflection, which improves the spatial resolution [9]. Alternatively, advanced etching techniques can be used to create a silicon matrix of pores, which are subsequently filled with a scintillator [10]. The silicon pore walls can be oxidized [11] or metallised [12] in order to obtain an array of scintillating waveguides, whose operating principle is similar to scintillating optical fibres. It has been demonstrated that it is possible to improve the signal to noise ratio close to the theoretical limit for a specific spatial resolution and X-ray dose [13].

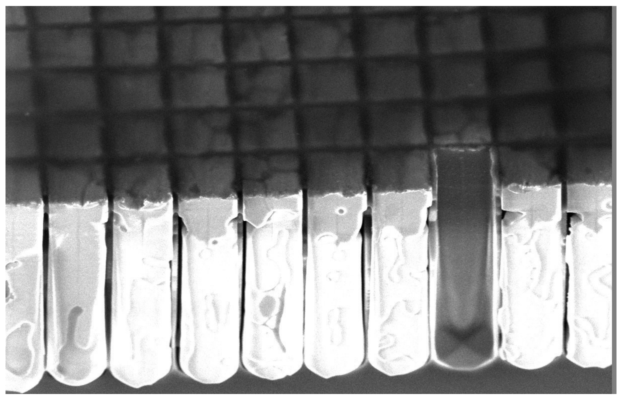

Figure 3: Scanning electron micrographs of a pore array filled with CsI(Tl) from [13].

1.5.3 Strip detectors

Strip detectors are popular in high energy physics. Strip arrays in one or two dimensions are suitable for following the path of a high energy particle. Attempts have been made to use detectors with crossed strips for X-ray imaging. In astronomy applications, strip detector systems are successful. The position of a specific X-ray absorption is determined from the coincident pulses between two strips. One problem that occurs is that the speed of the ASIC limits the photon intensity, since only one pulse at a time can be retrieved. For medical imaging this is a problem since the exposure time must be short enough to ensure that the patient does not move. In commercially available medical systems scanning of a moving 1D-strip array is a successful method. The strips are put "edge-on" towards the beam, and the absorption path for the photons becomes the full strip length that is of the order of 1 cm [14].

1.5.4 Pixel detectors

Pixel detectors form the main concept of this thesis. A detector matrix consisting of pixellated diodes can be bump-bonded to a front-end readout chip [15]. Hence the pixel size defines the available space for the pixel readout electronics. Therefore design of pixellated readout systems requires deep submicron CMOS processes.

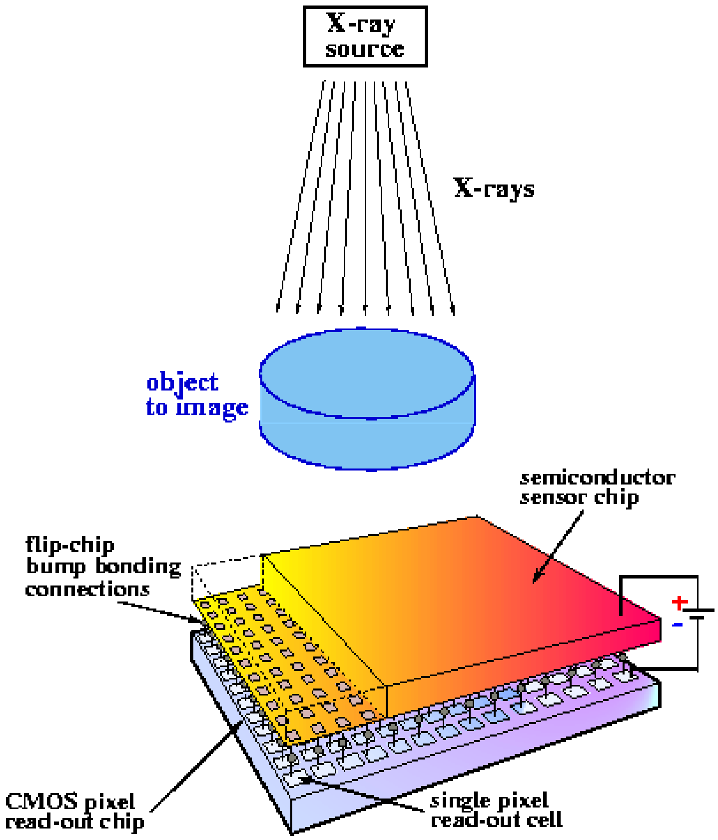

Figure 4: Schematics of the Medipix chip bump-bonded to a pixellated detector from [16].

The photon counting technique is well known in nuclear physics. The pulse shape of the discharge signal from a gas-chamber has, for a considerable time, been a common method for retrieving spectra in multi-channel readout systems. But these measurements are performed using a single detector connected to an external device containing the large-size front end electronics.

State of the art imaging systems such as the CCD (or film) works via a charge integrating principle. The sum of the charge accumulated in a pixel corresponds to the total X-ray energy absorbed by that pixel in the image. At present this is the standard technology for imaging applications. Quantum imaging has become possible due to advances in microelectronics, which allows the deigns and fabrication of chips with pixellated pulse processing front-end electronics with low noise. The measured charge pulse defines the energy of the absorbed photon, and it is possible to perform spectroscopic discrimination on each pixel. The front-end electronics is usually bump-bonded to the pixel detector.

Photon counting is a simple way of quantum imaging, when discrimination of low energies is used to cancel the readout noise. Through sweeping the threshold voltage and subtracting consecutive images a full spectrum can be achieved. One problem in pixellated detectors is that the energy threshold will vary between pixels due to variations in the amplifiers. Pixellated systems must therefore be equipped with an individual calibration of the threshold voltage for each pixel. This can be achieved by a threshold adjustment circuit in each pixel. The Medipix system is equipped with a 3-bits register in each pixel, which allows threshold adjustment in eight steps.

Several projects concerning photon counting pixellated detectors exist. An overview with brief descriptions of several projects can be found in [14].

2 THE MEDIPIX PROJECT

The Medipix project is a collaboration between 16 universities and research institutes including Mid Sweden University [16]. The project is coordinated by the CERN microelectronics group.

2.1 BRIEF DESCRIPTION OF MEDIPIX1

The Medipix1 chip, which became available in 1997, was the first full-scale quantum imaging ASIC for hybrid semiconductor pixel detectors [17]. The design was based on previous experiences of pixel chips for high-energy particle trackers. The pixel size is 170 x 170 μm^2 and they are arranged in a 64 x 64 matrix. The readout chip is designed in 1 µm SACMOS technology and each pixel is equipped with a preamplifier, a discriminator with 3 bits threshold adjustment and a 15-bit counter. Both Si- and GaAs detectors have been bump-bonded to the chip. The chipboard can be operated using a standard PC equipped with a data acquisition card and an analogue output card connected to an interface circuit called MUROS1 developed by NIKHEF. The user interface software for Medipix1 is Medisoft 3 described in [18].

2.2 BRIEF DESCRIPTION OF MEDIPIX2

The Medipix2 chip is a further development of Medipix1 [19]. One purpose was to reduce the pixel size to 55 x 55 µm2 to become competitive with state of the art CCD detectors and a further purpose was to introduce a high threshold for the energy window discrimination. 0.25 µm CMOS technology is used to construct the chip of size 1.4 x 1.6 cm2 containing 256 x 256 pixels [20]. Dead areas are minimized on three sides of the chip, so several detectors can be tiled to make a large area detector. The readout circuit in each pixel is improved by means of an individual leakage current compensation and a high energy threshold with 3 bits calibration. The counters are decreased to 13 bits, to obtain approximately the same area sensitivity as Medipix1. Both positive and negative charged inputs are accepted by the readout, so detector materials with large hole trappings such as CdTe can be used. The chipboard can be operated via a standard PC either by a USB serial adapter developed by IEAP or by a data acquisition card connected to an interface circuit called MUROS2 developed by NIKHEF. To operate the system, the software Medisoft 4 [21] was developed, and lately also the software Pixelman [22].

A redesigned version of Medipix2 called Mpix2MXR has also been developed. This chip is improved concerning for example radiation hardness, temperature dependence and leakage current compensations. The counter dynamic range is 11810 counts with overflow control [19].

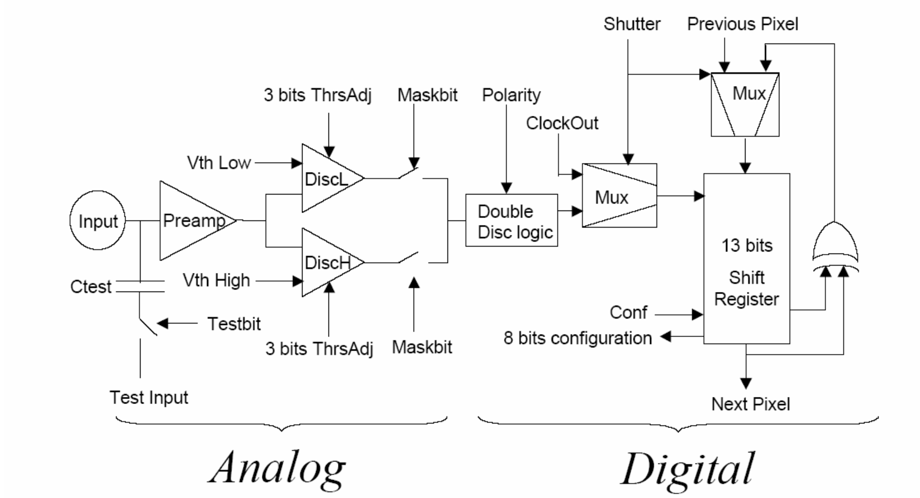

Figure 5: Description of the Medipix2 readout circuit for each pixel from [20].

2.3 BRIEF DESCRIPTION OF MEDIPIX3

Medipix3 will be developed to overcome the problem associated with charge sharing in Medipix2 and to allow simultaneous counting and readout. In paper IX in this thesis, charge summing schemes based on pixel to pixel communication were proposed. In the Medpix3 prototype, a scheme based on summing between four pixels (4PS) is implemented [23]. The prototype is fabricated in 0.13 µm CMOS technology with eight metal layers. The system can work either in *charge summing mode* or in *single pixel mode*, with the charge summing turned of. Another feature of Medipix3 is that the readout contains two counters and two thresholds for each pixel. The system can be configured for *Simultaneous Read-Write* operation, where one counter is read out while the other counts, or for *Sequential Read-Write*, here two threshold levels are available. The latter case makes imaging with three energy bins possible, as proposed in [24].

The normal working mode of the Medipix3 is *Fine Pitch Mode*, but one additional feature of the chip is that it can be bump-bonded on detectors with 110 µm pitch, i.e. four times the readout pixel area. This case with a large pixel size is called *Spectroscopic Mode*, since for each detector pixel 8 thresholds from the four readout pixels will be available for colour imaging. The ability for charge summing is also available in *Spectroscopic Mode*.

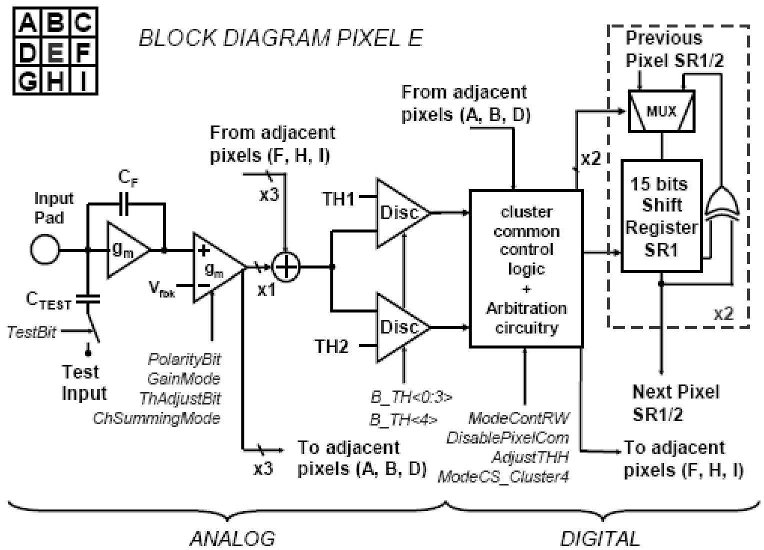

Figure 6: Description of the Medipix2 readout circuit for each pixel from [23].

3 CHARACTERISATION OF THE MEDIPIX SYSTEM

3.1 CHARGE SHARING IN PIXELATED DETECTORS

An important problem for the design of high resolution pixel detectors is that some of the induced charge will drift to neighbouring pixels and thus contribute in the wrong pixel position. This effect is called charge sharing. If the pixel size of a pixellated detector is small compared to the wafer thickness, charge sharing will be a serious problem and will reduce both spatial resolution and energy resolution of the detector [25].

When an image is taken, small details of the object will always be degenerated. The capability to show small details is referred to as spatial resolution. This is usually measured using the "line spread function" (LSF), which describes the extent to which a sharp edge will be sharp in the image. A "point spread function" can be defined as being analogous to LSF. The mechanisms that can cause the image to degenerate in an X-ray imaging system are:

- Beam geometry and scattering
- Quantisation error
- Absorption width
- X-ray fluorescence
- Charge drift
- Back scattering

Although the resolution is degenerated by charge sharing, it will have an even more drastic influence on the spectroscopic properties of the system. For a photon counting system, the spectroscopic properties of such a system are severely degenerated by the charge sharing phenomenon [1]. In the effective spectrum obtained by the system, high energy photons will be redistributed towards lower energies, as shown further on in this section. This occurs when a high energy photon hits the detector close to the border between two pixels and the charge cloud is distributed over both pixels. The event detected by the system is two photons which share the energy of the high energy photon.

Although several research projects concerning pixel detectors exists, the Medipix2 system is the only system which has reached such small pixel sizes that charge sharing has become a large problem. Due to the high resolution and the low noise of the Medipix system, it can be used as a tool to study the charge sharing phenomenon.

3.1.1 Beam geometry and scattering

Divergence of the X-ray beam and scattering of X-rays in air or in soft tissue will cause the image to degenerate. This problem does not depend on the detector technology, but to some extent X-ray scattering in soft tissue can be compensated for when using "colour" X-ray imaging.

3.1.2 Signal sharing from quantisation error

The quantisation error present in pixellated X-ray detectors exists in all digital imaging systems. Since the image is digitalized a diagonal line will be represented by a "stairway" where the pixel size defines the size of the steps as in Figure 7. The maximum width of the line spread function can therefore not be smaller than the pixel size [26]. This is the driving force behind the development of detectors with reducing pixel sizes.

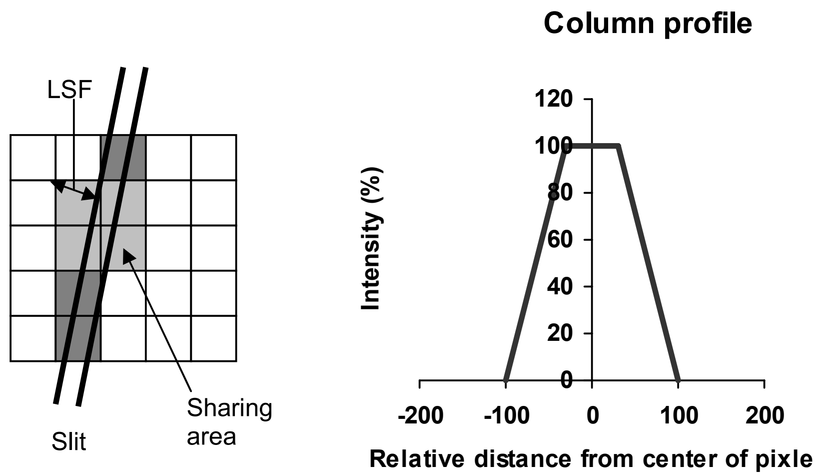

Figure 7: The line spread function, LSF, can be measured with an illuminated slit with smaller dimension than the pixels. In the illustration, the intensity for a pixel in a column will correspond to the LSF-value for the corresponding distance between the slit centre and pixel centre. The proportion between the plateau and the slope of the LSF depends on the width of the slit.

3.1.3 Signal sharing from X-ray absorption width

When an X-ray photon is absorbed in a semiconductor, a chain of events is initiated where the total energy is deposited. This process can involve locations in more than one pixel. In paper V and [10] different aspects of how the distribution of deposited energy can be calculated by simulations using the Monte Carlo simulator MCNP [27] are studied.

The cross section, which is the probability for absorption of X-ray photons in the detector, differs depending on the photon energy and on the detector material. Silicon is quite transparent and only about 10 % of the photons from a standard dental X-ray source are absorbed in a 300 μm silicon detector. Materials such as GaAs and CdTe are much better X-ray absorbers and can therefore offer increased quantum efficiency, as can be seen in Figure 8. But the superiority in electrical properties for silicon makes it an attractive detector material even though its absorption properties are poor.

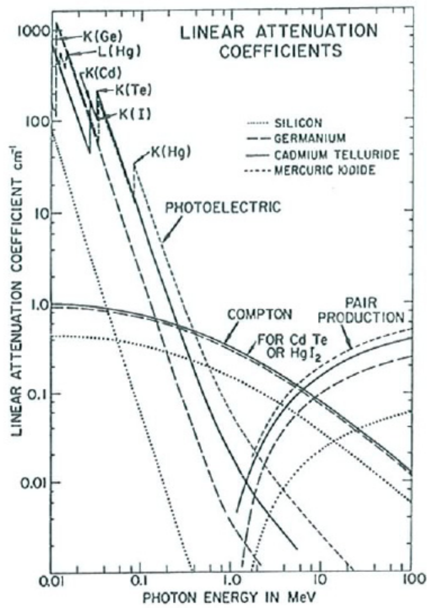

Figure 8: Photoelectric, Compton, and pair production linear attenuation coefficients for Si, Ge, CdTe and HgI_2 from [5]. K-shell absorption edges are shown.

3.1.4 Signal sharing from X-ray fluorescence

X-ray fluorescence is a process related to X-ray absorption. It occurs when an atom emits the absorbed energy as a new X-ray photon. The energy of the generated X-ray photon typically corresponds to the binding energy of a K-shell electron. The energy of fluorescent photons increases with atomic number. Fluorescent X-rays are emitted in any direction and can be absorbed again "far away" from the original absorbing position in the detector. If the effect of X-ray fluorescence is large, as it is for heavy atoms, it will cause serious degeneration of the image quality. When a CdTe-detector is irradiated using a 40 keV beam, approximately 43 % of the beam energy will be carried away by fluorescence. X-ray fluorescence for CdTe and GaAs is quantified in paper V. Although the effect of fluorescence is significant in CdTe and GaAs, the effect of charge drift is larger.

Table 1: Energies for fluorescence X-rays for some detector materials together with the escape energy if a 40 keV source is used.

Material	Kα-energy (keV)	Escape energy for a 40 keV source (keV)
Cd	23.17	16.83
Te	27.47	12.53
Ga	9.25	30.75
As	10.54	29.46

3.1.5 Signal sharing from charge drift

Charge drift is the single most important contribution to signal sharing, and therefore signal sharing is often referred to as charge sharing. The energy deposited by X-ray photons in a semiconductor generates a cloud of free electron-hole pairs.

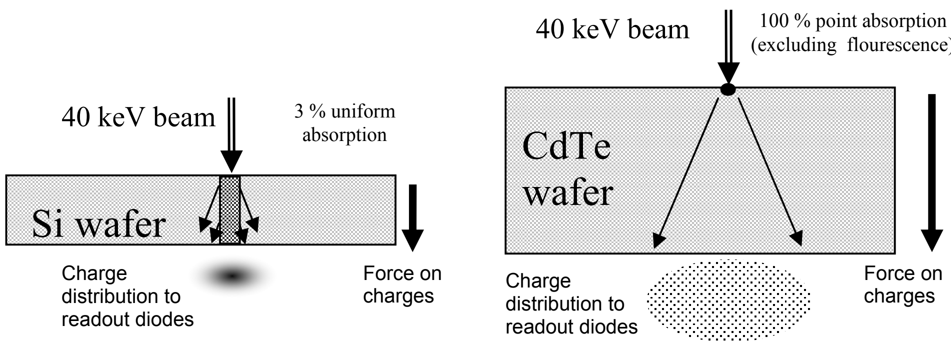

Figure 9: Illustration of charge sharing. In silicon the absorption path can be approximated by a uniform line through the detector. A normal wafer thickness is 300 μm so the charge has to travel 150 μm on average. In CdTe the absorption can be approximated as a point on the surface. The charge has to travel through the whole wafer which normally is 1 mm. In both cases the applied field is about 350 V/mm.

Normally a field is applied to force the induced charges to accelerate towards the contact for the readout electronics. But during the transport time the charge cloud will increase in size due to diffusion as illustrated in Figure 9. Over-depletion will suppress the diffusion and therefore to some extent improve the situation.

3.1.6 Signal sharing due to backscattering of X-ray photons

Backscattering of X-ray photons from underlying layers is a problem in the case of detector materials with low absorption such as silicon. In the Medipix system the detector chip is bump-bonded to the readout chip using an indium or tin/lead bump for each pixel. The size of the bump is comparable to the pixel size and it will reflect a significant amount of X-ray photons thus contributing to the charge sharing [28].

3.2 OBSERVATIONS OF CHARGE SHARING IN SLIT MEASUREMENTS

The most straightforward means of visualising that charge sharing is present in Medipix2 is to investigate the spatial resolution with slit measurements. To measure the line spread function, a 10 μm wide and 6 mm long slit was used. Since the slit is tilted, the line spread function can be achieved from the signal distribution in columns [26], as discussed in chapter 3.1.2.

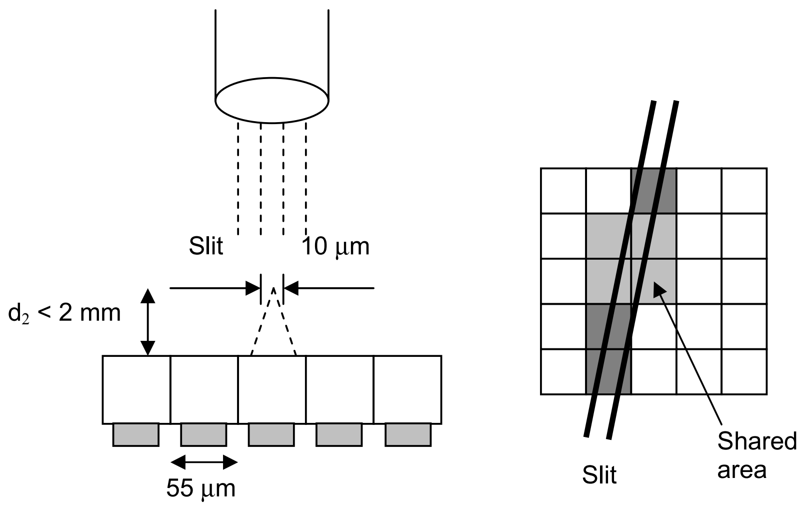

Figure 10: Experimental setup. The 10 µm slit is exposed by 70 keV X-rays.

The distance between the slit and the detector surface was approximately 2 mm, since the slit could damage the bonding wires between the readout chip and the circuit board if they had physical contact. The width of the focal spot point of the source is 100 µm. The divergence of the beam is small, since the distance of 350 mm between the slit and the source is much longer than that between the slit and the detector. The spot size of the X-ray beam on the detector after the slit can be estimated to 11 µm due to the width of the focal spot point.

Figure 11 displays an image of the slit obtained using a Medipix2 silicon detector and a wide energy threshold window. In this image the pixels with a centred slit can be clearly distinguished from the shared areas.

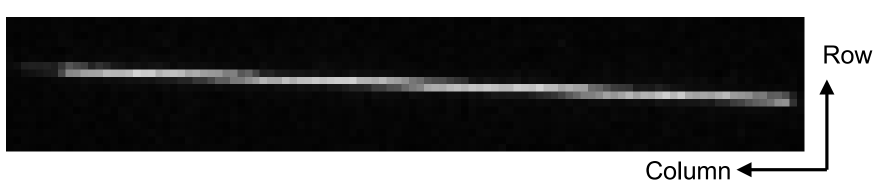

Figure 11: Image of a slightly tilted slit achieved using Medipix 2.

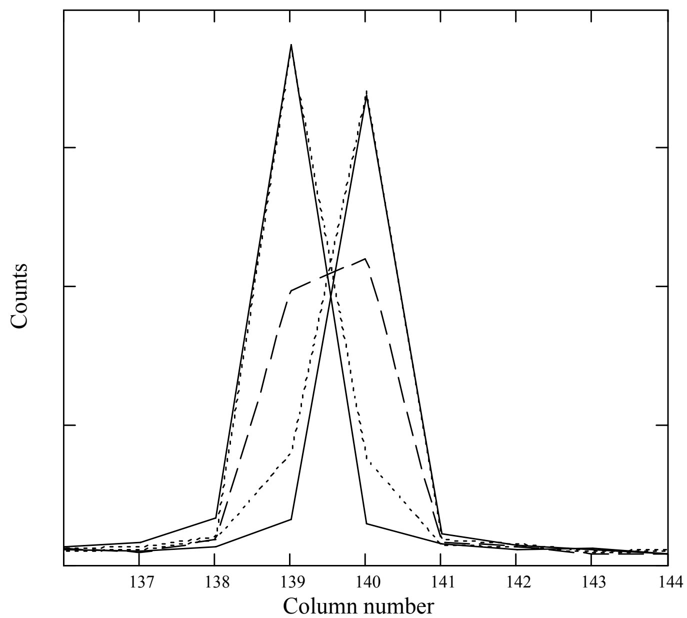

Figure 12: Row profiles of the slit in Figure 11.

The achieved row profile in Figure 12 is due to the geometrical position of the slit [26] and charge sharing properties [1] of the detector. The left and right solid lines correspond to rows where the centre of the slit is placed exactly in front of the centre of pixel columns 139 and 140 respectively. The signal achieved by the neighbouring pixels is due to charge sharing only. The signal due to charge sharing does not exceed 10 %. The dashed line shows a row where the centre of the slit lies exactly in between pixel columns 139 and 140. The dotted lines correspond to rows where the spot size is close to the border, but does not overlap the neighbouring pixel.

3.2.1 Colour images of a slit

It is possible to compose RGB images of a slit, by combining three images achieved with three different energy windows. The dental X-ray source has a wide spectrum seen in Figure 1. The low energy image is assigned to red (10 – 15 keV), the medium energy to green (25 – 30 keV) and the high energy to blue (43 – 47 keV). If the full spectrum is present the resulting colour will be white. The reason for this rather low RGB scheme is the shift of the recorded spectrum due to charge sharing discussed in chapter 3.3.4.

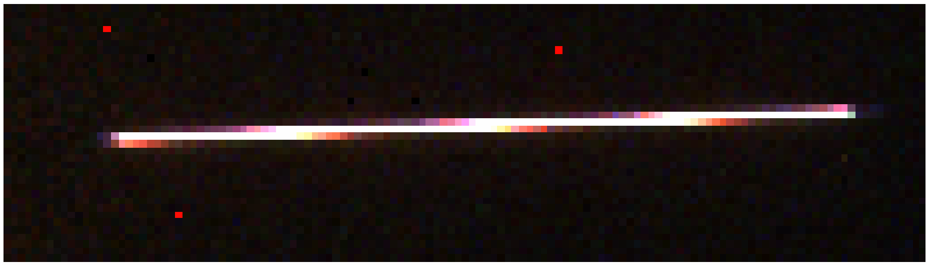

Figure 13: Colour image of a 10 µm slit achieved with Medipix2 with a 300 µm thick silicon detector and a dental X-ray source.

It can be noted in Figure 13 when the slit is centred the pixel colour is white, which means that the full spectrum range is recorded. The red colour corresponds to pixels not illuminated that are reached by the charge cloud from an illuminated neighbour pixel.

The image of the slit on a CdTe detector in Figure 14 shows a width of approximately 400 µm. The increase in width is due to charge drift and fluorescence as discussed in chapter 3.3.2.

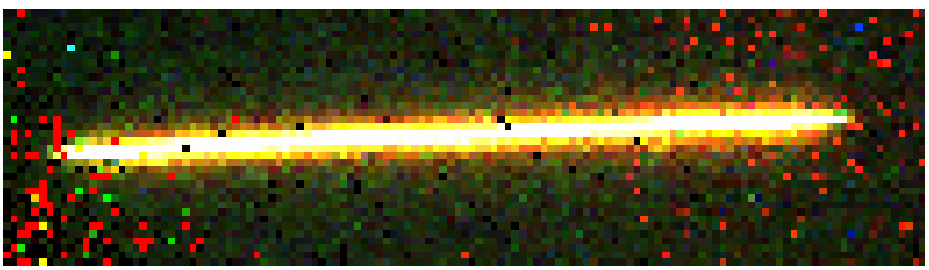

Figure 14: Colour image of a 10 µm slit achieved with Medipix2 with a 1 mm thick CdTe detector and a dental X-ray source.

3.2.2 Slit profiles with low threshold discrimination

The column profiles for this slightly tilted slit are more interesting than the row profile, since it corresponds to the LSF [26] and offers information concerning the signal as a function of the position in the pixel. If these column profiles are studied for different low threshold discrimination levels, information about signal sharing properties can be obtained.

The lower curves displayed in Figure 15 show the series of the signal distributions along the columns for the detector with a tilted slit. The dotted curves correspond to a low level of the lower threshold. For the dashed curves, the lower energy counts are discriminated by applying a 22 keV higher value of the lower threshold.

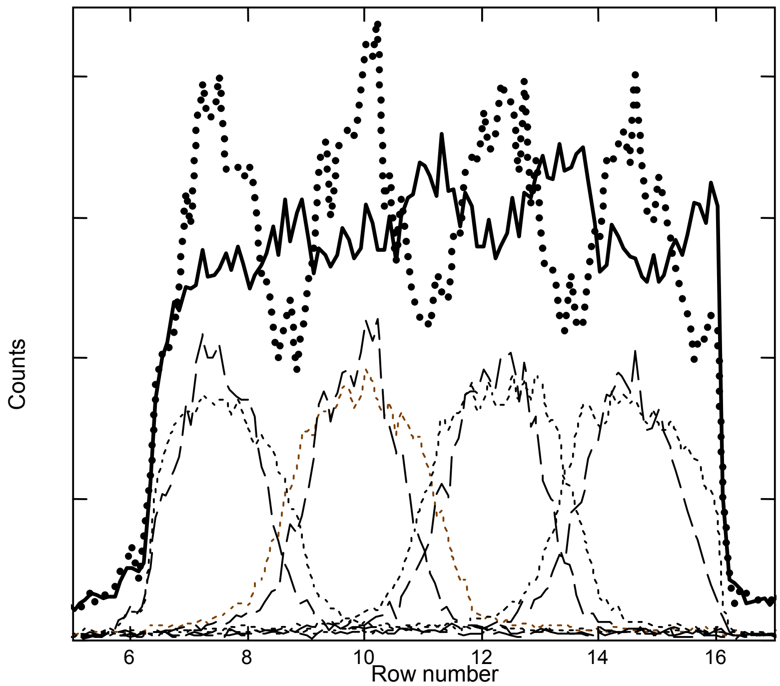

Figure 15: The lower curves are column profiles of two images of the slit obtained using different threshold values. The dotted profiles correspond to a low threshold and the dashed profiles to a high threshold.

The peaks of the profiles correspond to pixels where the slit intersects with the centre of the pixel, while the crossing of profiles corresponds to the border between pixels. It can be seen that plots for the high threshold are always narrower than those for the low threshold. This means that discrimination of lower energy counts reduces the influence of the shared signal and therefore improves the resolution. This can be explained as a suppression of charge sharing, where the counts originating from charge clouds shared between two pixels will be discriminated for the high threshold setting. A conclusion that can be drawn is that increasing the lower energy threshold decreases the signal contribution from the shared high energy photons.

Other information can be extracted by summing the columns (upper thick lines in Figure 15). The dotted thick lines correspond to a higher threshold than the solid thick line. If all generated charge is collected, then the signal equal to the sum of the signals over a row for separate columns, should not exhibit any changes as a function of row number. This is the case if the intensity of the X-rays beam is constant along the slit. From Figure 15 it can be seen that the modulation of the sum of the signals occurs in the case, when lower energy photons are excluded. In the borders the signal drops showing that the collection of charge is different for different thresholds. This is due to charge sharing. The signal originating from shared photons with a low energy is suppressed if the threshold is increased. Therefore the sum over a row decreases for high thresholds, when the slit intersects the gap between two pixel columns. The sum for the lower threshold shows a slightly higher count rate in between the pixels. For low thresholds photons absorbed near a pixel border will be counted twice, since the charge cloud from the photon is divided between the two pixels.

3.2.3 Slit profiles for a 1 mm CdTe detector

In the case of a 1 mm thick CdTe detector, the charge cloud on the readout side of the wafer becomes larger than a pixel for low energies. Row profiles corresponding to the line spread function can be achieved for CdTe in the same manner as was discussed for silicon. The achieved profiles show a width larger than one pixel. For a low energy setting as in Figure 16 an inverse modulation can be seen.

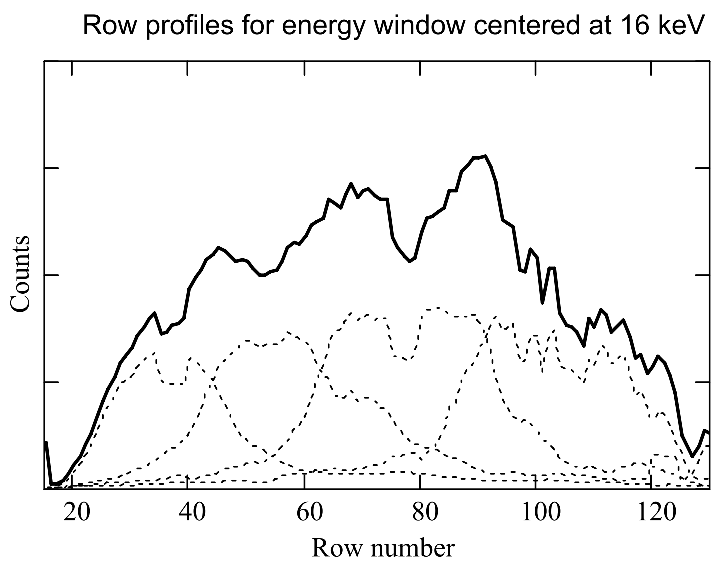

Figure 16: Column profile for two pixels and their sum for a slightly tilted slit on a CdTe detector. The threshold energy window is 3 keV wide with middle energy value at 16 keV.

In Figure 17 this modulation disappears and the sum of the profiles becomes uniform. For a higher energy window as in Figure 18 the strongest signal comes from the centre of the pixel, indicating that discrimination takes place for shared counts on the border between the pixels. The widths of the profiles are however still wide compared to profiles for a silicon detector.

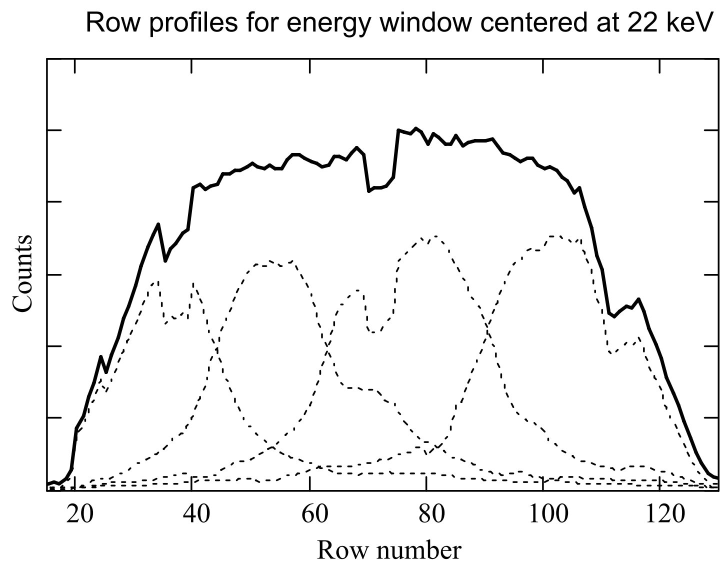

Figure 17: Column profile for two pixels and their sum for a slightly tilted slit on a CdTe detector. The threshold energy window is 3 keV wide with middle energy value at 22 keV.

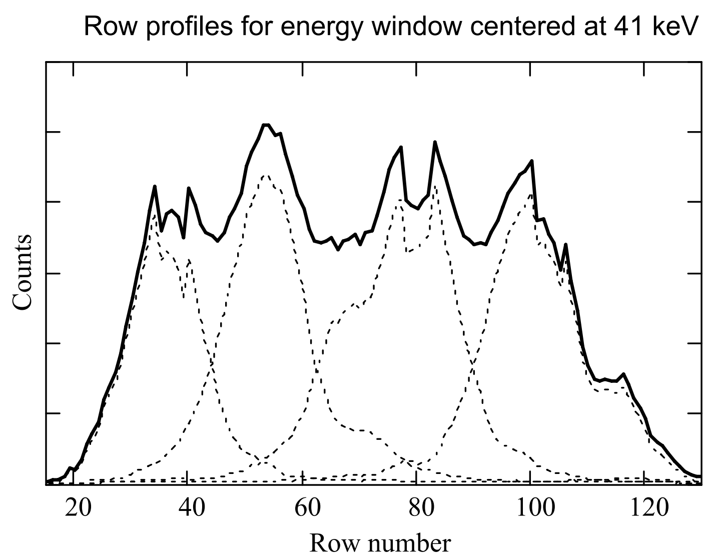

Figure 18: Column profile for two pixels and their sum for a slightly tilted slit on a CdTe detector. The threshold energy window is 3 keV wide with middle energy value at 41 keV.

3.3 SIMULATIONS OF DETECTOR PERFORMANCE

Computer simulations are important for gaining understanding about the basic physical phenomena leading to particular experimental results. The ever-increasing computer power leads to simulation models which have higher and higher degrees of complexity. The computer environment for simulations in this thesis is the Electronic Design Computer Centre at Mid Sweden University. The mainframe is a Sun Fire 15K StarCat with 72x - 900 MHz CPUs, 288 Gbyte of memory and 3.93 Tbyte of RAID5 disk space.

The purpose of the simulations described in this chapter is to reproduce the different measurements in this thesis and thereby provide understanding about the charge sharing mechanism in Medipix2 detectors. Simulations of X-ray absorption, X-ray fluorescence and backscattering have been performed using MCNP [27]. Simulations of charge drift have been performed using Medici [29] and GEMS [1]. The latter simulator is based on a full band Monte Carlo method and has been developed to explore the characteristics of novel materials and novel devices [30]. All simulations in the following sections are done using 10 um wide beam of 40 keV photons, except the flood image simulations in section 3.3.4.

3.3.1 Simulations of X-ray absorption in silicon

When the Medipix2 chip is equipped with a 300 µm thick silicon detector, it can be used for imaging with good spatial resolution, in spite of the charge sharing problem. Simulations of one pixel in 300 µm silicon using MCNP gives a quantum efficiency of 3.4 % and an absorption profile according to Figure 19. The X-ray absorption is approximately uniform through the detector, but scattering events broaden the half width of the beam to about 12 µm.

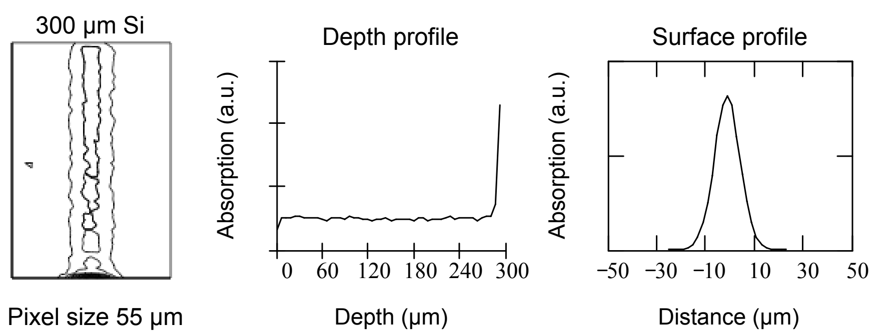

Figure 19: Simulation in MCNP showing the absorption profile in 300 µm Si for a 10 µm wide source with monochrome 40 keV X-rays. The plot to the left is a contour plot of a pixel of the detector along the beam (horizontal axis scaled 4 times); the plots in the middle and to the right are profiles along and perpendicular to the beam.

The increase in absorbed energy at the bottom of the pixel is due to X-ray fluorescence from the bump-bonds [28]. This fluorescence is sometimes referred to as "backscattering". The bump-bonds can consist either of Indium or of a mixture of Tin and Lead. Backscattered X-rays are considered in paper VII, since they will give a contribution of low energy counts in the achieved spectrum [28]. In Figure 20 the energy spectrum due to fluorescence in Lead/Tin and Indium are shown.

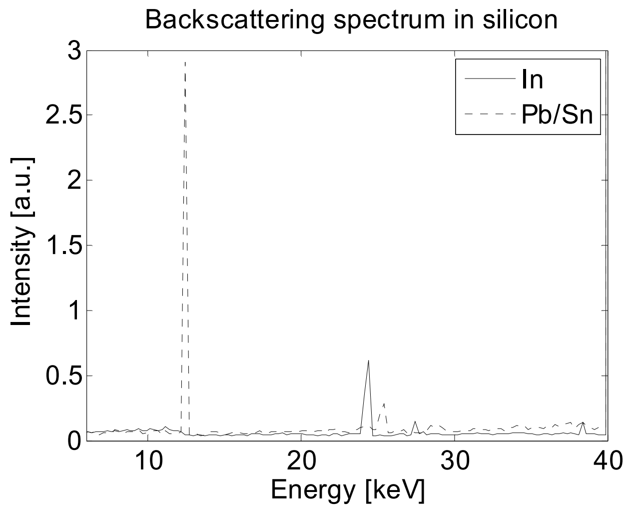

Figure 20: Spectrum achieved from MCNP due to fluorescence from a bump bond consisting of Indium or Lead/Tin.

The Medipix detectors characterised in this thesis contain bump bonds of Lead/Tin, so this spectrum is more interesting. The Kα energy for Tin at 25 keV can be observed. The distinct peak at 12 keV originates form the L-shell in Lead. For sources with higher energy the Kα energy for Lead at 75 keV could be expected to occur. The backscattered radiation can be seen as a spherically radiating source at the bottom of the pixel as in Figure 21.

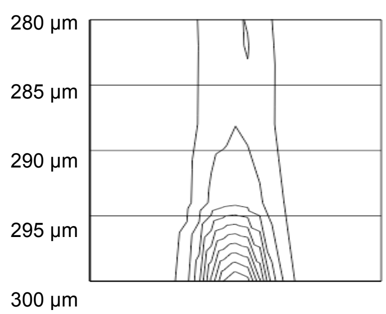

Figure 21: Detail of the contour plot to the left in Figure 19, showing the absorption profile in a pixel bottom up to 20 µm above the bump bond.

A contribution of backscattering from the silver glue (7 µm thick on the back side of the ASIC) and from the copper ground plate will also be present in the detector [31]. In the case of a narrow beam on one single pixel this fluorescence will be radiated spherically through the ASIC and affect an area of approximately 500 pixels. Therefore backscattering from silver glue has been omitted in the model. It is implied in [32] that the main backscattering contribution comes from the bump bonds.

Medipix chips with 700 µm thick silicon detectors are available. Simulations using MCNP give a quantum efficiency of 7.3 % and an absorption profile according to Figure 22. The X-ray absorption is approximately uniform through the detector, but scattering events broaden the beam to about 13 µm.

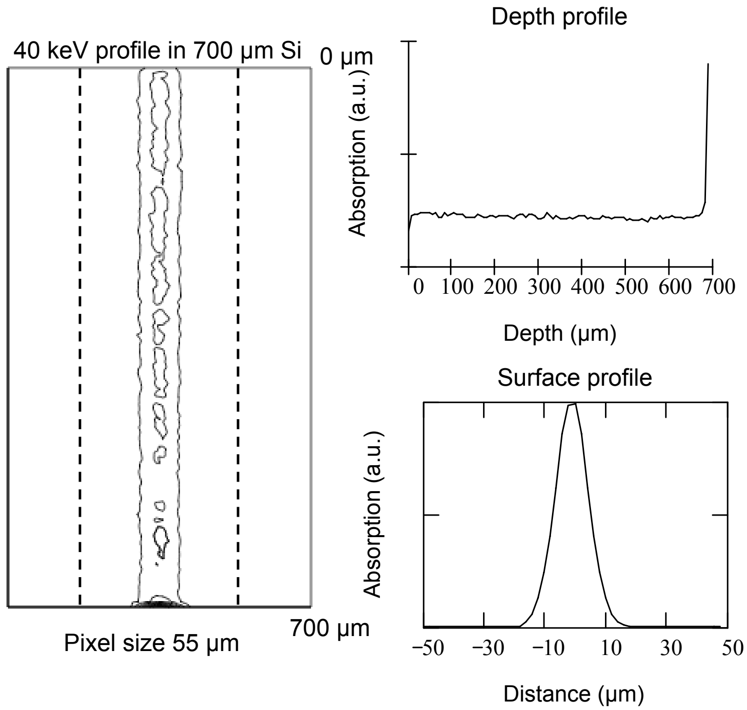

Figure 22: Simulation in MCNP showing the absorption profile in 700 µm Si for a 10 µm wide source with monochrome 40 keV X-rays. The plot to the left is a contour plot of a slice of the detector along the beam (horizontal axis scaled 4 times); the plots to the right are profiles along and perpendicular to the beam.

Due to improved quantum efficiency and almost no increased Compton scattering, the 700 µm thick silicon detector would be a better choice than the 300 µm silicon detector. However, degeneration of the spatial and spectral resolution of thick silicon detectors occurs because of charge sharing. Another complication discussed in chapter 3.4.2 and in paper VII involves alignment problems in thick detectors.

3.3.2 Simulation of X-ray absorption in CdTe

Almost all direct absorptions of 40 keV photons in a CdTe detector take place close to the detector surface, as can be seen in Figure 23. However, the influence of fluorescence causes significant degeneration of the quantum efficiency of one single pixel. MCNP-simulations show that due to fluorescence only 70 % of the incoming X-rays will deposit their energy inside the 55 µm pixel. Some fluorescence X-rays will be emitted upwards, but 22 % of the incoming energy from the beam will be deposited in other pixels of the detector and thus the image will be degenerated.

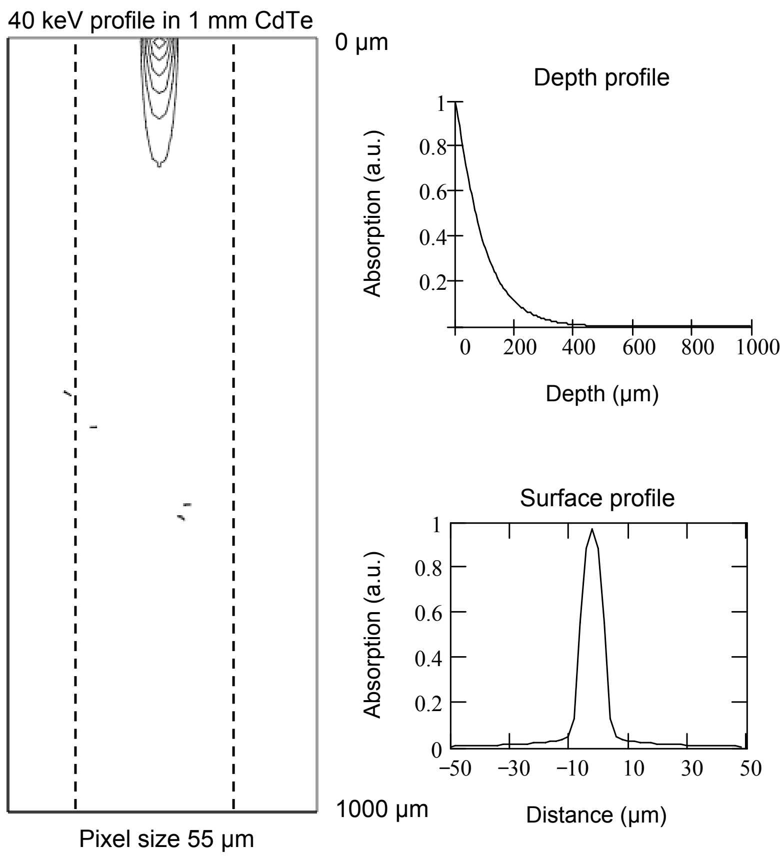

Figure 23: Simulation in MCNP showing the absorption profile in 1 mm CdTe for a 10 µm wide source with monochrome 40 keV X-rays. The plot to the left is a contour plot of a slice of the detector along the beam (horizontal axis scaled 4 times); the plots to the right are profiles along and perpendicular to the beam.

Imaging using a 1 mm thick CdTe detector requires discrimination of energies below 30 keV in order to eliminate image contributions from fluorescence. If only Compton scattering were present, the spatial resolution of CdTe would be similar to silicon, apart from considerably improved quantum efficiency. In paper V simulations using MCNP of the fluorescence spectrum in different detectors were presented. The resulting spectra can be seen in Figure 24. The distinct peaks are escape peaks, or the remaining energy of the incoming photon after the transfer of energy to a core electron of an atom. When the atom is de-excitated the released fluorescent X-ray photon will have a range of some hundred micrometers, so the probability that it is absorbed in the same pixel as the incoming photon is low.

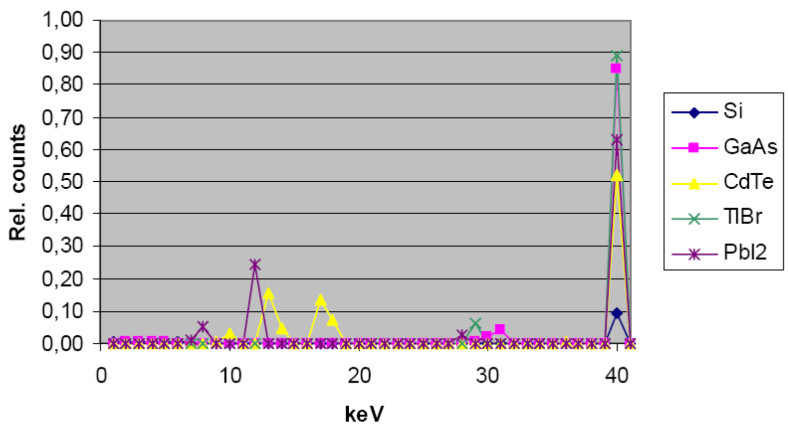

Figure 24: Simulation in MCNP of the resulting spectrum when different detector materials are illuminated with a 10 µm wide beam with monochrome 40 keV X-rays. The escape peaks in the various materials can bee clearly seen.

3.3.3 Simulations of charge drift for a narrow beam

In paper V and paper VI simulations of charge transport with MEDICI for a CdTe detector were presented. In Figure 25 a typical absorption event is illustrated.

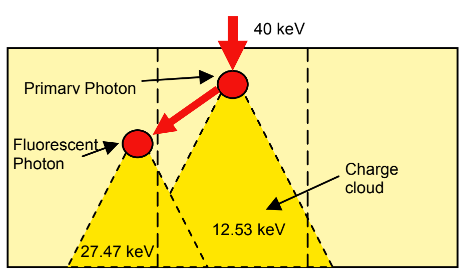

Figure 25: Schematic sketch of a typical X-ray event in a detector of a high-Z material. A fluorescent photon is emitted and captured outside the pixel. The charge cloud from both absorption events widens by diffusion during drift towards the readout electrode.

The simulation shows that the charge cloud of a 40 keV photon will become larger than the pixel size when it reaches the readout electrode, see Figure 26. Without charge summing between pixels it is therefore impossible to detect the full energy of an X-ray photon by means of a 1 mm CdTe detector.

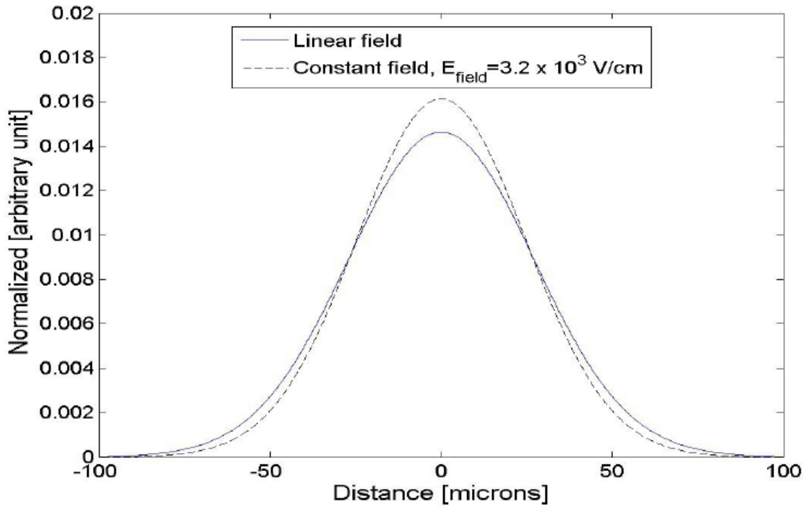

Figure 26: Extension of the charge cloud at the pixel contact for 40 keV photons captured in a 1 mm thick CdTe detector biased at 300 V. Both the constant field case (compensated material) and the linear field case (diode like structure) give the same result for this specific case.

3.3.4 Simulations of charge sharing with GEMS

With a pixel size as small as 55 x 55 µm, charge sharing is a significant effect, as stated in [1]. The simulations show that for the pixel size 50 x 50 μm^2, measured energy spectra will be highly distorted and the line spread function of an image of a slit will be broadened. Three levels of Monte Carlo simulations for a pixellated detector system are performed. Photon transport is simulated with MCNP. The full band charge transport is simulated using GEMS. The results are interpreted at the system level using a Monte Carlo methodology for a detector array implemented in Matlab. Since the GEMS simulations are very timeconsuming, a large number of absorption events have been pre-calculated. This GEMS-generated database is used as the input to the system level Monte Carlo scheme in order to directly extract charge sharing information from the silicon detector, for a given absorption profile from MCNP. Simulated and measured spectra of an X-ray tube have been compared in paper IX.

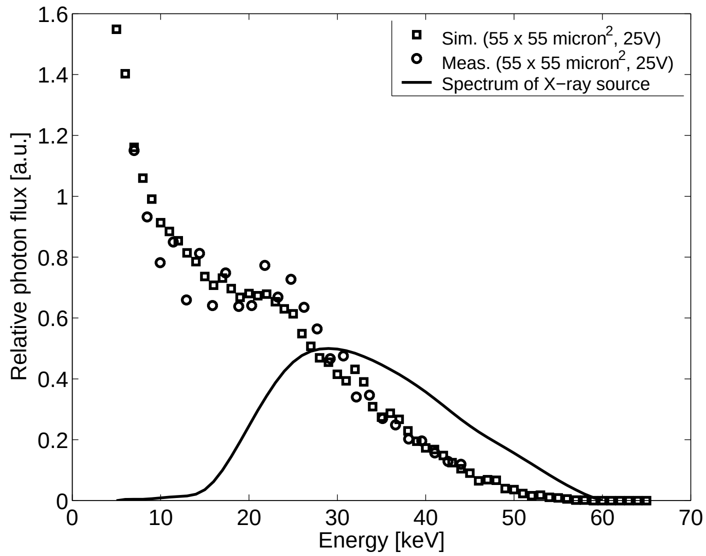

Figure 27: Comparison between simulated and measured spectra for the Medipix2 system. The bias voltage of 25 V corresponds to the depletion voltage of the detector. The solid line shows the actual spectrum of the source.

The achieved spectrum shows that at the depletion voltage the Medipix2 system with a 300 μm silicon detector is unable to resolve the spectrum of a dental X-ray source. As seen in Figure 28, the charge sharing is suppressed if the bias voltage is increased. But even at 100 V bias voltage, which is close to the breakdown voltage of the 300 μm silicon detector, the achieved spectrum is far from the original spectrum of the source.

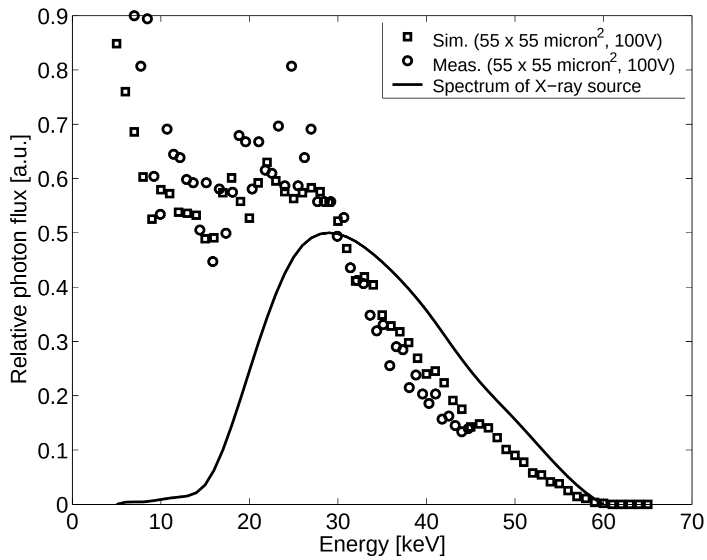

Figure 28: Comparison between simulated and measured spectra for the Medipix2 system when the detector bias is 100 V.

3.4 MEASUREMENTS WITH A NARROW MONOCHROME BEAM

Measurements on Medipix2 using a monochrome source were performed at ESRF in Grenoble, France [33]. The purpose of these measurements was to isolate specific contributions to the charge sharing process for Si- and CdTe-detectors. These measurements are described in papers V and VI for CdTe-detectors and in paper VII for Si-detectors.

The actual beam line delivered an intense and monochrome beam consisting of 40 keV photons. The beam size was approximately 900x900 µm but it was limited to a 10x10 µm square with two crossed slits. The detector was mounted perpendicularly to the beam.

3.4.1 Measurements on a 1 mm thick CdTe detector

The measured point spread function for the beam on a CdTe-detector is shown in Figure 29. When the discriminator level is close to the energy of the source, the signal on the neighbouring pixels is three orders of magnitude lower in intensity. However if the energy threshold falls below the fluorescence energies of CdTe, a strong signal is present on the neighbouring pixels and a significant signal is observable even at a distance of 165 µm from the beam. This agrees with simulations of X-ray absorption and fluorescence using MCNP, as seen in Figure 29.

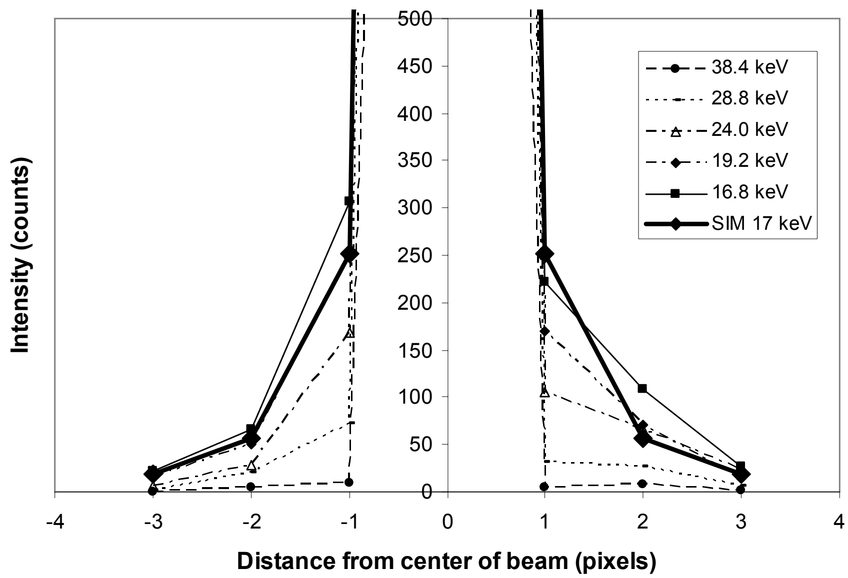

Figure 29: Measurement of the signal in neighbouring pixels of a CdTe detector for different threshold energies. The bold line indicates the simulated response due to fluorescence, without taking charge transport into account.

The spectrum achieved from the centred pixel offers more information regarding what is actually happening in the detector. In Figure 30 a spectrum achieved using a 2.1 keV wide threshold window is shown. The plateau for lower energies is expected if charge sharing and fluorescence are present, so it is evident that, although the beam is centred, a fraction of the photons will deposit a part of their energy outside the pixel. The neighbouring pixel shows a spectrum without an actual energy peak, with a significant count rate at low energies. The spectrum intensity of the neighbour slowly decreases to zero when the energy becomes close to 40 keV. The photon energy 40 keV cannot be present in the readout from the neighbouring pixel since no photons are absorbed in this pixel. The shape of the spectrum for this neighbouring pixel is typical when the dominant process is charge sharing.

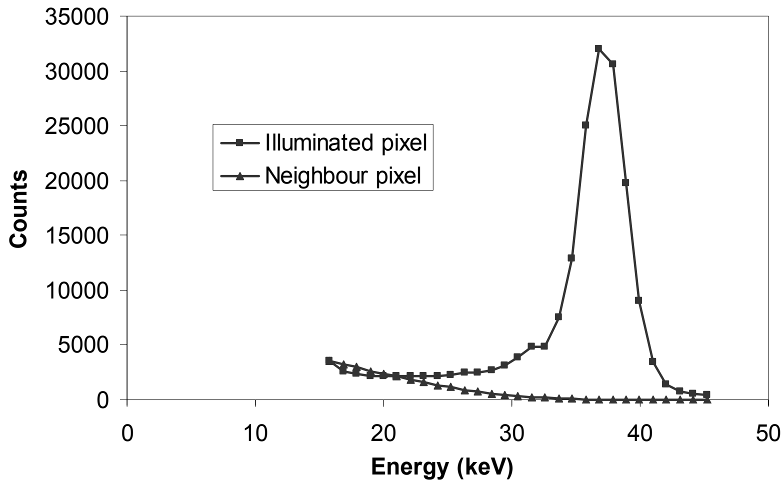

Figure 30: Spectrum achieved from a CdTe detector when the beam is centred on one pixel. The charge sharing spectrum from the neighbouring pixel is also presented. The spectrum is achieved using a 2.1 keV wide threshold window.

A small tail towards higher energies can be seen in Figure 30. In Figure 31 this low energy tail is shown to a level above 90 keV. Note that above the double energy (80 keV) the spectrum intensity drops to almost zero. This indicates that the high energy tail originates from double counts, where two photons hit the pixel within the time resolution of the input amplifier.

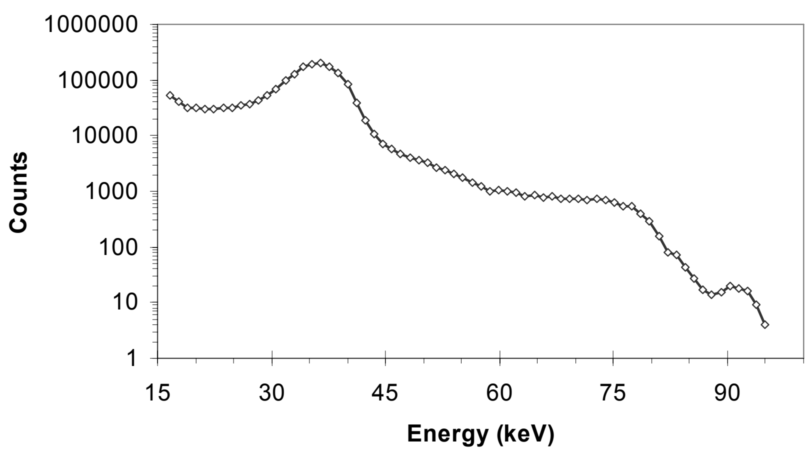

Figure 31: Spectrum on a CdTe detector to study the high energy tail originating from double counts.

Measurements of the spectral response when the beam is scanned over the pixel area provide information of the charge drift in the detector. These measurements in paper VI are very noisy, but in Figure 32 it is evident that the simulated size of the charge cloud in Figure 26 is reasonable.

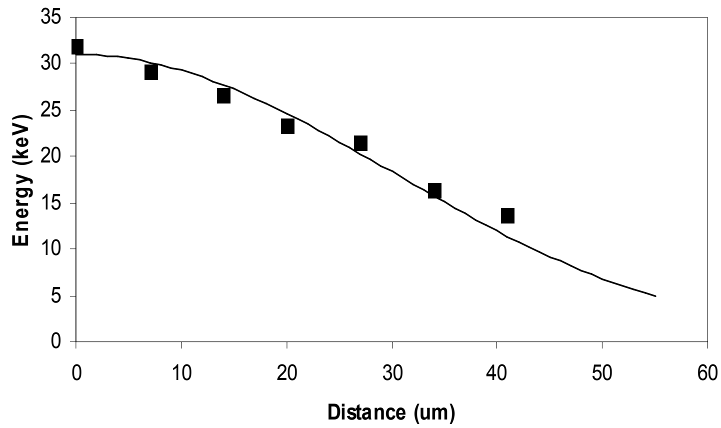

Figure 32: Position of the energy peak as a function of beam distance form the centre of the pixel. The line shows the simulation results. The dots represent experimental data without correction for incomplete charge collection.

For low energy settings of the lower threshold on the present 1 mm CdTe-detector, the spatial resolution is insufficient. Bright details in an image will be smeared out over a distance of approximately 400 µm, as in Figure 14. Since the charge cloud is as large as the pixel size, the energy information will be highly dependent on the position of photon absorption in the pixel. Therefore no relevant energy information can be recorded using a CdTe detector on Medipix2 under flood illumination. With charge summing schemes for the closest pixels, the charge drift problem can be corrected, but still fluorescence will distort the energy information, unless charge summing schemes for about 7x7 pixels are implemented.

3.4.2 Measurements on 300 µm and 700 µm thick Si detectors

In paper VII measurements of a narrow beam on a 300 µm silicon detector are reported. Figure 33 displays a spectrum achieved from a low threshold scan. This generates a cumulative spectrum which can then be differentiated. The spectrum is achieved from a pixel where the narrow monochrome beam is centred. A plateau for lower energies due to charge sharing is present in the differentiated spectrum, since there is a slope in the cumulative spectrum. The simulations in chapter 3.3.1 reveal that this charge sharing is due to backscattering from the bump bond. The charge cloud is not sufficiently large to reach neighbouring pixels when the beam is centred in a pixel. The low energy slope in the cumulative spectrum can be reproduced if Indium or Tin/Lead is present below the detector in the MCNP model.

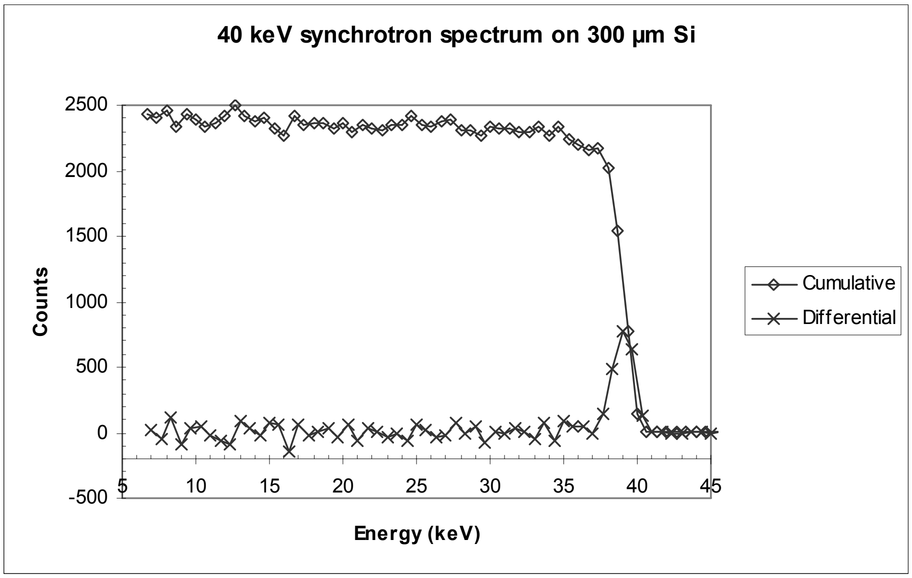

Figure 33: Spectrum of the 40 keV source achieved from a low threshold scan with a 300 µm thick Si detector.

To be able to see how the charge sharing influences the spectrum, the beam was moved from the centred position towards the border of the pixel. The best spectrum should be achieved with the beam centred above a pixel (0 µm), while the beam position on the border between two pixels (28 µm) should give a minimal contribution of 40 keV counts. The charge drift for this measurement situation has been simulated using GEMS. The simulation results compared to the measurements are presented in Figure 34. To reproduce the slope of the 40 keV edge in the spectra, a readout noise level of 80 electrons had to be added, which corresponds to the expected value. The soft bending at about 38 keV for some positions indicates that a part of the charge cloud has escaped from the pixel. The presence of lower energies is mainly due to backscattering. In paper VII both aligned and 2° tilted beams are studied. The tilt of the beam introduces a beam widening, but the position sensitivity will become quite complex. If the beam is tilted, charges created close to the detector surface will reach the readout on a shifted position compared to charges created close to the readout. Charge clouds created close to the surface have a long drift path and will result in wider clouds reaching the readout. Note that the peak shift for the border position is reproduced in the simulation if the beam is tilted, which indicates that the simulation accuracy is reasonable.

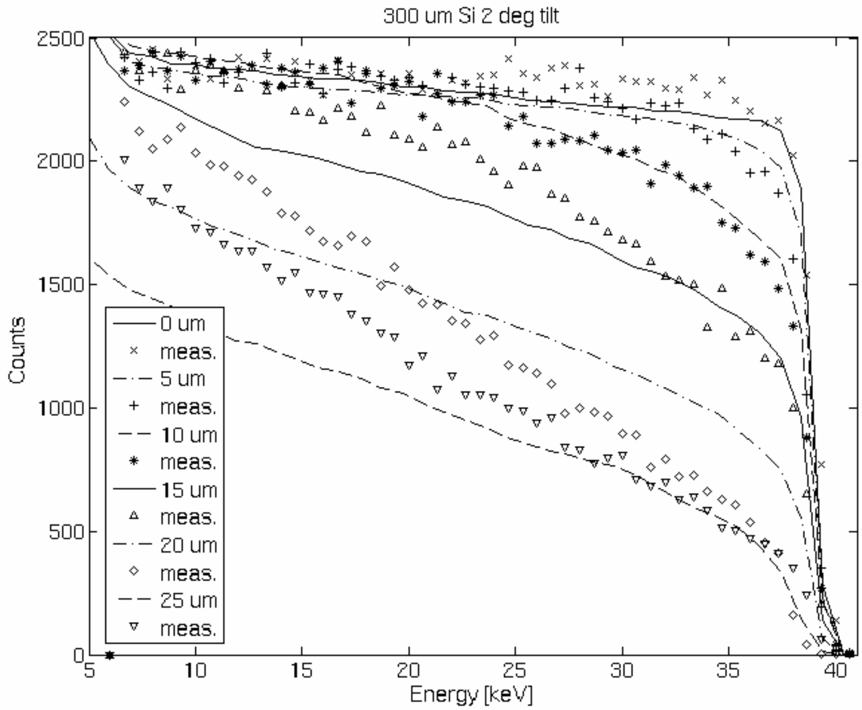

Figure 34: Comparison of measured and simulated cumulative spectra for a narrow 40 keV beam on a 300 µm thick silicon detector. The beam is tilted 2°.

Widening of the charge cloud due to angular misalignment of the incoming beam on the detector is illustrated in Figure 35. If the actual tilt is 2º, the beam absorption width will be significantly increased by approximately 10 µm for a 300 µm detector and 24 µm for a 700 µm detector. Alignment problems will hence have a large impact on thick silicon detectors

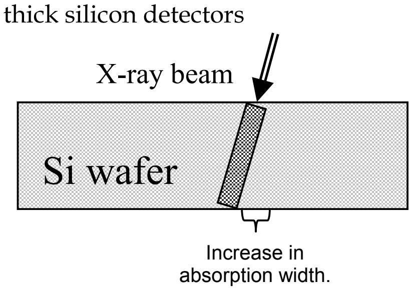

Figure 35: Illustration of the increase in absorption width due to a slight tilt of the incoming beam.

When these measurements were performed on a 700 µm thick silicon detector, the achieved spectra for a centred beam showed much less distinct energy edges than those for 300 µm. The charge sharing in 700 µm silicon is expected to be stronger than in 300 µm, since the average charge transport path is 200 µm longer. When the measurements are compared with GEMS simulations in Figure 36 the agreement is reasonable.

Centring of a tilted beam is a complex problem according to simulations. For some angles the 7 µm position will show a more distinct energy edge than the centred position, which also appears to be the case in the measurements The simulated peak shift for the 28 µm position cannot be found in the measurements, which indicates either that the centring of the beam is not correct or that the beam tilt is lower than 2°.

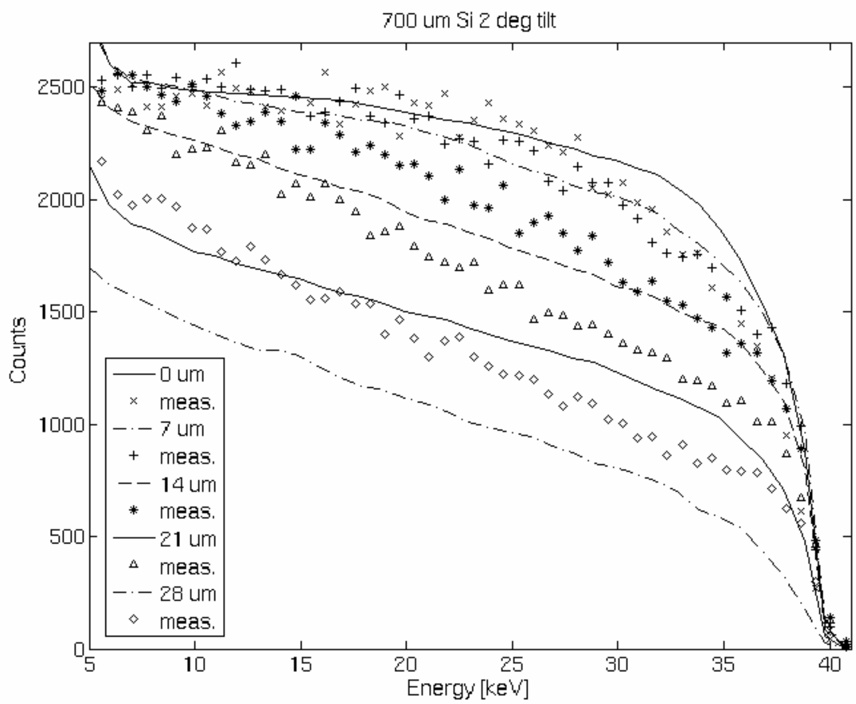

Figure 36: Comparison of measured and simulated cumulative spectra for a narrow 40 keV beam on a 700 µm thick silicon detector. The beam is tilted 2°.

3.5 DESIGN STRATEGIES TO OVERCOME CHARGE SHARING

3.5.1 The 3D-detector structure

One important conclusion can be drawn when paper I is compared to [1], namely that crosstalk between pixels due to charge transport is suppressed in a 3D structure compared to a traditional planar structure. This is because the electric field between the n- and p-contacts of the pixel in the 3D-structure forms a potential well forcing the charges to drift to the "correct" pixel. The field is perpendicular to the incoming photons so the drift path of the charges will not be longer than half a pixel diagonal, as seen in Figure 37. In a planar silicon detector the average drift path will be half that of the detector wafer thickness.

A Medipix1 system equipped with a silicon 3D-detector is demonstrated in [34]. It is argued that the charge sharing can be reduced by a factor of ten compared to a similar planar detector design with four times the bias voltage.

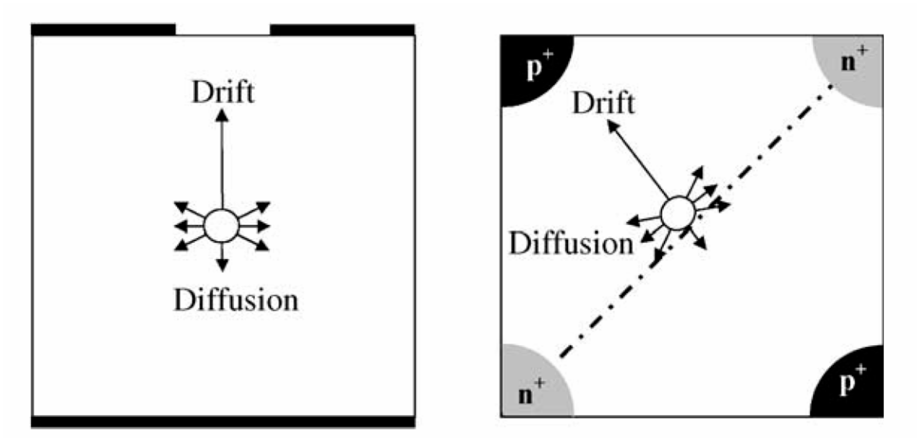

Figure 37: Principal difference between charge sharing in: (left) a 2D pixel detector viewed from the side, and (right) a border (tilted 45º) between two 3D pixels viewed from above.

Another advantage of the 3D design is the possibility to increase the quantum efficiency of silicon detectors by constructing thick detectors, theoretically without increasing the charge sharing. For planar detectors without charge sharing correcting schemes, the gain in quantum efficiency for increased thickness is lost since the increased charge sharing reduces the spatial and spectral resolution.

A problem for a thick silicon 3D-detector is that the source alignment perpendicular to the detector will become important, see section 3.4.2. When the detector is thick compared to the pixel pitch, a small misalignment will cause the photon paths to cross several pixels. Then, details of the object will be smeared out over several pixels, which causes degeneration in both the spatial and spectral resolutions.

For highly absorbing materials the ability to construct thick detectors is not so important, but here the gain in charge sharing is larger since the photons are absorbed close to the surface and the charges have to travel through the entire detector wafer, as mentioned in section 3.1.5. Fabrication of GaAs 3D-detectors is demonstrated in [35].

3.5.2 Charge summing pixel to pixel communication

The problem associated with charge sharing in planar pixellated detectors structures can be overcome if the readout electronics can sum the charge of several pixels for simultaneous events. This solution is mentioned in [20] and one possible low level implementation is presented in [36]. In paper IX, different summing schemes were compared. Summing of charges between pixels will unfortunately always provide additional noise. The noise will increase as the square root of the number of contributing pixels. Four different charge assignment schemes were evaluated concerning their energy resolution and increase in readout noise.

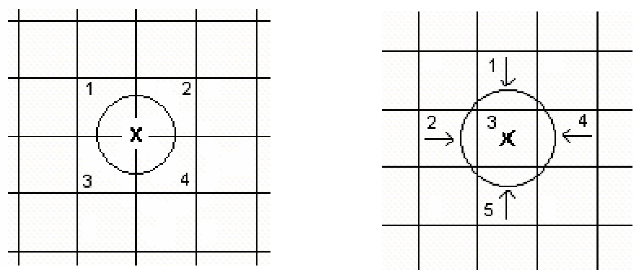

Figure 38: Four pixel summing configuration (4PS) to the left and five pixel summing configuration (5PS) to the right.

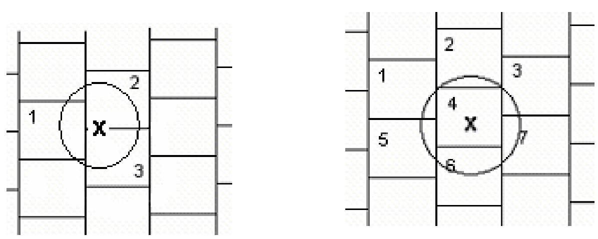

Figure 39: Three pixel summing configuration (3PS) to the left and seven pixel summing configuration (7PS) to the right. These schemes requires a Odd Column Shifted Matrix (OCSM)

The readout electronics must firstly decide the pixel to which to assign the position of simultaneous shared events and this will be the position of highest signal value. The energy level is however based on the sum of charges for this pixel and its neighbours. For the non-symmetric configurations (4PS and 3PS) the neighbouring pixels are not defined, therefore an additional logic step is required to decide which set of pixels should be summed. But this will actually increase the covered area of the non-symmetric schemes, since for example a corner hit will be assigned to the most appropriate set of pixels.

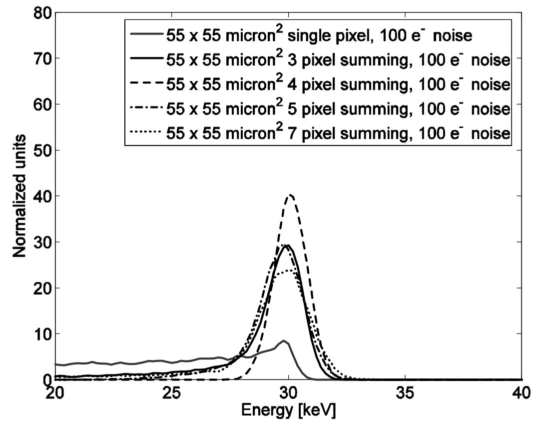

Figure 40: Simulated energy spectra for different charge assignment schemes assuming a mono-energetic 30 keV X-ray source. The assumed electronic noise level is 100 electrons.

The charge summing scheme to be implemented in the Medipix3 is suggested to be (4PS) [23]. This charge sharing correction will solve much of the problem associated with charge sharing due to charge drift. It can however not compensate for all of the charge sharing due to fluorescence that occurs in for example a CdTe detector, see chapter 3.4.1. To solve this problem, a correcting scheme for 7x7 pixels should be required, which will probably introduce too much noise, and might also be difficult to implement with a 0.13 process on the actual pixel size. But CdTe detectors with 110 µm or 165 µm pixels might be an alternative to achieve energy information utilising the better quantum efficiency of the CdTe detector.

3.6 IMAGE CORRECTION FOR THE MEDIPIX SYSTEM

Before an X-ray imaging system can be used, the system must be calibrated to compensate for non-uniformities in the individual detector and in the readout chip. These calibrations must consider the actual application of the system, i.e. the energy and intensity of the X-ray tube. The most well known calibration is “flat field correction”, which must be done for both integrating and photon counting systems. Most readout systems are also designed with a compensation for leakage current. For photon counting system some consideration must be given as to how the threshold settings that discriminates unwanted energies are to be calibrated.

3.6.1 Flat field correction

All detector systems will contain imperfections either in the readout or in the detector which causes different quantum efficiencies for different pixels. This is referred to as fixed pattern noise and is observed when the detector is irradiated by a uniform X-ray beam. From the signal S_n for each pixel in this flat field image a gain factor G_n can be achieved as follows:

$$G_n = \frac{1}{S_n} \cdot \frac{\sum_{n=1}^{N} S_n}{N} \tag{1}$$

The number of pixels on the detector is N. The flat field correction is normalised using the average number of counts on the detector to preserve the achieved count rate of the image. At full depletion a fluctuation pattern due to radial doping non-uniformities can be observed in most detectors [37]. This effect is considerably reduced by over-depletion. The gain map is thus valid for the specific bias voltage applied to the detector.

Normally a large number of flat field images are averaged in order to reduce the statistic noise in the gain map [14]. Another detail for increasing the accuracy of the gain map is to use the full dynamic range of the counters. For a silicon detector the histogram resolution is narrow and flat field images can be achieved close to the maximum number of counts. However, for CdTe-detectors the non-uniformities of the detector are much larger than for Si and the histogram resolution is therefore very wide. The achievable flat field image is then significantly below that of the maximum number of counts. Gain factors corresponding to counter readings of the maximum number of counts will not produce a properly corrected image. In the first version of the Medipix2 chip, the counters will restart from zero once they have reached the maximum number of counts (8192). A small number of "over-counted" pixels in the gain map can thus case considerably degeneration to the image quality.

Something that must be taken into consideration is that the value of the gain factor in flat field correction depends on the energy of the incoming photon [38]. If the number of photons of a specific energy is Φ_e, then the number of counts S_e for a detector thickness t will be described by:

$$S_e = \Phi_e \left(1 - e^{-\alpha_e \cdot t}\right) \tag{2}$$

Since the linear attenuation coefficient α_e is strongly energy dependent, it can be concluded that the flat field correction only works properly for a limited photon energy interval. This is a problem when images taken using a wide spectrum source require correction. In the object, radiation hardening of the source spectrum takes place, meaning that low energy photons are more likely to be absorbed in the object. So the average photon energy is higher in the low intensity parts of the image than in the bright parts.

A flat field correction method, which compensates for radiation hardening in tomography applications, is proposed in [39]. The method uses a set of aluminium test samples of varying thicknesses. The measured transmission *f(x)* can be assumed to correspond to the sample thickness according to:

$$f(x) = \mathbf{O} + \mathbf{A} \cdot e^{\mathbf{G} \cdot x} \tag{3}$$

The set of measurements is fitted to this equation for each individual pixel, and a flat field correction consisting of three matrices is achieved. The achieved gain map is valid for objects consisting of materials with transmission spectra equal to the material of the test samples.

3.6.2 Threshold calibration

The applied threshold voltage in a pixellated system will not correspond to exactly the same discrimination energy in each pixel. The Medipix system is designed with a three-bit threshold adjustment and a test pulse intended to calibrate the threshold for each pixel. The test pulse charges a capacitor at each pixel to a specified voltage and then discharges the capacitance into the corresponding readout. It is then possible to scan the threshold for each calibration setting and observe at which setting discrimination of the capacitive charges occurs for each pixel. In this way a uniform threshold setting is achieved for the whole readout matrix. This procedure is referred to as the ANIN test [18]. There are problems associated with equalizing the threshold settings of the matrix with the ANIN test. It is not possible to construct a chip with exactly the same capacitance in the test capacitor of each pixel. Another method used to equalize the threshold settings of the chip is to equalize the edge of the noise floor. This method, supported by the software Medisoft 4.1 and Pixelman, is at present the standard method used in the equalization of the threshold for Medipix2.

The equalisation described above only takes into account the electronics and not the conversion layer and the bump bonds. It is possible to generate an "absolute" calibration mask that considers the whole system by using a source with a known narrow spectrum [40].

If the energy window capability of the Medipix2 system is going to be utilized, the high energy threshold must also be calibrated. Otherwise the fluctuation in the high energy threshold values will introduce large variations in count rates for different pixels for narrow energy windows. The high threshold mask can be generated by taking images of a wide spectrum X-ray source while the energy window is decreased [41]. When the high threshold for an individual pixel falls below the low threshold, this high threshold will be switched off for this pixel and the count rate will increase significantly. It is also possible to use the ANIN test signal instead of a source. This way to achieve a calibration mask for the high threshold is implemented in pixelman.

3.6.3 Proposed method for energy dependent threshold calibration

A problem considered in paper II is that the threshold setting for individual pixels does not vary linearly with energy. Therefore the threshold equalisation is energy dependent. The behaviour of the cumulative function for individual pixels varies within a wide range for different thresholds. Therefore, it is impossible to create a single calibration mask for all energies. The mask is valid for only a narrow energy range due to the variation in the individual cumulative functions.

This range can be estimated from analysis of the cumulative functions for the pixels. The noise floor corresponds to the lowest energy that is possible to resolve with the system. Therefore the quality of the equalization, achieved from the noise floor, degenerates for threshold settings at high energies.

To solve this problem a method of generating threshold masks for different energies was proposed in paper II. In the study, the Medipix1 system and a 70 keV dental X-ray source with wide spectrum were used. The produced masks will be "absolute", since both detector and channel stationary influences are included, and it is not necessary to use a special calibration source for the creation of correction masks, which simplifies the calibration. For mask creation, histograms of image series were obtained for different thresholds. These histograms correspond to threshold distributions for particular energy thresholds. The model for the histograms was created assuming our standard dental X-ray source. To find suitable parameters, such as the threshold range, it is possible to vary the FWHM (full width half maximum) in the model, until the histograms correspond to experimental data. When creating a mask, it is possible to use the principle of a "flat" correction, since the number of counts from individual pixels is proportional to an integral, which depends on the threshold. The spectral non-uniformity of the detector can be compensated for by the same procedure, if the spectral content of X-rays is similar for each pixel. This is valid, when the number of photons per pixel is sufficiently large (32000). As a result, the image is divided into a number of separate arrays with different count rates and this procedure can be executed for each energy level requiring investigation. Based on these arrays, mask files narrowing the threshold distribution to close to the theoretical limit, were prepared.

This approach can be called a spectral "flat" correction principle, assuming that the threshold distribution dominates the image noise. The histogram shows the distribution of count rates for the pixels of the detector. For the Medipix1 detector and photon energies from 30 – 70 keV, the effective spectrum $\tau(E)$ is close to the source spectrum $S(E)$. The number of pixels in the histogram, h, and the number of detected photons, g, are functions of the threshold of the pixels and can be expressed as $h = f(g)$ or:

$$h(th) = \frac{R(th - th_0)}{S(th) / \Delta_s} = f\left(\int_{th}^{E_{max}} S(E)dE \right) = f(g(th)) \qquad (4)$$

Figure 41 shows a graphical representation of this function. The function *R* can be approximated by a Gaussian distribution which has a half width Δ_R. When Δ_R/Δ_S << 1, the left part of Eq. (4) represents the threshold distribution. The value is normalised with the factor Δ_S.

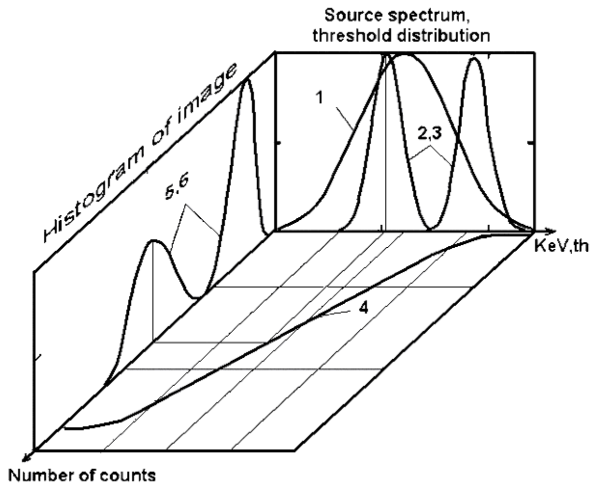

Figure 41: Qualitative description of how histograms relate to the spectra threshold distributions. 1- effective source spectrum from the wide spectrum X-ray source, 2 and 3- pixels threshold distributions for two applied thresholds, 4- cumulative function for pixels, 5 and 6- histograms of images from Medipix1 for threshold distribution 2 and 3, respectively.

Based on this model histograms were created. The model assumes a Gaussian distribution of *R* and a standard X-ray dental source with a 70 keV spectrum. Varying the FWHM of the threshold distribution, the theoretical histograms in Figure 42a were similar to those of the experimentally obtained histograms in Figure 42b. The images were taken using Medipix1 in the threshold scan regime.

Each histogram in Figure 42 represents an image for a particular threshold voltage. From this data the best fit to the experiment was found when the ratio $\Delta_R/\Delta_S \approx 1/7$. The threshold distribution found is $\Delta_R \approx 0.06$ V, assuming that the source distribution is $\Delta_S \approx 0.4$ V. Histograms for thresholds closer to the ends of the spectra do not fit the histograms given by the model because of noise. For low thresholds, high noise exists because of detector and amplifier limitations, for higher thresholds on the other hand the signal is low, and the statistical noise increases.

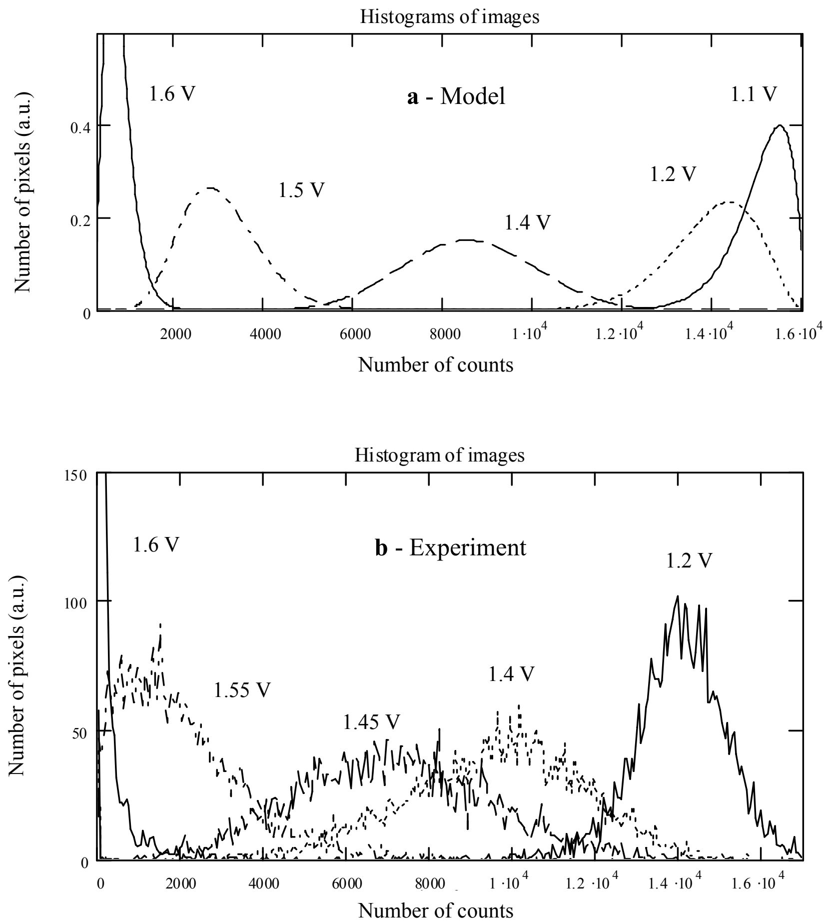

Figure 42: Model – (a) and experimental histograms of flat field images– (b) for different thresholds voltages.

After achieving the range of the count rate distribution from the histogram in Figure 42, it is possible to split the image into the number of levels in the system correction mask. The transformed image contains seven layers describing the resulting mask. After applying this mask the width of the distribution of photo counts was reduced by a factor of 3 compared to the width without a mask. The narrowing of the distribution can be seen on the histograms of these images in Figure 43. A comparison of the achieved histogram of the image after correction can also be made with a theoretical histogram for a perfect seven-level calibration describing the limits of such a correction with this source and system. It is possible to create an optimal compensation mask for each case, because the shape of the histogram of the corrected image depends on parameters such as the number of levels in the calibration mask, the noise to signal ration, etc.

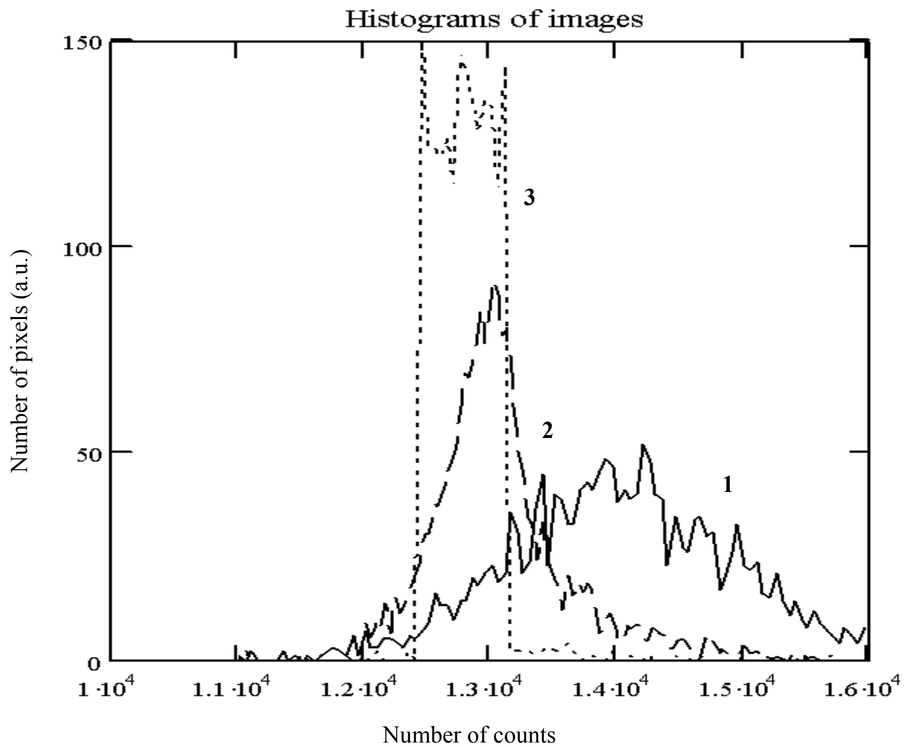

Figure 43: Histograms of image taken without (1) and with (2) mask, compared to a histogram for the calculated image with mask (3).

Using the parameters of the Medipix1 system with a dental X-ray source, the achieved spectral resolution can be estimated. The total range of the threshold energy adjustment for Medipix1 with a dental X-ray source is of the order of 40 keV, which may result in a contrast change of the order of 80 %. In this case changing the contrast of an image by for example 1 % could be achieved by an energy shift of the order of 0.5 keV. Using these estimations, the limits of resolution can be found because of the minimal contrast difference, which can be detected for two images or objects. Such a minimum can be found, when two images are taken using the same conditions on two separate occasions. The resulting minimal contrast is about 2 %, which corresponds to 1 keV. The corresponding standard resolution for 3 sigma is ≈ 3 keV, which is close to the limit of spectral resolution for this system due to Poisson noise, when the number of photons is of the order of 10^4 per pixel. This case corresponds to the highest spatial frequency for the image. The contrast is expected to increase if the spatial frequency decreases. Note that the minimal contrast deteriorates as the threshold rises.

4 POSSIBILITIES FOR PHOTON COUNTING APPLICATIONS

The photon counting principle opens up new perspectives for X-ray imaging. Since photon counting systems are equipped with an energy threshold, the principle is sometimes referred to as "colour X-ray imaging". The difference in absorption for different "colours" can be used to discern materials in the object. This feature is useful in medical imaging. Today some diseases such as brittle-bone disease are diagnosed by the subtraction of two images taken using two different sources with two narrow energies. This method is called "K-edge subtraction" since it uses the fact that the absorption of photons differs above and below the K-edge energy of a specific atom. For a photon counting system with two energy bins this examination can be done using only one X-ray exposure. In paper VIII it was demonstrated that identification of K-edge energies is possible with Medipix2, if charge sharing is compensated for.

Materials can also be distinguished although no K-edge energy is present in the actual X-ray spectrum. In section 4.1 a method from paper III based on the energy variation in absorption is proposed. This method can be used to distinguish between aluminium and silicon for electronic industry applications. Such methods can also be of interest for fibre quality control in the paper and pulp industry [42].

One important reason behind the development of photon counting systems is to improve the quality of medical imaging and thus to be able to reduce the dose delivered to patients [43]. The possibility of dose reduction with photon counting systems has been demonstrated for dental imaging [44] and mammography imaging [45]. Further image improvement can be achieved by energy weighting algorithms as described in section 4.4. The X-ray energy influence on the image quality is studied in paper IV and briefly described in chapter 4.3.

4.1 MATERIAL RECOGNITION

A thickness-independent method for material recognition using the ratio of absorption coefficients is proposed in paper III. The different dispersion of absorption for the materials can be expressed through the linear absorption coefficient α and depends on the material and on the energy of the X-ray photons. From absorption data tables the energy dependence of α can be achieved. If the thickness of the object is unknown, a convenient material parameter to identify is $K = \alpha_1/\alpha_2$, which is equal to the ratio of the logarithms of two measured transmissions $\ln(t_1)/\ln(t_2)$. If a database of K for different materials and energies is created, this method can be used for material recognition independent of the thickness of the materials.

To evaluate the method an object consisting of two 0.5 mm thick slabs of silicon and aluminium were used for X-ray imaging with Medipix1. The X-ray absorption for silicon and aluminium is very similar over the range of the 70 keV dental source, and differs only for lower energies. Hence the possibility to distinguish between silicon and aluminium is a relevant test of the capability of the Medipix1 detector.

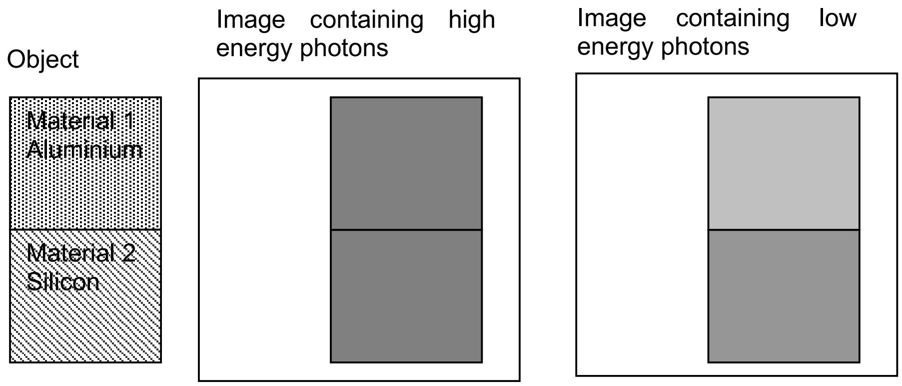

Figure 44: Object consisting of two materials and expected images for different photon energies.

For low energy photons, an image should show an evident difference in the relative contrast between the materials, as shown in Figure 44. But with the Medipix1 system it is not possible to discriminate the high energy counts. The system has one threshold that can only discriminate the low energy counts. The relative contrast for a low threshold value is an average over the spectral width from the applied global threshold to the highest energy achieved.

Series of images of the aluminium and silicon object were taken using different energy thresholds. As expected, it was not possible to distinguish between the materials in a high-energy image. For lower energy threshold values the images were studied using histograms as in Figure 45, and it was possible to resolve two distinct peaks and hence identify the region in the image for each material. The resolution of contrasts found by histograms was close to the limit of the system due to the statistical noise of the signal.

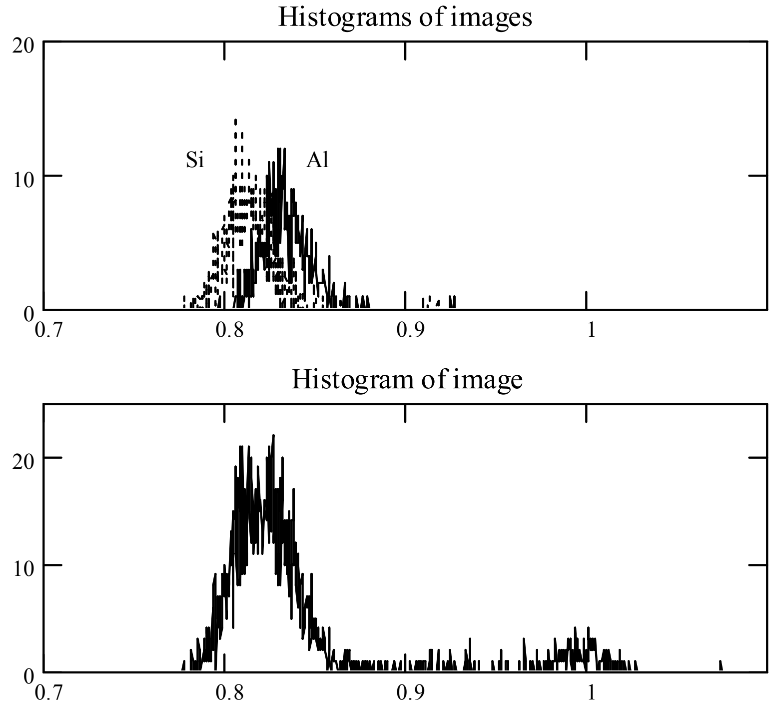

Figure 45: Absorption induced histogram shift. Upper figure: selected known regions. Lower figure: the whole detector.

When the regions were known, it was possible to average the transmission over the regions and calculate the relative contrast between the regions. The relative contrast between the materials for each value of the low threshold was calculated using:

$$\text{Relative contrast} = \frac{t_{Si} - t_{Al}}{t_{Si}} \tag{8}$$

The difference of the average relative contrast between the two materials versus threshold after applying a flat field correction is shown in Figure 46. For the averaging an area of about 100 pixels was used.

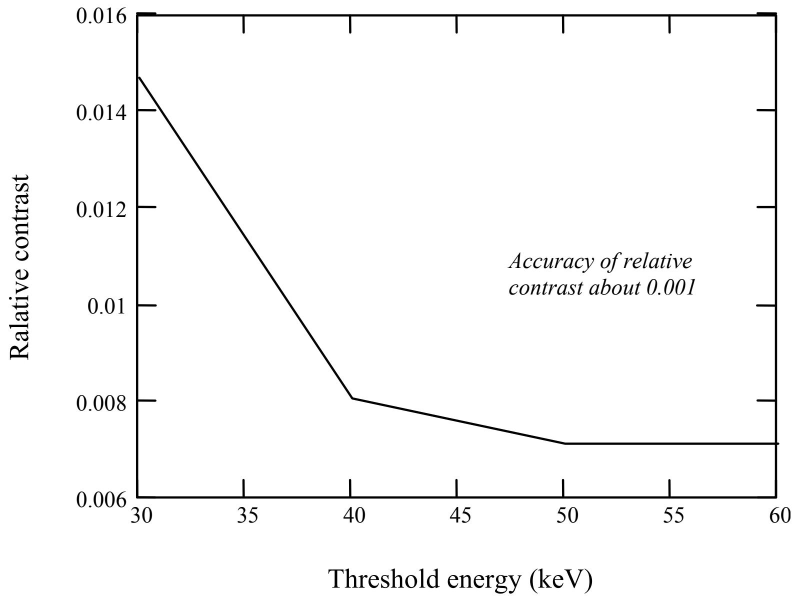

Figure 46: Contrast calculated from measurements; the areas are averaged on 100 pixels.

Another subject concerning the application of this method is the recognition of materials when the object contains mixed or overlapping materials. The proposed method can be extended to this case, but transmission measurements for a larger number of energies are required.

4.2 WINDOW THRESHOLDS

One improvement to the design of Medipix2 compared to Medipix1 is that an upper threshold has been introduced. Therefore all energies outside a small energy window can be excluded from the images. Without this window such data can only be achieved by differentiation of two images with small differences in the lower threshold settings. To prepare the data for paper III, differentiation of images taken using Medipix1 were primarily intended to be used. Differential images are expected to give a higher relative contrast between the two materials to be distinguished. But the noise of the differential images increased more than the contrast. Therefore differential data were not used in paper III.

For Medipix2 designed with a threshold energy window, a better signal-to-noise ratio was expected, since the statistical noise is not doubled in the differentiation of images. Some speculations on the subject of comparing signal to noise ratios for systems such as Medipix1 without and Medipix2 with threshold window can be made. The differential method requires two images and $(S/N)_{Medipix1} = (S_1 - S_2)/2N_{1,2}$, where $N_{1,2}$ is proportional to $\sqrt{S_{1,2}}$, so that

$(S/N)_{Medipix1}$ is proportional to $(S_1 - S_2)/2\sqrt{S_{1,2}}$. At the same time for window threshold $(S/N)_{Medipix2} = S/\sqrt{S}$, where $S = S_1 - S_2$. Then the ratio between window threshold and only low threshold systems will be $R_{2/1} = (S/N)_{Medipix2}/(S/N)_{Medipix1} = 2\sqrt{S_{Medipix1}/S_{Medipix2}}$. The advantage of the window threshold method is obvious. Unfortunately the achieved SNR for images using Medipix2 is much lower than for Medipix1 [46]. This is due to two mechanisms:

1. Medipix2 has a much smaller pixel size than Medipix1 and thus the statistics for each pixel must also be smaller. One pixel on Medipix1 covers approximately 9 pixels on Medipix2. If the sum of the signals for these 9 pixels on Medipix2 is taken then the noise will become $\sqrt{9 \cdot S}$ and the ratio between the detectors become $R_{2/1} = \frac{2}{3}\sqrt{S_{Medipix1}/S_{9 \cdot Medipix2}}$.
2. Charge sharing which destroys the energy information necessary to achieve a difference in contrast between the two compared materials.

Due to these mechanisms the result achieved with Medipix1 in chapter 4.1, that it is possible to distinguish between aluminium and silicon, is not likely to be achieved with Medipix2.

With the Medipix3 system, it is possible to work in "spectroscopic mode", with four readout pixels bump bonded to one detector pixel. The detector pixel pitch will then be 110 µm, almost as in the Medipix1 system. If the noises of the counters are negligible, the SNR will be improved as discussed above, and a better material resolution than that what is achieved in chapter 4.1 might be possible.

At present spectroscopic X-ray imaging is merely used in astronomy applications, where the images must contain many energy bins to provide useful information revealing for example the material composition of a star. Due to the low photon flux in astronomy it is more suitable to use crossed strip detectors connected to an external multichannel readout, than to use pixellated detectors.

If less accuracy in spectroscopic resolution is required, then the energy information can be visualised by colour coding or contrast enhancing techniques such as energy weighting discussed in chapter 4.4. This can enable the use of energy resolved X-ray imaging in new types of applications. If three energy bins are available, then for example RGB colour coding can be used to visualise the energy information of the image. The possibility of obtaining three energy channels with two thresholds and two counters as in Medipix3 is demonstrated in [24]. In the next two sections it is demonstrated that contrast enhancement is possible with photon counting systems.

4.3 ENERGY DEPENDENT IMAGING

The possibility of achieving better contrast in dental images by selecting specific X-ray energies has been investigated in paper IV. By applying both the low and high energy thresholds of the Medipix2 chip, only a narrow interval of the spectrum of a 70 keV standard dental source is selected. Images of a lower jaw are taken using a setup similar to a dental X-ray imaging system. A Medipix chip with a 300 μm thick silicon detector is mounted inside the jaw.

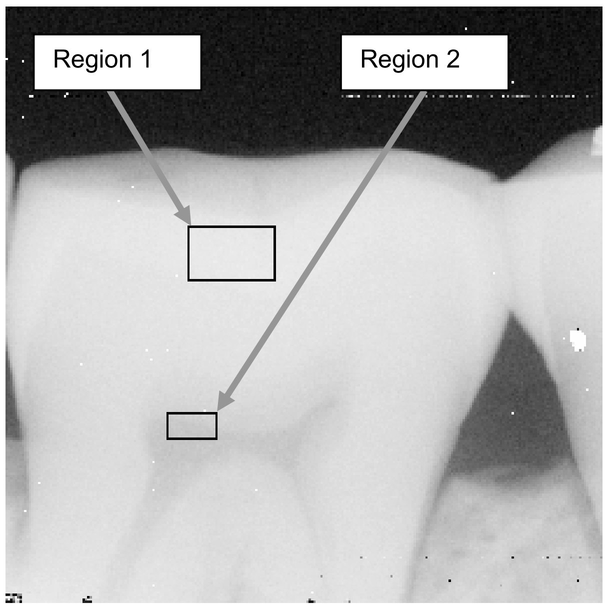

Figure 47: Image of a tooth achieved with Medipix2. Two regions with high respectively low X-ray absorption are defined to study the contrast variation.

To obtain a quantitative measurement of the image quality, one region with high photon absorption and one with low photon absorption were defined for the tooth, see Figure 47. The contrasts for these two regions of interest relative to the part of the image above the tooth were extracted. It is relevant to investigate the contrast as it is dose independent. If the contrast is improved, more noise can be tolerated in the image and thus the dose to the patient can be reduced.

A window of 4 keV was used. This window was used to sweep the available energy spectrum and achieve the energy dependence of the contrasts of the defined regions of the tooth, see Figure 48. It can be concluded that the relative contrast can be improved from 0.59 for the full spectrum to 0.70 when a narrow energy interval centred at 30 keV is applied. A maximum relative contrast near this energy could be expected, since at this energy, region 1 is still absorbing strongly while region 2 is beginning to become transparent [47].

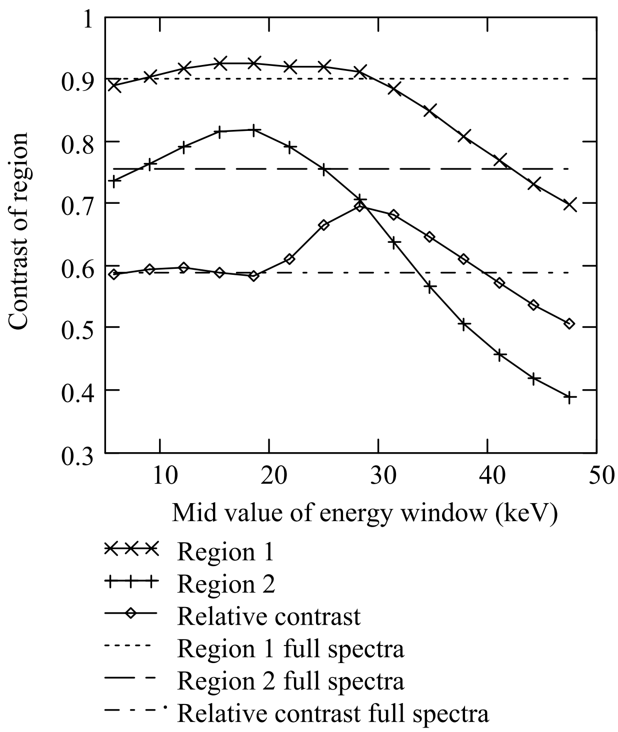

Figure 48: Achieved contrast for the two defined regions of the tooth and the relative contrast between these regions for a series of 4 keV wide energy windows. The measurements are compared to the value for a full spectrum.

The main conclusion was that it is possible to improve the contrast in dental images by selecting specific X-ray energies. The relative contrast between the parts of the tooth with the highest and lowest absorptions respectively increases by 18 % when the energy spread of the X-rays is narrowed from the full spectrum to a 4 keV window centred around 30 keV. The result implies that it is possible to reduce the dose delivered to dental imaging patients by improving the energy profile of dental sources, or by applying energy weighting algorithms to improve the image quality.

A simple way to generate a colour X-ray image of the tooth in Figure 47 is to use RGB coding for three energy windows within the source spectrum. The colour image of a tooth in Figure 49 is achieved from the images of Figure 4 in paper IV, where the red, green and blue colours are assigned respectively.

Figure 49: Colour X-ray image of a tooth achieved with Medipix2 with a 300 µm thick silicon detector.

4.4 ENERGY WEIGHTING TO IMPROVE THE IMAGE QUALITY

Energy weighting is a method available for implementing the possible improvements of "colour" imaging into clinical X-ray imaging. From the previous chapter on dental imaging it can be concluded that the small tail of high energy photons from the full source spectrum lowers the relative contrast significantly. In a multi-channel photon counting system, the quality of images can be improved by applying an optimal energy weighting algorithm. From theoretical considerations it is proposed in [48] that the optimal weighting factor for mammography applications is $w = 1/E^3$. It should be noted that a charge integrating system corresponds to choosing $w = E$ while a photon counting system without energy weighting corresponds to the choice of $w=1$. Therefore a charge integrating readout can be said to give unwanted energy weighting favouring high energy photons. This means that using a photon counting principle as in the Medipix system already introduces a significant improvement compared to the state-of-the-art imaging systems with charge integrating readout.

Introducing the energy weighting algorithm for mammography examinations can increase the SNR by up to a factor of 1.9 or reduce the dose by up to a factor of 2.5 compared to integrating systems [48]. A system with only 3 energy channels can still achieve 90 % of this improvement [49]. The Medipix3 system which contains several channels is therefore very promising for the future work on the reduction of doses to patients.

4.5 K-EDGE IDENTIFICATION

It is possible to identify the presence of specific atoms in a test sample, if the atoms have K-edge energy in the range of the X-ray source spectrum. The absorption cross section for this atom will be significantly larger for photons with energy just above the K-edge energy than for photons with slightly lower energy. In paper VIII the attenuation of the source spectrum for some different test samples were studied. In Figure 50 the presence of K-edge energies for Iodine (33 keV), Tin (29 keV) and Gadolinium (50 keV) can be distinguished. The measurement setup is described in Figure 51.

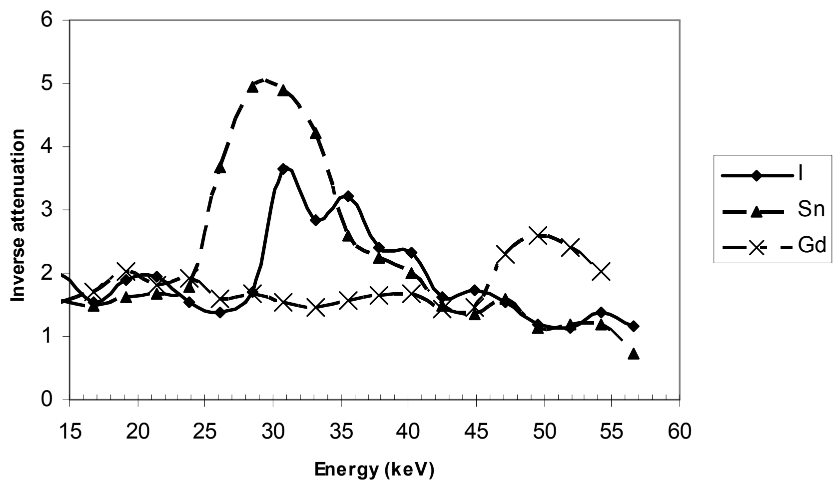

Figure 50: Inverse attenuation spectra for test samples of Iodine, Tin and Gadolinium. The inverse attenuation spectrum is the reference spectrum divided by the transmission spectrum for the test sample.

Photon counting systems such as Medipix can be used for K-edge identification of materials, if:

1. Charge sharing is corrected for.
2. At least two energy channels are available.

In the measurements in Figure 50, charge sharing was suppressed by using a narrow beam centred on one pixel. The beam was collimated with two crossed 10 µm slits, and each energy reading corresponds to one exposure.

The conclusion of paper VIII is that K-edge identification is possible with systems such as Medipix3 where charge sharing correcting schemes as described in paper IX are implemented. The material content can be visualised by colour coding schemes as briefly discussed in chapter 4.2.

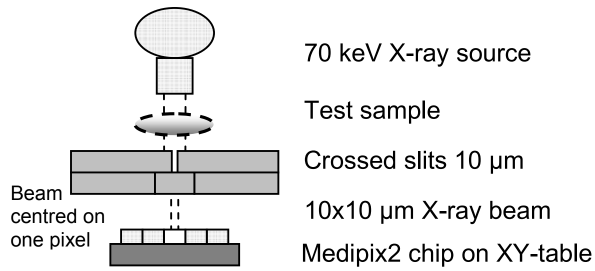

Figure 51: Schematic sketch of the measurement setup used in paper VIII.

One interesting application for K-edge identification is imaging with contrast agents. A contrast agent is a fluid with high X-ray absorption used to fill a void in an object. An example application is the X-ray evaluation of seed, in which bad seed will have a void inside which will be filled with fluid and become black on the image.

5 SUMMARY OF PUBLICATIONS

Papers III, IV and VIII in this thesis relate to chapter 4 and concern the practical applications of photon counting systems. This includes image correction, material recognition and improvements to the image quality in dental imaging. Papers II, VI and VII concern characterisation of the MEDIPIX system described in chapter 3. Paper V describes simulations for different detector materials, while paper I contain simulations of electrical properties in a silicon 3D-detector.

5.1 PAPER I

Simulations to demonstrate that charge sharing properties are better in 3D-detector structures than in planar pixellated detectors.

5.2 PAPER II

A simple method to create threshold calibration masks for specific energy intervals is described. A standard threshold equalisation towards the noise edge will not be valid for high energy threshold settings. For wide spectrum measurements, a set of calibration masks can be extracted to cover the whole energy interval.

5.3 PAPER III

A method to distinguish between different materials utilizing differences in absorption for different X-ray energies is proposed. It is demonstrated that Medipix1 can distinguish between aluminium and silicon, although these materials have smooth (no K-edges) and quite similar absorption spectra in the range 10-100 keV. The method is independent of the thickness of the samples.

5.4 PAPER IV

Colour X-ray imaging are exemplified by studies of dental images with Medipix2. It is concluded the image contrast can be improved by 18 % compared to a full spectrum image.

5.5 PAPER V

Simulation of the spectral response for pixellated detectors made of different materials. The spectral response of a pixel is degraded by effects such as X-ray fluorescence, Compton scattering, charge spreading during charge transport, misalignment of the beam and charge trapping. For high-Z materials and high photon energies X-ray fluorescence becomes an important degrading mechanism.

5.6 PAPER VI

A 1 mm thick CdTe detector with 55 µm pixels was characterised using a narrow mono-energetic 40 keV beam. X-ray fluorescence generates hits in neighbouring pixels with a range of several pixels. Charge sharing causes severe loss of energy information for imaging applications. To achieve full charge collection for the actual geometry, charge summing over several pixels must be implemented.

5.7 PAPER VII

Silicon detectors, 300 µm and 700 µm thick, with 55 µm pixels were characterised using a narrow mono-energetic 40 keV beam. Measurements of position-dependent spectra can be reproduced by Monte Carlo simulations of the charge transport. Assumptions for readout noise and backscattering of X-rays from the bump bonds can be verified.

5.8 PAPER VIII

Attenuation spectra of different test samples were achieved using a wide energy X-ray source. It was demonstrated that K-edge energies revealing the material content could be identified. In the study the charge sharing of one pixel was suppressed by crossed slits.

5.9 PAPER IX

A comparison is given of different charge summing schemes for use in the design of pixellated readout electronics. A scheme which does not significantly increase the electronic noise can be used to compensate for charge sharing in 50 µm size pixellated detector systems.

5.10 AUTHOR'S CONTRIBUTIONS

The author of this thesis has had the main responsibility for papers II, III, IV, VII and VIII. For paper I the contribution was in supplying model input for the simulations. For papers V and IX the contribution was in supplying measurements. For paper VI the contribution was in the preparation of the readout system in the measurement setup and measurement data analysis.

6 THESIS SUMMARY

The work contained in this thesis deals with photon counting detector systems. Possible improvements in the image quality due to the photon counting principle are discussed in Chapter 4. These improvements could reduce the dose given to patients in dental and mammography applications. Another area discussed is material recognition utilizing spectroscopic imaging, which finds applications in process industry, safety, and quality control. Image correction methods are also studied.

Chapter 3 presents a characterisation of the Medipix2 system aimed towards a better understanding of charge sharing. Charge sharing schemes to be implemented in the Medipix3 system are presented, which are expected to solve the problem associated with charge sharing.

6.1 DOSE REDUCTION IN MEDICAL IMAGING

It is proved in paper IV that it is possible to achieve significant improvements in the image quality of dental examinations by introducing "colour" X-ray imaging systems. Energy weighting is one method used to implement the possible improvements of "colour" imaging into clinical imaging. It is proposed in [48] that the optimal weighting factor for mammography applications is $w = 1/E^3$. Introducing the energy weighting algorithm for mammography examinations can reduce the required dose by up to a factor 2.5 compared to integrating systems. It can be noted that in a charge integrating system, which is state-of-the-art at present, the energy weighting factor is $w = E$. In a photon counting system the energy weighting factor is $w = 1$, which is closer to the ideal factor. As photon counting systems like Medipix3 containing several channels are being developed, then energy weighting algorithms can be implemented in these systems. At this point the system might be ready to be transferred from applied research into product development in the medical industry.

6.2 MATERIAL RECOGNITION

Photon counting systems open up new perspectives for X-ray imaging. The difference in absorption for different "colours" can be used to discern materials in the object. Today some diseases are diagnosed from analyses of the material content found by K-edge subtraction. For a photon counting system with two energy bins this examination is possible using only one X-ray exposure. In paper III a method for material recognition using a wide spectra source for situations where no K-edge energy is available is proposed. It is demonstrated that the Medipix1 system with only a low energy threshold can distinguish between silicon and aluminium, although the absorption for these materials is very similar over the range of a standard dental source. The method is thickness independent and can be extended to distinguish between regions with mixed or overlapping materials. It is also demonstrated that K-edge identification is possible with Medipix2, if charge sharing is suppressed. This can be used in applications for medical imaging utilizing contrast agents.

6.3 IMAGE CORRECTIONS METHODS

It is shown in section 3.6 that for energy dependent X-ray imaging the validity of the standard method of flat field correction for full spectrum imaging is limited. Interpolation methods for flat field corrections for specific energies must be implemented. The threshold calibration for individual pixels is also energy dependent. In paper II a method for generating threshold masks for different energies is proposed. In the study, the Medipix1 system and a 70 keV dental X-ray source with wide spectrum is used.

6.4 CHARACTERISATION MEASUREMENTS OF MEDIPIX2

Due to the size of the charge cloud, 55 µm is close to the physical limitation of pixel size for a planar 300 µm silicon detector. Photon counting systems can be used for full spectrum imaging without too much loss of spatial resolution due to charge sharing but at the cost of reduced quantum efficiency. But the spectral information that is important for energy weighting and material recognition is strongly distorted due to charge sharing as seen in section 3.3.4. But although the spectral information is partly lost for the pixel size 55 µm, energy dependent imaging can still improve the image quality as shown in paper IV.

For a 700 µm thick detector, the alignment of the detector relative to the source and the object becomes very important, since the angle between the centre and the border along the pixels is only 2.2°. The charge sharing is much stronger in 700 µm Si compared to 300 µm Si; which can be understood by geometrical considerations.

In relation to CdTe, it unfortunately appears that a statement in [25] is true. In this paper it is implied that a pixel size below 55 µm for photon counting systems is impossible for a 1 mm thick CdTe detector due to charge sharing. It is concluded in paper V that the size of the charge cloud is as large as the pixel size when it reaches the readout electrode. However there remains a significant possibility of improving the quantum efficiency if high-Z materials could function as good X-ray detectors. A requirement is that the quality of these materials has to be improved giving better uniformity and reduced charge trapping.

6.5 CONCLUSIONS FROM THE MEXIPIX2 PROJECT

The outcome of the Medipix2 project is an X-ray imaging sensor based on single photon processing which have been tested in a large number of applications. Since the device is noiseless it has a very high dynamic range, with the lower limit defined by the background radiation and the upper limit defined by the speed of the electronics. Spectroscopic imaging can be done either by sweeping one threshold and subtracting images or by sweeping both thresholds operating in window mode. However the spectroscopic information is deteriorated by the charge sharing. The project has resulted in an enormous increase in the knowledge of the physics of small pixels. This knowledge will be necessary since the development towards smaller and smaller pixel sizes will probably continue.

For X-ray colour imaging to become a reality, the limitations to the spectral resolution due to charge sharing must be solved. It is very promising that charge summing schemes are to be implemented in Medipix3. This will probably solve the problem associated with charge sharing induced by charge diffusion.

For practical applications it is sometimes profitable to choose a larger pixel size, since 55 x 55 μm^2 is not always required. The Medipix3 design will have the option to bump-bond detectors with 110 μm pixel pitch. If charge summing is applied to this larger pixel pitch, then CdTe detectors might work properly in spite of the large range of fluorescence photons.

If energy weighting algorithms were to be implemented, pixellated readout systems with at least three energy bins are required. Three bins will also make colour schemes as proposed in [24] possible. Three bins is also a possibility in the Medipix3 design.

But detector improvement must also be considered. An alternative approach to suppressing charge sharing is to use the 3D-detector structure instead of planar pixellated detectors. The transverse electric field in the 3D-structure forces the electron to drift to the correct pixel. For silicon it is possible to increase the quantum efficiency by constructing thick detectors, theoretically without increasing the charge sharing. For high absorbing materials, the advantage of 3D-design is in the gain involved in the charge transport path. Although the photons are absorbed close to the surface, the charges only have to travel half a pixel diagonally, and can then pass through the whole wafer through the doped contact.

The striving for smaller pixel sizes will continue, independent of the question as to whether it is the 3D-detector or the charge sharing corrections in the pixellated readout that will prove to be the most successful. The development in both these areas will in any case continue. In the longer perspective the 3D-detector might offer the possibility of avoiding the physical limitation that the diffusion of the charge cloud introduces into the planar detector, that is the ratio between the pixel size and the wafer thickness. In the future it might be possible to reach below 25 μm in resolution for a 1 mm thick 3D-detector.

7 REFERENCES

[1] H.-E. Nilsson, E. Dubaric, M. Hjelm, K. Bertilsson, “Simulation of photon and charge transport in X-ray imaging semiconductor sensors”, *Nuclear Instruments and Methods in Physics Research A* 487 (2002) 151.

[2] *Introduction to Radiobiology*, M. Tubiana, J. Dutreix, A. Wambersie, Taylor & Francis 1990, ISBN 0-85066-763-1.

[3] G. Rikner, *Silicon diodes as detectors in relative dosimetry of photon, electron and proton radiation fields*, PhD thesis, Uppsala University, Sweden 1983, ISBN 91-554-1448-6.

[4] B. Mikulec, *Single Photon Detection with Semiconductor Pixel Arrays for Medical Imaging Applications*, PhD thesis, University of Vienna, Austria, June 2000, CERN-THESIS-2000-021.

[5] *Radiation Detection and Measurement*, 3:rd ed., Glenn F. Knoll, John Wiley and Sons Inc., 2000, ISBN 0-471-07338-5.

[6] S.M. Gruner, M.W. Tate, E.F. Eikenberry, “Charge-coupled device area x-ray detectors”, *Review of Scientific Instruments* 73, no. 8, pp. 2815-2842, August 2002.

[7] *Physics of Semiconductor Devices*, 2:nd ed., S. M. Sze, John Wiley and Sons Inc., 1981, ISBN 0-471-05661-8.

[8] E. Dubaric, C. Fröjdh, M. Hjelm, H.-E. Nilsson, M. Abdallah, C. S. Petersson, “Monte Carlo simulations of the imaging properties of scintillator coated X-ray pixel detectors”, *Nuclear Science Symposium Conference Record, 2000 IEEE* ,Volume: 1 , 15-20 Oct. 2000, Pages:6/282 - 6/285.

[9] T. Jing, C.A. Goodman, J. Drewery, G. Cho, W.S. Hong, H. Lee, S.N. Kaplan, A. Mireshghi, V. Perez-Mendez, D. Wildermuth, “Amorphous silicon pixel layers with cesium iodide converters for medical radiography”, *IEEE Transactions on Nuclear Science,*Vol. 41 no. 4, Aug. 1994, pp. 903-909.

[10] M. Hjelm, B. Norlin, H.-E. Nilsson, C. Fröjdh and X. Badel, “Monte Carlo simulation of the imaging properties of scintillator-coated X-ray pixel detectors”, *Nuclear Instruments and Methods in Physics Research A* 509 (2003) 76.

[11] P. Kleimann, J. Linnros, C. Fröjdh and C.S. Petersson, “An X-ray imaging pixel detector based on scintillator filled pores in a silicon matrix”, *Nuclear Instruments and Methods in Physics Research A* 460 (2003) 15-19.

[12] X. Badel, J. Linnros, P. Kleimann, B. Norlin, E. Koskiahde, K. Balpas, S. Nenonen, C. S. Petersson and C. Fröjdh, “Metallized and Oxidized Silicon Macropore Arrays Filled With a Scintillator for CCD-Based X-ray Imaging Detectors”, *IEEE Transactions on Nuclear Science*, Vol. 51, no. 3, June 2004, pp. 1006-1010.

[13] X. Badel, B. Norlin, P. Kleimann, L. Williams, S. Moody, G. Tyrrell, C. Fröjdh, J. Linnros, Performance of Scintillating Waveguides for CCD-based X-ray Detectors, Submitted to IEEE Transactions on Nuclear Science.

[14] B. Mikulek, “Development of segmented semiconductor arrays for quantum imaging”, *Nuclear Instruments and Methods in Physics Research A* 510 (2003) 1.

[15] E. H. M. Heijne, P. Jarron, "Development of silicon pixel detectors: An introduction", *Nuclear Instruments and Methods in Physics Research A* 275 (1989) 467.
[16] Medipix webpage (http://medipix.web.cern.ch/MEDIPIX/)
[17] M. Campbell, E. H. M. Heijne, G. Meddeler, E. Pernigotti, W. Snoeys, "Readout for a 64 x 64 Pixel Matrix with 15-bit Single Photon Counting", *IEEE Transactions on Nuclear Science*, vol 45 (3), 751-753, June 1998
[18] G. Bardelloni, E. Bertolucci, A. L. J. Boerkamp, D. Calvet, M. Conti, M. Maiorino, P. Russo, J. L. Visschers, "A New Read-out System for an Imaging Pixel Detector", Nuclear Science Symposium Conference Record, 2000 IEEE ,Volume: 2 , 15-20 Oct. 2000 Pages:12/57 - 12/60 vol. 2.
[19] X Llopart, *Design and characterization of 64K pixels chips working in single photon processing mode*, Mid Sweden University Doctoral Thesis 27, Sweden May 2007, ISBN 978-91-85317-56-1.
[20] X. Llopart, M. Campbell, R. Dinapoli, D. San Segundo and E. Pernigotti, "Medipix2, a 64k pixel readout chip with 55 μm square elements working in single photon counting mode", *IEEE Transactions on Nuclear Science*, vol. 49, 2279-2283, October 2002
[21] M. Conti, M. Maiorino, G. Mettivier, M. C. Montesi, P. Russo, "Preliminary Test of Medisoft 4: Control Software for the Medipix2 Readout Chip", *IEEE Transactions on Nuclear Science*, vol. 50 (4), 869-877 August 2003.
[22] Pixelman webpage (http://www.utef.cvut.cz/medipix/)
[23] R. Ballabriga, M. Campbell, E. H. M. Heijne, X. Llopart, L. Tlustos, "The Medipix3 Prototype, a Pixel Readout Chip Working in Single Photon Counting Mode with Improved Spectrometric Performance", *proceedings of Nuclear Science Symposium IEEE 2006*, October 2006, San Diego, USA.
[24] Jan Lundgren, Mattias O'Nils, Bengt Oelmann, Börje Norlin, Suliman Abdalla, "An Area Efficient Readout Architecture for Photon Counting Color Imaging" *Nuclear Instruments and Methods in Physics Research A* (2007), 6 February 2007.
[25] G. Pellegrini, M. Chmeissani, M. Maiorino, G. Blanchot, J. Garcia, M. Lozano, R. Martinez, C. Puigdengoles, M. Ullan, P.Casado, "Performance Limits of a 55-μm Pixel CdTe Detector", *IEEE Transactions on Nuclear Science*, vol. 53 (1), 361-366, February 2006.
[26] M.S. Passmore, R. Bates, K. Mathieson, V. O'Shea, M. Rahman, P. Seller, K. M. Smith, "Characterisation of a single photon counting pixel detector", *Nuclear Instruments and Methods in Physics Research A* 466 (2001) 202.
[27] J.F. Briesmeister (Ed.), *MCNP—A General Monte Carlo N—Particle Transport Code*, Version 4C, Manual, 2000.
[28] M. Hoheisel, A. Korn, J. Giersch, "Influence of backscattering on the spatial resolution of semiconductor X-ray detectors", *Nuclear Instruments and Methods in Physics Research A* 546 (2005) 252.
[29] Avant! Corporation, *Medici, Two-Dimensional Device Simulation Program*, Version 2001.2, User's Manual, TCAD Buissness Unit, Fremont, CA, USA, 2001.
[30] Mats Hjelm, *Monte Carlo Simulations of Homogeneous and Inhomogeneous Transport in Silicon Carbide*, PhD Thesis, KTH, Royal Institute of Technology, Sweden 2004.

[31] Alexander Korn, Markus Firsching, Gisela Anton, Martin Hoheisel, Thilo Michel, ”Investigation of charge carrier transport and charge sharing in X-ray semiconductor pixel detectors such as Medipix2”, *Nuclear Instruments and Methods in Physics Research A* (2007), 6 February 2007

[32] Jürgen Durst, Gisela Anton, Thilo Michel, ”Discriminator threshold dependency of the zero-frequency DQE of photon-counting pixel detectors”, *Nuclear Instruments and Methods in Physics Research A* (2007), 6 February 2007

[33] ESRF webpage (http://www.esrf.fr/)

[34] V.A. Wright, W.D. Davidson, J.J. Melone, V. O’Shea, K.M. Smith, L. Donnohue, L. Lea, K. Robb, S. Nenonen and H. Silpila, “3-D Medipix: A new generation of X-ray detectors”, *Nuclear Instruments and Methods in Physics Research A* 546 (2005) 319.

[35] Patrick Roy, G. Pellegrini, A. Al-Ajili, R. Bates, L. Haddad, J. Melone, V. O’Shea, K. M. Smith, V. Wright and M. Rahman, “Study of irradiated 3D detectors”, *Nuclear Instruments and Methods in Physics Research A* 509 (2003) 132.

[36] Suliman Abdalla, Hans-Erik Nilsson, Bengt Oelmann, “Circuit Implementation of Mechanism for Charge-Sharing Suppression for Photon-Counting Pixel Arrays”, *proceedings of the IEEE Norchip Conference*, Oulo, Finland 2005.

[37] L. Tlustos, D. Davidson, M. Campbell, E. Heijne and B. Mikulec, “Fixed pattern deviations in Si pixel detectors measured using the Medipix1 readout chip”, *Nuclear Instruments and Methods in Physics Research A* 509 (2003) 102.

[38] D.W. Davidson, C. Fröjdh, V. O’Shea, H.-E Nilsson, M. Rahman, “Limitations to flat-field correction methods when using an X-ray spectrum”, *Nuclear Instruments and Methods in Physics Research A* 509 (2003) 146.

[39] J. Jakubek, T. Holý, S. Popísil, D. Vavrík, “Tomography for XRDD”, *Nuclear Instruments and Methods in Physics Research A* 531 (2004) 307.

[40] D. Niederlöhner, Ch. Bert, J. Giersch, K. -F. Pfeiffer, G. Anton, ” Threshold characterisation of the Medipix1 chip”, *Nuclear Instruments and Methods in Physics Research A* 531 (2004), 68.

[41] J. Karg, D. Niederlöhner, J. Giersch, G. Anton, ” Using the Medipix2 detector for energy weighting”, *Nuclear Instruments and Methods in Physics Research A* 546 (2005) 306.

[42] T. Eriksson, P. Nilsson, Ö. Sundvall, Chapter 8 pp.125-133, ”On-Line Pulp Quality Monitoring”, in: *Paper Recycling Challenge: Volume IV – Process Control & Mensuration*, M. R. Doshi & J. M. Dyer (Eds.), ISBN 0-9657447-4-4, Doshi and Associates, Inc., Appleton, WI, 1999, pp. 125-133 (Chapter 8).

[43] R. Amendolia, E. Bertolucci, M. G. Bisogni, U. Bottigli, A. Ceccopieri, M. A. Ciocci, M. Conti, P. Delogu, M. E. Fantacci, P. Maestro, V. Marzulli, E. Pernigotti, N. Romeo, V. Rosso, P. Rosso, A. Stefanini, S. Stumbo, ”MEDIPIX: a VLSI chip for a GaAs pixel detector for digital radiology”, *Nuclear Instruments and Methods in Physics Research A* 422 (1999) 201 and erratum *Nuclear Instruments and Methods in Physics Research A* 440 (2000) 258.

[44] J. Watt, D. W. Davidson, C. Johnston, C. Smith, L. Tlustos, B. Mikulec, K.M. Smith, M. Rahman, “Dose reduction in dental X-ray imaging using Medipix”, *Nuclear Instruments and Methods in Physics Research A* 513 (2003) 65.

[45] G. Mettivier, M. C. Montesi, P. Russo, Phys. “First images of a digital autoradiography system based on a Medipix2 hybrid silicon pixel detector”, *Phys. Med. Biol. 48 (2003) N173*

[46] K.-F.G. Pfeiffer, J. Giersch, G. Anton, “How good is better? A comparison between the Medipix1 and the Medipix2 chip using mammographic phantoms”, *Nuclear Instruments and Methods in Physics Research A* 531 (2004) 246.

[47] J. Ludwig, A. Zwerger, K.W. Benz, M. Fiederle, H. Braml, A. Fauler, J.P. Konrath, “X-ray energy selected imaging with Medipix II”, *Nuclear Instruments and Methods in Physics Research A* 531 (2004) 209.

[48] D. Niederlöhner, J. Karg, J. Giersch, G. Anton, ”The energy weighting technique: Measurements and simulations”, preprint submitted to *Nuclear Instruments and Methods in Physics Research A.*

[49] J. Giersc, D. Niederlöhner, G. Anton, ”The influence of energy weighting on X-ray imaging quality”, *Nuclear Instruments and Methods in Physics Research A* 531 (2004) 68.

PAPER I

Monte Carlo simulation of the response of a pixellated 3D photo-detector in silicon

P a p e r I

ELSEVIER

Nuclear Instruments and Methods in Physics Research A 487 (2002) 136–141

NUCLEAR INSTRUMENTS & METHODS IN PHYSICS RESEARCH Section A

www.elsevier.com/locate/nima

Monte Carlo simulation of the response of a pixellated 3D photo-detector in silicon

E. Dubarić[a,b,*], H.-E. Nilsson[a], C. Fröjdh[a], B. Norlin[a]

[a] *Department of Information Technology and Media, Mid-Sweden University, Holmgatan 10, SE-851 70 Sundsvall, Sweden*
[b] *Solid State Electronics, Department of Microelectronics and Information Technology, Royal Institute of Technology (KTH), Electrum 229, SE-164 40 Kista, Sweden*

Abstract

The charge transport and X-ray photon absorption in three-dimensional (3D) X-ray pixel detectors have been studied using numerical simulations. The charge transport has been modelled using the drift-diffusion simulator MEDICI, while photon absorption has been studied using MCNP. The response of the entire pixel detector system in terms of charge sharing, line spread function and modulation transfer function, has been simulated using a system level Monte Carlo simulation approach. A major part of the study is devoted to the effect of charge sharing on the energy resolution in 3D-pixel detectors. The 3D configuration was found to suppress charge sharing much better than conventional planar detectors.

PACS: 07.05.Tp; 07.07.Df; 07.85.Fv; 85.60.Gz; 87.59.−e

Keywords: Monte Carlo simulation; Three-dimensional; X-ray; Detector; Silicon; Charge sharing

1. Introduction

Improved process techniques, like laser drilling and dry etching that make it possible to drill deep holes and to dope and fill them, have made a new silicon detector approach very interesting. The suggested detector structure, as shown in Fig. 1(a), which was first suggested by Parker et al. in Ref. [1], has the potential to solve the shortcomings of the current silicon X-ray detectors. Another structure that has been suggested is to fill the holes with a scintillating material in order to improve the light detection efficiency and the spatial resolution [2]. The short distance between the charge collecting electrodes leads to shorter drift times, higher electric fields, and smaller operating voltages. Initial simulations of the detector structure in Fig. 1(b) suggest that an applied bias of ~1 V is needed to fully deplete the device. There are other possible detectors layout, like the hexagonal structure, but the one in Fig. 1(b) has a simple matrix format very well suited for direct conversion to standard digital image formats.

In this work, we have used a Monte Carlo approach on the system level to investigate the response for a 3D X-ray pixel detector in silicon in terms of charge sharing, line spread function (LSF) and modulation transfer function (MTF).

*Corresponding author. Tel.: +46-6014-8879; fax: +46-6014-8830.
E-mail address: ervin.dubaric@ite.mh.se (E. Dubarić).

0168-9002/02/$ - see front matter
PII: S0168-9002(02)00957-9

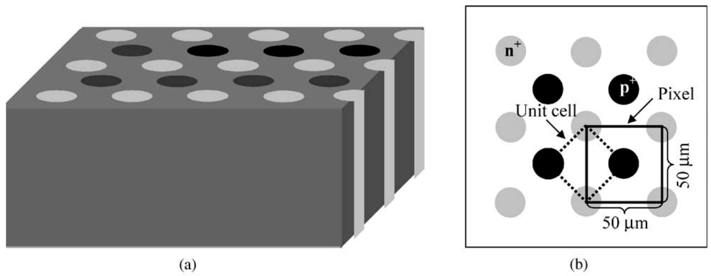

Fig. 1. (a) Three-dimensional X-ray pixel detector structure, (b) unit cell and simulated structure.

2. Charge sharing

Constraints within medical and dental X-ray imaging, such as patient dose reduction and higher resolution, demand detector structures with better spatial resolution. One possible solution to meet these constraints is smaller pixel dimensions. A major drawback with shrinking pixel sizes is that the charge sharing between two adjacent pixels becomes more pronounced. The charge sharing has a large impact on the energy resolution in a photon counting system, since the pulse height will not correspond to the energy of the photon. In the energy spectrum this effect results in a redistribution of the signal towards lower energies. Other drawbacks with smaller pixel size are lower signal-to-noise ratio and smaller dynamic range. A methodology to determine an optimal pixel size is presented in Ref. [3].

There is a conceptual difference between charge sharing in 2D and 3D X-ray detectors. In a 2D detector, the X-ray photon induced charge cloud will diffuse during its drift towards the charge collecting electrode, i.e., the drift does not suppress the charge sharing, whereas in a 3D detector the charge sharing is suppressed by the drift, see Fig. 2. This means that the charge sharing should be less severe in the latter detector type, which consequently should have better performance.

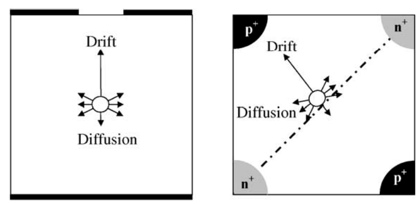

Fig. 2. Principal difference between charge sharing in: (left) a 2D pixel detector, and (right) a 3D pixel detector.

2.1. Charge sharing study using MEDICI

In order to make an initial study of the charge sharing in the suggested 3D structure, simulations of the transient of single photon absorption were performed using the commercial 2D-semiconductor device simulator MEDICI from Avant! Corp. [4]. The simulator solves numerically and self-consistently Poisson's equation in two dimensions, electron and hole continuity equations, and electron and hole current equations. Recombination mechanisms implemented in the simulator include Shockley Read Hall (SRH), Auger and band-to-band statistics.

In Fig. 3, the simulated unit cell (see Fig. 1) is presented. The stars indicate the simulated points of photon absorption in the detector. Due to the symmetry of the device, only half of it was

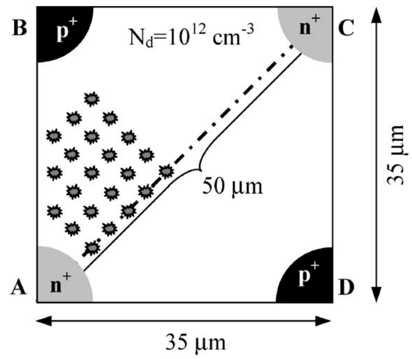

Fig. 3. Simulated unit cell. The stars indicate the location of a single photon absorption.

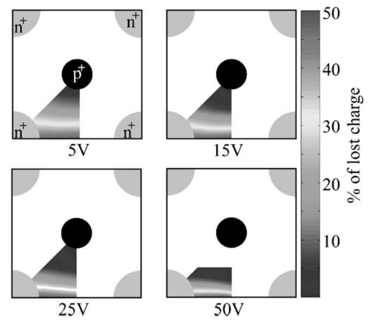

Fig. 4. Simulated percentage of charge sharing at different bias levels.

simulated. In the simulations we have assumed a point-like mono-energetic X-ray source of 30 keV. The number of electron hole pairs created at this energy level is approximately 8310, corresponding to a peak carrier concentration of $5 \times 10^{16}\,\mathrm{cm}^{-3}$. Default silicon material parameters and standard drift-diffusion transport parameter values in MEDICI were used. It should be noted that 3D plasma effects in the charge cloud have been neglected. A full 3D drift-diffusion simulation is needed in order to take these effects into account. However, for the drift distances and the electric field strength considered in this work, this approximation is of minor importance.

In Fig. 4, the percentage of collected charge for different biases at contact **B** is presented. As can be seen, the region sensitive to charge sharing is decreased by a factor of two when the applied voltage is increased by a factor of 10. The main reason for this can be understood by considering the relation between drift time and diffusion. The diffusion equation and its solution can be written as [5]

$$\frac{\partial \Delta n}{\partial t} = D_n \frac{\partial^2 \Delta n}{\partial x^2} \tag{1}$$

$$\Delta n = \left[\frac{\Delta n_0}{2\sqrt{\pi D_n t}}\right] \mathrm{e}^{-(x^2/4D_n t)} \tag{2}$$

where Δn is the excess carrier concentration, D_n is the diffusion constant and Δn_0 is the peak excess concentration at $t = 0$. Using this approximation it is possible to write the charge spread as

$$\Delta x = 4\sqrt{D_n t} \tag{3}$$

where Δx is the full width at 37% of the top value. This simple expression shows that there is a square root relation between charge spread and drift time. The symmetry of the 3D detector is such that the drift path a charge cloud experiences will be independent of the bias voltage. The electric field along the drift path will change and thus the drift time. An increase in the voltage bias with a factor of 10 will decrease the drift time with approximately the same factor. The corresponding decrease in charge spread will thus be $1/\sqrt{10} = 0.3$. Charge spread is directly related to the size of the charge sharing regions in the detector, which explains the simulation results.

2.2. *System level Monte Carlo simulation of the imaging performance*

The charge collection in a 3D detector is different from charge collection in 2D detectors. In the 2D detector, the charge cloud is spherical and the charge collection at the detector surface can be described using a radial distribution. However, in a 3D detector the charge-collecting electrode is a cylinder, and as the charge cloud moves closer to the collecting electrode, the cloud will be reduced in size and transformed into a non-spherical shape. At the system level the details regarding the shape and size of the charge cloud is not important, as long as the overall charge sharing effects close to the pixel boundaries are accurately modelled. An advantage with the 3D detector is that the charge sharing is not dependent on the depth of the absorption event as in the 2D detector. This indicates that it is possible to use a system level Monte Carlo model developed for 2D detectors to estimate the effect of charge sharing on the system performance, if a proper radial charge distribution is used. The choice of radial charge distribution should be such that it reproduces the charge sharing characteristics of the 3D-pixel detector.

The system level Monte Carlo simulation is performed using the following algorithm:

For each simulated photon:

1. Select photon energy according to the distribution function of the X-ray source.
2. Select the position of the X-ray absorption randomly according to the 3D-energy deposition distribution function obtained using MCNP [6].
3. Assigned charges to the pixel electrodes using the fixed radial charge distribution.

A more detailed description of the system level Monte Carlo model is presented in Ref. [7].

In order to verify that our model provides reasonable results, we have applied our model to the same 3D-detector structure as used in the experiments presented by Kenney et al. [8]. They used a ^{55}Fe X-ray source to study the energy resolution of a 3D-strip detector with a strip spacing of 200 μm. The measured full-width-at-half-maximum (FWHM) was 618 eV. In Fig. 5, the energy spectrum obtained by simulation of the same detector structure using a narrow peak X-ray source (FWHM value of 590 eV) is presented. The energy spectrum obtained is similar to what has been observed experimentally, which shows that the simulation model provides reasonable accuracy.

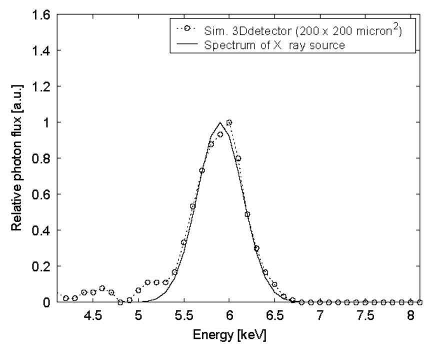

Fig. 5. Simulated energy spectrum for a 200 μm strip detector illuminated with a narrow-peak X-ray source similar to the ^{55}Fe source used in Ref. [8].

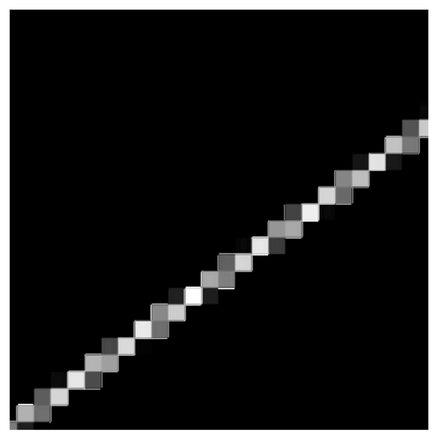

Fig. 6. The simulated image of a 10 μm wide slit on top of a 3D detector with a pixel size of $50 \times 50\ \mu m^2$.

As a measure of the image resolution of an X-ray pixel detector, the LSF and the MTF are commonly used [9]. An experimental way to get the MTF is based on the X-ray illumination of a slit, which is tilted with respect to the detector array and placed on top of it. The LSF is then obtained by plotting the intensity in each pixel as a function of the distance l between the centre of the

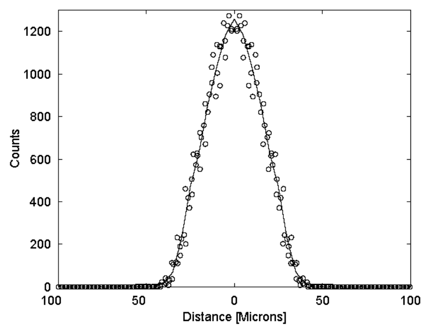

Fig. 7. Extracted line spread function (LSF) from the image in Fig. 6.

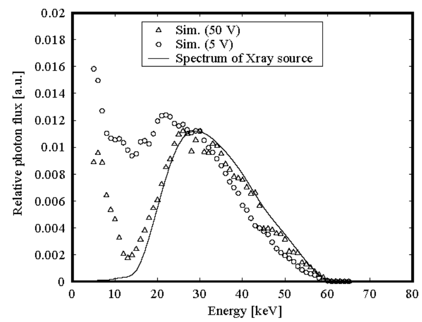

Fig. 9. Simulated energy spectrum for a 3D detector with a pixel size of $50 \times 50\,\mu m^2$ at 5 and 50 V bias.

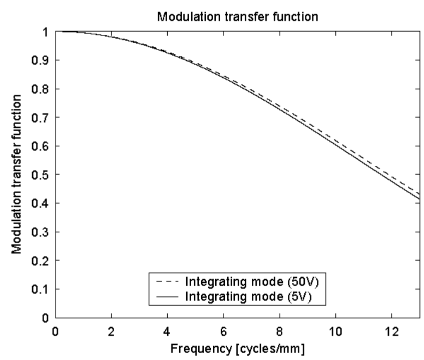

Fig. 8. Modulation transfer function (MTF) for a 3D detector with a pixel size of $50 \times 50\,\mu m^2$ at 5 and 50 V bias.

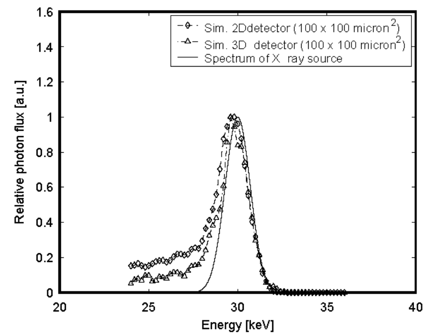

Fig. 10. Comparison of simulated energy spectrum for 2D and 3D detectors with a pixel size of $100 \times 100\,\mu m^2$.

pixel and the position of the slit; the MTF is the Fourier transform of the LSF. Fig. 6 presents the simulated image of a $10\,\mu m$ slit on top of a 25×25 pixel detector array while the corresponding LSF is presented in Fig. 7.

In Fig. 8, the MTF for the bias conditions of 5 and 50 V is presented. According to the MEDICI simulations the charge sharing at 50 V should be lower than 5 V. The effect of this difference can be seen in Fig. 9, where the simulated energy spectrum from a flood exposure of a dental X-ray source is presented. There is a large difference between the 5 and 50 V bias. The large difference in the energy spectrum is not visible in the spatial resolution (see Fig. 8). The main reason for this can be found in the way the spatial resolution is extracted. The spatial resolution is first of all limited by the pixel size. As long as the pixel size is much larger than the charge spread, the spatial resolution will be limited by the pixel size. A more detailed discussion regarding the effect of charge sharing on the spatial resolution can be found in Ref. [7].

In Fig. 10, the simulated energy spectrum for both 2D and 3D configurations are compared. The X-ray source used has a narrow peak at 30 keV with a FWHM of 1.66 keV. The simulated 3D detector had a bias of 10 V, which is needed in order to fully deplete the $100 \times 100\,\mu m^2$ pixel detector. The energy resolution of the 3D detecor at this bias is significantly better than the resolution of the 2D detector. The difference will be even larger at a bias voltage of 50 V.

3. Conclusions

In this paper, we have studied the charge sharing effects in a 3D X-ray pixel detector for dental applications by simulations using a drift-diffusion transport model. The charge sharing at the pixel boundary has been studied as a function of different bias voltages. This study has been used to set up a system level Monte Carlo simulation model in order to model the imaging properties of 3D-detector systems. Both spatial and energy resolution have been studied. A comparison with the experimental energy resolution obtained for 200 μm slit detector in Ref. [8] shows that the model can reproduce the experimental result, which indicates that the model has a reasonable accuracy. The simulated energy spectrum for a 3D detector with a pixel size of $50 \times 50\,\mu m^2$ and illuminated by a standard dental X-ray source, show that under these conditions a high bias voltage is needed in order to suppress the distortion due to charge sharing. A detailed comparison of the charge sharing in lateral detectors and 3D detectors show that the charge sharing is significantly lower in the 3D detector. The charge sharing in 3D detectors is mainly reduced due to a higher electric field, a shorter drift path and localisation of the charge to one pixel due to the potential well structure in 3D detectors.

Acknowledgements

The Mid-Sweden University in Sundsvall, Sweden, and the KK-Foundation, Sweden, are gratefully acknowledged for their financial support.

References

[1] S.I. Parker, C.J. Kenney, J. Segal, Nucl. Instr. and Meth. A 395 (1997) 328.
[2] P. Kleimann, J. Linnros, C. Fröjdh, C.S. Petersson, Nucl. Instr. and Meth. A 460 (2001) 15.
[3] Ting Chen, et al., Proc. SPIE 3965 (2000) 1.
[4] Avant! Corporation, MEDICI, Two-dimensional Device Simulation Program, Version 4.1, User Manual, TCAD Business Unit, Freemont, CA, USA, 1998.
[5] B.G. Streetman, Solid State Electronic Devices, 4th Edition, 1995, p. 123.
[6] Los Alamos Monte Carlo Group, MCNP-4B General Monte Carlo N-Particle Transport Code, Los Alamos National Laboratories Report LA-12625-M, 1997.
[7] H-E. Nilsson, E. Dubaric, M. Hjelm, K. Bertilsson, Nucl. Instr. and Meth. A 487 (2002), 151, these proceedings.
[8] C.J. Kenney, et al., IEEE Trans. Nucl. Sci. NS-48 (2001) 189.
[9] A. Workman, D.S. Brettle, Dentomaxillofacial Radiol. 26 (1997) 139.

PAPER II

Spectroscopy applications for the Medipix photon counting X-ray system

Paper II

Available online at www.sciencedirect.com
SCIENCE DIRECT®
ELSEVIER
Nuclear Instruments and Methods in Physics Research A 531 (2004) 251–257
NUCLEAR INSTRUMENTS & METHODS IN PHYSICS RESEARCH Section A
www.elsevier.com/locate/nima

Spectroscopy applications for the Medipix photon counting X-ray system

A. Manuilskiy, B. Norlin*, H-E. Nilsson, C. Fröjdh

Department of Information Technology and Media, Mid-Sweden University, SE-85170 Sundsvall, Sweden

Available online 23 June 2004

Abstract

Since the Medipix system is a photon counting system with selectable threshold, it is possible to use it as a spectroscopic device, which is sensitive to the energy of the incoming photons. One feature of the Medipix system is the possibility to adjust the threshold for each pixel by a three-bit mask. A simple method for creating threshold equalisation masks for different threshold settings including both detector and channel stability influences is proposed. The method is suitable for systems using X-ray sources with a wide energy range, since the threshold adjustment is energy dependent. This is an alternative to the well-known method for correction of non-uniformity, which uses mono energetic sources.

The proposed method is based on the analysis of histograms of series of images. The model for the histograms was created assuming a standard dental X-ray source, which allows mask-creating parameters such as threshold range to be found. This procedure can be performed for each of the energies of interest. Based on these arrays, mask files that narrowed the threshold distribution close to the theoretical limit, were prepared. The limit of the spectroscopic resolution for the system was measured by analysing histograms for a series of flat images under identical conditions.

PACS: 07.07.Df; 07.85.−m; 07.85.Nc; 87.57−s; 87.59.−e

Keywords: X-ray; Imaging; Pixel detector; Medipix; Spectroscopy

1. Introduction

Imaging using X-rays is very important for many applications. In the framework of the Medipix collaboration, colour imaging with X-rays is promising for new imaging applications. Since the Medipix system is a photon counting system with a selectable threshold [1] or threshold window [2], it is possible to use it as a spectroscopic device, which is sensitive to the energy of the incoming photons. The system can for example be used to achieve the spectrum of an unknown source, for material recognition and other applications. Since it is an imaging system it can be used for energy dependent scattering experiments instead of position sensitive detectors.

One of the main parameters of a spectroscopic device is spectral resolution. The factors limiting

*Corresponding author. Tel.: +46-60-1485-94; fax: +46-60-1484-56.

E-mail address: borje.norlin@mh.se (B. Norlin).

0168-9002/$ - see front matter
doi:10.1016/j.nima.2004.06.013

the resolution are source and channel noise and system non-uniformity. The noise limits the minimal contrast that can be obtained with the spectroscopic device. In the alternative where the contribution of the threshold non-uniformity dominates, the spectral and contrast resolution will increase with decreasing threshold non-uniformity. This can be understood by describing the cumulative $\mathrm{Cum}(\mathrm{th}_0)$ function for the Medipix1 detector as

$$\mathrm{Cum}(\mathrm{th}_0) = \int_{E_{\min}}^{E_{\max}} R(\mathrm{th}-\mathrm{th}_0) \int_{th}^{E_{\max}} S(E)\tau(E)\,\mathrm{dE}\,\mathrm{d(th)} \quad (1)$$

where $R(\mathrm{th}-\mathrm{th}_0)$ is the threshold energy distribution function with half-width Δ_R, when the threshold energy (th_0) is applied, $S(E)$ the X-ray source spectrum function with half-width Δ_s, $\tau(E)$ photons to charge energy dependent conversion for the detector, $S(E)\tau(E)$ can be said to be "the effective spectrum" and $E_{\min}$ and $E_{\max}$ the minimum and maximum photon energy for the source spectrum. High resolution can be achieved when the cumulative function approaches a step function. The spectral resolution corresponds to the case when the width of $S(E)\tau(E)$ is small compared to Δ_R and as follows from Eq. (1) is determined by the half width of the threshold distribution. It is important to determine the contribution of the factors mentioned above to the spectral resolution. When a high spectral resolution is important, a spectral correction mask for the Medipix 1 system must be applied to compensate for threshold non-uniformity. Usually this correction mask is achieved by using a calibration source with narrow spectra [3,4] or a special test signal [5,6]. However, in practice, when measurements for a wider spectral interval are required, it is difficult to use this method.

2. Histogram properties and mask preparation

One of the effective ways to obtain important correction masks parameters is to analyse histograms of images from Medipix1 exposed to an X-ray source with a wide spectrum and a flat spatial intensity distribution. Assuming that different pixels receive the same number of photons and the spectral content is also identical, we can then apply a spectral "flat" correction principle, since the threshold distribution dominates the image noise. The histogram gives the distribution of pixels with a certain count rate for the detector. For a typical silicon detector and photon energies from 30 to 70 keV, we can assume that $\tau(E)$ is a smooth function with small changes. The shape of the effective spectrum is then close to the shape of source spectrum $S(E)$ and the density of number of pixels per unit interval of threshold values is proportional to

$$h(\mathrm{th}) = \frac{R(\mathrm{th}-\mathrm{th}_0)}{S(\mathrm{th})/\Delta_s} \quad (2)$$

where the number of detected photons is proportional to

$$g(\mathrm{th}) = \int_{\mathrm{th}}^{E_{\max}} S(E)\,\mathrm{d}E. \quad (3)$$

Both h and g are functions of the threshold of pixels (th) and they can be expressed as $h(\mathrm{th}) = f(g(\mathrm{th}))$ or

$$\frac{R(\mathrm{th}-\mathrm{th}_0)}{S(\mathrm{th})/\Delta_s} = f\left(\int_{\mathrm{th}}^{E_{\max}} S(E)\,dE\right). \quad (4)$$

This function is presented graphically in Fig. 1. The function R can be expressed approximately by a Gaussian distribution with half width Δ_R. When $\Delta_R/\Delta_0 \ll 1$ then the left hand side of Eq. (4) represents the threshold distribution.

In order to create a correction mask for a chosen threshold the following algorithm may be used.

(1) Determine a histogram of the flat field image.
(2) Find the limits of the count rates for the image.
(3) By using histograms transform the count rates to threshold to find the range of the Medipix 1 parameters Vth and Vthadj.
(4) Transform the image to a mask by splitting the image into discrete correction levels equal to the number of bits in the correction mask.

Based on Eq. (4) a model of histograms was created. The model assumes a Gaussian distribu-

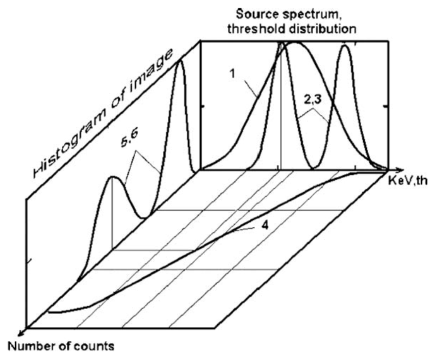

Fig. 1. Qualitatively description of how histograms relate to spectrum and threshold distribution. 1—effective source spectrum; 2 and 3—pixels threshold distributions for two applied thresholds; 4—cumulative function for pixels, described by Eq. (3); 5 and 6— histograms of images from Medipix1 for threshold distribution 2 and 3, respectively. A wide spectrum X-ray source with a flat intensity spatial distribution is applied.

tion of R and a standard X-ray dental source with a 60 keV spectrum. The spectrum was taken from [7]. By varying the parameter Δ_R of the threshold distribution the theoretical histograms in Fig. 2a could fit the experimentally obtained histograms in Fig. 2b. Each histogram represents an image for a particular threshold voltage. The images were taken using Medipix1 in the threshold scan regime.

3. Experimental results and discussion

From the data in Fig. 2 the best fit to the experiment was found to be when $\Delta_R \approx 0.06$ V and $\Delta_S \approx 4$ V, which corresponds to ratio $\Delta_R/\Delta_S \approx 1/7$. Histograms for thresholds closer to the ends of the spectra do not fit the histograms given by the model because of noise. For low thresholds high noise exists because of detector and amplifier limitations, while on the other hand for higher thresholds the signal will be low and the statistical noise will increase. Because of the noise for low thresholds, noise counts with lower energy rather than the minimum source energy will be measured experimentally. Therefore the measured cumulative function will not have saturation at lower threshold values, as shown in Fig. 3.

Another important factor that must be taken into account is the changing behaviour of the cumulative functions for individual pixels when the threshold is changed. Fig. 3 shows the wide variations in range for the cumulative functions for individual pixels for different thresholds. Therefore, it is impossible to create a single calibration mask valid for the whole energy range. Note that it is even possible for the individual cumulative functions to cross.

The best range for creating a mask is:

- The range of thresholds with low noise, and
- The linear part of the cumulative function.

The method proposed allows a set of correction masks for a wide range of energy to be created in a simple manner. The results for one global threshold are presented in this paper. After achieving the range of the count rate distribution from the histogram (Fig. 2b), the image can be split into the number of levels in the correction mask of the system. The transformed image (Fig. 4) contains seven layers describing the achieved mask. The histogram of these transformed images (Fig. 5) shows that the distribution is close to Gaussian. After applying this mask the width of the distribution of photo counts (Fig. 6a) was decreased by a factor of 3 compared to that without a mask (Fig. 6b).

The narrowing of the distribution can also be seen in the histograms of these images (Fig. 7). The histogram of the image achieved after correction can also be compared to a theoretical histogram for perfect seven levels calibration describing the limits of such a correction with this source and system.

Possibilities exist to create an optimal compensation mask for each case because the shape of the histogram of the corrected image depends on parameters such as the number of levels in the calibration mask, noise to signal ratio, etc.

By using the parameters of the Medipix1 system with a dental X-ray source the achieved spectral resolution can be estimated. The total range of the adjusting threshold energy for Medipix1 with a

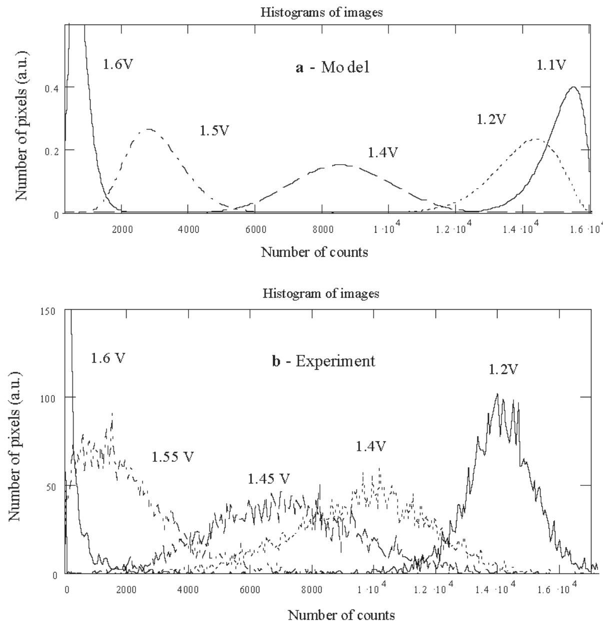

Fig. 2. Model (a) and experimental (b) histograms of flat field images for different threshold voltages.

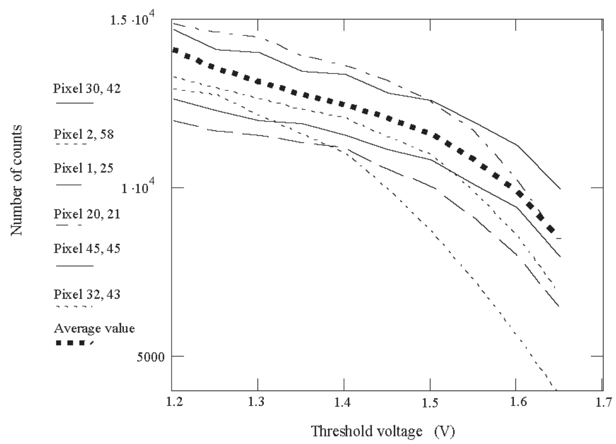

Fig. 3. Cumulative functions for different individual pixels and whole matrix.

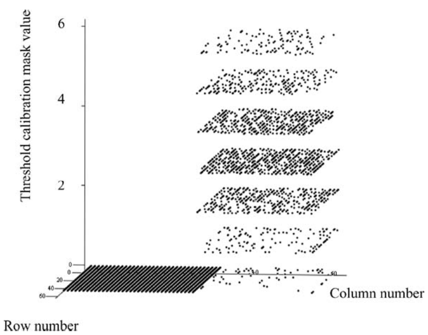

Fig. 4. Pixels distribution between threshold calibration mask values. (Column numbers 1–30 not used.)

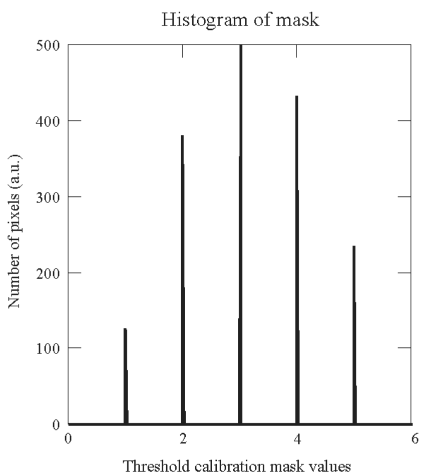

Fig. 5. Distribution of pixels for different threshold calibration mask values.

dental X-ray source is of the order of 40 keV, where a signal change of the order of 80% might be achieved. In this case changing the signal of an image, by for example 1%, could be achieved by an energy shift of the order of 0.5 keV. By using

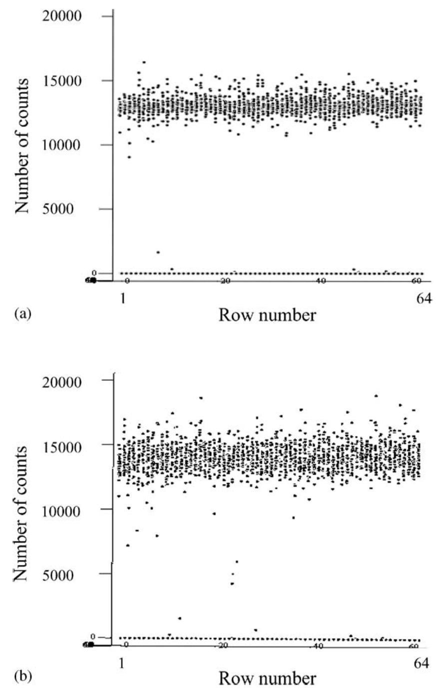

Fig. 6. Distributions of photon counts in image: (a) after and (b) before applying mask.

these estimations the limits of resolution can be found because of the minimal signal or contrast difference, which can be detected for two images or objects. Such a minimum can be found when two images are taken under the same conditions. The histogram of the ratio of two flat field images is presented in Fig. 8. As a result, the minimal contrast is approximately 2% of that corresponding to 1 keV and energy resolution ≈ 3 keV. This is close to the limit of the spectral resolution for this system due to Poisson noise for a single pixel when the number of photons is of the order of 10^4 per pixel. This case

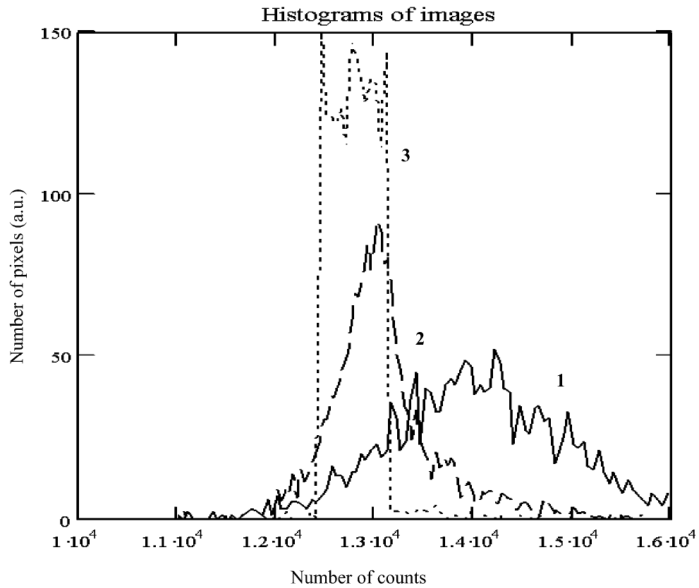

Fig. 7. Histograms of image taken without (1) and with (2) mask compared to histogram for calculated image with mask (3).

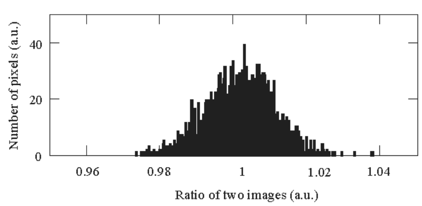

Fig. 8. Histogram of the ratio of two flat field images taken under identical conditions.

corresponds to the highest spatial frequency for the image. The contrast can be expected to increase if the spatial frequency decreases, since the noise is suppressed by averaging. It should be noted that the minimal detectable contrast deteriorates for higher threshold settings, where the signal decreases.

4. Conclusions

A method for creating correction masks for Medipix1 system with a dental X-ray source is proposed. It is not necessary to use special calibration sources for creating such correction masks, which makes the calibration much easier.

The mask is valid within a narrow energy range due to the variation in the individual cumulative functions. This range can be estimated by analysing the cumulative functions for the pixels.

After compensation, the estimated spectral resolution was about 3 keV, which is close to the limit of the spectral resolution for this system due to Poisson noise for a single pixel.

References

[1] B. Mikulec, Ph.D. Thesis, University of Vienna, Austria, June 2000, CERN-THESIS-2000-021.
[2] X. Llopart, M. Campbell, R. Dinapoli, D. San Segundo, E. Pernigotti, IEEE Trans. Nucl. Sci. 49 (2002) 2279.
[3] D. Niederlöhner, Ch. Bert, J. Giersch, K.-F. Pfeiffer, G. Anton, preprint Elsevier Science 20 November 2002.
[4] B. Mikulec, M. Campbell, G. Dipasquale, C. Schwarz, J. Watt. Nucl. Instr. and Meth. A 458 (2001) 352.
[5] R. Amendolia, E. Bertolucci, M.G. Bisogni, U. Bottigli, A. Ceccopieri, M.A. Ciocci, M. Conti, P. Delogu, M.E. Fantacci, P. Maestro, V. Marzulli, E. Pernigotti, N. Romeo, V. Rosso, P. Rosso, A. Stefanini, S. Stumbo, Nucl. Instr. and Meth. A 422 (1999) 201; erratum Nucl. Instr. and Meth. A 440 (2000) 258.
[6] E. Bertolucci, M. Conti, G. Mettivier, P. Russo, S.R. Amendolia, M.G. Bisogni, U. Bottigli, A. Ceccopieri, M.A. Ciocci, P. Delogu, M.E. Fantacci, P. Maestro, V.M. Marzulli, E. Pernigotti, N. Romeo, V. Rosso, A. Stefanini, S. Stumbo, Nucl. Instr. and Meth. A 422 (1999) 242.
[7] H.-E. Nilsson, E. Dubaric, M. Hjelm, K. Bertilsson, Nucl. Instr. and Meth. A 487 (2002) 151.

PAPER III

Material recognition with the Medipix photon counting colour X-ray system

P a p e r III

Available online at www.sciencedirect.com
SCIENCE DIRECT
Nuclear Instruments and Methods in Physics Research A 531 (2004) 265–269
NUCLEAR INSTRUMENTS & METHODS IN PHYSICS RESEARCH Section A
www.elsevier.com/locate/nima

Material recognition with the Medipix photon counting colour X-ray system

B. Norlin*, A. Manuilskiy, H.-E. Nilsson, C. Fröjdh

Department of Information Technology and Media, Mid-Sweden University, SE-85170 Sundsvall, Sweden

Available online 23 June 2004

Abstract

An energy sensitive imaging system like Medipix1 has proved to be promising in distinguishing different materials in an X-ray image of an object. We propose a general method utilising X-ray energy information for material recognition. For objects where the thickness of the materials is unknown, a convenient material parameter to identify is $K = \alpha_1/\alpha_2$, which is the ratio of the logarithms of the measured transmissions $\ln(t_1)/\ln(t_2)$. If a database of the parameter K for different materials and energies is created, this method can be used for material recognition independent of the thickness of the materials.

Series of images of an object consisting of aluminium and silicon were taken with different energy thresholds. The X-ray absorption for silicon and aluminium is very similar for the range 40–60 keV and only differs for lower energies. The results show that it is possible to distinguish between aluminium and silicon on images achieved by Medipix1 using a standard dental source. By decreasing the spatial resolution a better contrast between the materials was achieved. The resolution of contrasts shown by the histograms was close to the limit of the system due to the statistical noise of the signal.

PACS: 07.07.Df; 07.85.−m; 07.85.Nc; 78.70.Dm; 81.70.−q; 87.57−s; 87.59.−e

Keywords: X-ray; Imaging; Pixel detector; Medipix; Spectroscopy

Introduction

By using the Medipix1 system as a spectral sensitive detector matrix it is possible to obtain colour X-ray images of objects. Different applications for colour X-ray images are proposed within the framework of the Medipix collaboration. One application is to use energy discrimination as a method for improving the image quality for medical imaging [1]. Dose reduction in dental imaging [2] and mammography imaging [3] are issues of main importance for people's health in society. To be able to discriminate energy that is not required is also interesting in autoradiography [4] and electron microscopy [5].

This article will focus on investigating the spectroscopic information in an achieved image. A method to distinguish between different

*Corresponding author. Tel.: +46-60-1485-94; fax: +46-60-1484-56.
E-mail address: borje.norlin@mh.se (B. Norlin).

0168-9002/$ - see front matter © 2004 Elsevier B.V. All rights reserved.
doi:10.1016/j.nima.2004.06.015

materials in an object is proposed. For example, the materials Si and GaAs are expected to be easily distinguished if we have two images taken with different photon energies. This method can be used in characterisation of electronics production or in fibre quality control in the paper and pulp industry [6].

For many materials the attenuation of the X-rays in the range of energies from 10 to 100 keV can be expressed as an exponential function [7]

$$\frac{I}{I_0} = e^{-\alpha \cdot d} \tag{1}$$

where I_0 and I are the intensities before and after the absorber, respectively, and α is the absorption coefficient of the material which depends on the material and on the energy of the X-ray photons. The energy dependence of α plotted in Fig. 1 was achieved from absorption data [8]. The parameter α can serve as one of the attributes for identifying materials in the object when measuring the transparencies of a sample with a known thickness.

To identify materials in a sample with unknown thickness it is not possible to use the absolute parameter α. Instead we specify the parameter K as

$$K = \frac{\alpha_1(E_1)}{\alpha_2(E_2)}. \tag{2}$$

This parameter K can be extracted from two images taken for two different X-ray energies, E_1 and E_2, convenient for transmissions measurement of the object. In this case

$$K = \frac{\ln(t_1)}{\ln(t_2)} \tag{3}$$

where t_1 and t_2 are transmissions of the object for two energies. For this identification to work, it is important to achieve high accuracy in the measurements of K. This accuracy depends on the minimal detectable contrast of the images, according to $\Delta\alpha \sim \Delta t/t$, and this can be shown by differentiating (1). Fig. 2 presents two different ways of viewing the parameter K for Si, GaAs and CdTe, which may be helpful when choosing appropriate ranges of energies for practical applications. Fig. 2a presents K versus the energy E_2 if $E_1 = 30$ keV and Fig 2b presents K versus E_2, but with $E_2 - E_1 = 10$ keV. From these plots it is possible to find the two energies where the parameters K are sufficiently different to enable measurement to take place. For example, it is possible to distinguish Si from GaAs by extracting K for two images ($E_1 = 40$ keV and $E_2 = 60$ keV) on different parts of the images. (The suitable energy range also depends on the value of the transmissions and should be chosen so that the transmission of object is sufficient).

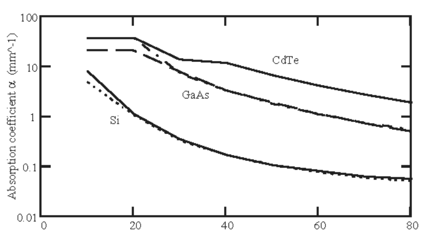

Fig. 1. The absorption coefficient α in mm^{-1} versus photon energy in keV extracted from experimental data [8] for different samples of Si, GaAs and CdTe.

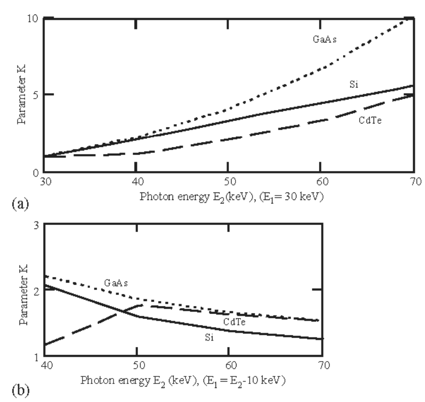

Fig. 2. The parameter $K = \alpha_1/\alpha_2$ extracted from Fig. 1 expressed in two different ways to help choose appropriate energies. (a) K versus the energy for α_2 if the energy for α_1 is 30 keV and (b) K versus the energy for α_2, but with the energy for α_1 kept 10 keV lower.

2. Method

Two different cases of colour imaging can be distinguished here. The first is when narrow spectrum sources are used and the second is when a wide spectra source such as a dental source is used. If a narrow spectra source is used, different energies are achieved by changing the source. For the proposed method to work using Medipix1, the whole threshold distribution [1] should be lower than the photon energies of the source. If not, the image will be lost for pixels with a threshold above the source energy. The sources are supposed to have energy distributions that do not overlap the threshold distribution. The pixel with the highest threshold energy should be able to count all incoming photons from the source. In this case the spectral selectivity of the Medipix1 system is not used. The threshold calibration is actually not necessary; a flat-field compensation to suppress noise can be applied afterwards. The ability for material recognition is limited by the different kinds of noise in the system. Due to the Poisson noise of incoming photons, the minimal detectable contrast is expected to be of the order of 1%, in the case of maximum exposure, i.e. when the number of counts is 32,768 on one pixel. For sufficiently transparent objects with informative spatial spectra below maximal frequency (smallest object details larger than the detector pixel size), the minimal detectable contrast will be lower, by several factors, and will be below 1%. It can be expected that the spectral resolution is proportional to the reverse spatial frequency.

The situation when a wide spectral source, such as a dental X-ray source that overlaps the threshold distribution, differs from the previously mentioned situation as the source defines the spectral resolution. To determine the spectral resolution in this case, the threshold or threshold window should be scanned within a defined energy range to obtain differential images. To achieve a reasonable spectral resolution a correction of the threshold distribution is required. When taking differential images it is important to use both flat-field and spectral corrections. Flat-field correction can be done in post-processing but spectral correction should be done with a threshold correction mask before taking images. Note that in the range of energies where the absorption spectrum is a smooth function of photon energy (i.e. no resonance) it is sufficient to use a flat field correction. This is valid when the width of the threshold distribution is much narrower than the source spectra and smaller than the spectral interval between energies of interest [9].

For images taken with a wide energy source, but with different energy thresholds, it is important to know how the threshold affects individual pixels. The cumulative function for individual pixels, showing the number of photons above the specified threshold energy, varies strongly between pixels, as shown in Fig. 3. To measure these cumulative functions, series of images with specified threshold were achieved. It can be seen that for individual pixels the behaviour appears to be definitely varying as a function of the applied threshold.

Hence the calibration of thresholds must be done separately for narrow threshold intervals. This is not important in narrow spectra source imaging, but it has practical consequences for differential colour imaging in a wide energy range.

3. Experiment

Spectral measurements should be done for energies within the dynamic range of the cumulative function, which depends on both the transmission spectra and the source spectra. For Medipix1 using a dental source, the half-width of the threshold distribution corresponds approximately to $\frac{1}{7}$ of the spectral width of the source, in threshold units this corresponds to 0.06 V [9]. A threshold scan range of the order of 0.40 V was applied during these experiments, so that the scan range was much wider than the threshold distribution. It can be seen that in this case there is no need to have a narrower spectral distribution of the thresholds to achieve the necessary resolution for measurements of transmissions for two X-ray energies.

To investigate whether the proposed method could work with reasonable accuracy when applied to Medipix1, materials with very similar absorption spectra were chosen for measurements.

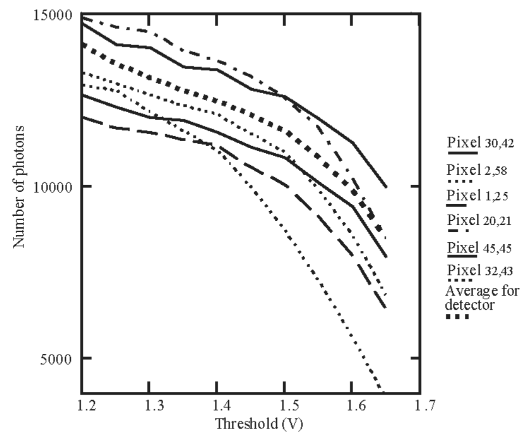

Fig. 3. Counting rate versus threshold energy for different individual pixels and average for whole matrix. Indexes correspond to the number of row and column for a pixel.

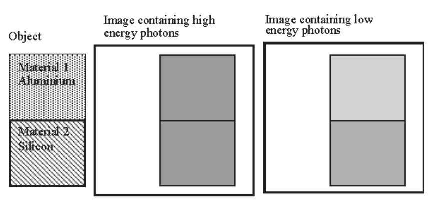

Fig. 4. Object consisting of two materials and expected images for different photon energies.

aluminium and silicon are materials that have quite smooth behaviour in the range 10 100 keV. Small percentage differences in transmission can be expected for the same thickness of materials. The difference decreases, when the photon energy increases from 30 to 70 keV. An object consisting of two 0.5 mm slabs, one of aluminium and one of silicon, were used for the measurements (Fig. 4). Series of images of the aluminium and silicon object were taken with different energy thresholds.

The difference of the average relative contrast between the two materials versus the threshold after applying a flat field correction is shown in Fig. 5. For averaging, an area of about 100 pixels was used. The relative contrast between the materials was calculated using:

$$\text{Relative contrast} = \frac{t_{Si} - t_{Al}}{t_{Si}} \tag{4}$$

where t_{Si} and t_{Al} are the average transmissions for the corresponding material.

Since the Medipix1 system can only discriminate low energy counts, the contrast achieved for low thresholds (Fig. 5) is an average over the spectral width from the applied global threshold to the highest energy achieved. As expected it was not possible to distinguish between the materials in high-energy images. For lower energies we could distinguish between the different materials by averaging the contrast for lower spatial frequencies in the image (Fig. 5) or by analysing histograms shown in Fig. 6. In the histogram for the whole detector, it is possible to distinguish two peaks that correspond to different areas with different materials. By analysing this histogram the regions of different materials can be identified. The histograms for these two regions are clearly resolved. By extracting separate histograms it is possible to actually distinguish between the absorption of aluminium and silicon. The resolution of contrasts found by the histograms was

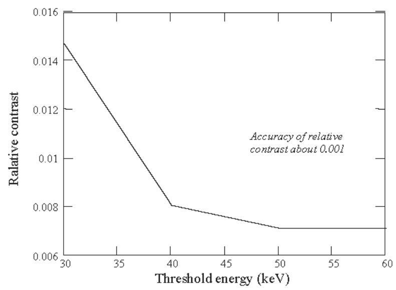

Fig. 5. Calculated contrast from measurements, areas averaged on 100 pixels.

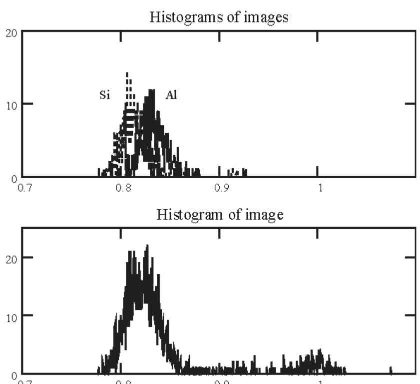

Fig. 6. Absorption induced shift of peak of histogram. Upper figure: selected known regions. Lower figure: the whole detector.

close to the limit of the system due to the statistical noise of the signal.

4. Discussion

Differential images are expected to give a higher contrast of an object, but in this case when Medipix1 was used, the noise of the differential images increased more than the contrast. Therefore we did not use differential images with the Medipix1 system. But for Medipix2 designed with a threshold energy window, better signal-to-noise ratios can be expected, since doubling of the statistical noise will not occur during the differentiation of two images.

Another subject concerning the application of the method is the recognition of materials if the object contains mixed or overlapping materials. The proposed method can be extended to this case but transmission measurements for a larger number of energies will be required.

5. Conclusions

A thickness independent method for material recognition using the ratio of absorption coefficients K is proposed. With this method it is possible to apply a flat field correction principle, in the case where the absorption spectra is a smooth function of photon energy. Experimental results show that it is possible to distinguish between aluminium and silicon (which have close X-ray absorption properties) on images achieved by Medipix1 using a standard dental source. By decreasing the spatial resolution a better contrast between the materials was achieved.

References

[1] B. Mikulec, Ph.D. Thesis, University of Vienna, Austria, June 2000, CERN-THESIS-2000-021.

[2] J. Watt, D.W. Davidson, C. Johnston, C. Smith, L. Tlustos, B. Mikulec, K.M. Smith, M. Rahman, Nucl. Instr. and Meth. A 513 (2003) 65.

[3] G. Mettivier, M.C. Montesi, P. Russo, Phys. Med. Biol. 48 (2003) N173.

[4] E. Bertolucci, M. Conti, G. Mettivier, M.C. Montesi, P. Russo, Nucl. Instr. and Meth. A 478 (2002) 109.

[5] A.R. Faruqi, D.M. Cattermole, R. Henderson, B. Mikulec, C. Raeburn, Ultramicroscopy 94 (2003) 263.

[6] T. Eriksson, P. Nilsson, Ö. Sundvall, On-line pulp quality monitoring, in: M.R. Doshi, J.M. Dyer (Eds.), Paper Recycling Challenge: Volume IV—Process Control & Mensuration, ISBN 0-9657447-4-4, Doshi and Associates, Inc., Appleton, WI, 1999, pp. 125–133 (Chapter 8).

[7] D. Vavrik, J. Jakubek, J. Visschers, S. Pospisil, C. Ponchut, J. Zemankova, Nucl. Instr. and Meth. A 487 (2002) 216.

[8] NIST Physical Reference Data; http://physics.nist.gov/PhysRefData/.

[9] A. Manuilskiy, B. Norlin, H.-E. Nilsson, C. Fröjdh, Nucl. Instr. and Meth. A (2004), this issue [doi: 10.1016/j.nima.2004.06.013].

PAPER IV

Energy dependence in dental imaging with Medipix2

Paper IV

Available online at www.sciencedirect.com
SCIENCE DIRECT®
Nuclear Instruments and Methods in Physics Research A 546 (2005) 19–23
NUCLEAR INSTRUMENTS & METHODS IN PHYSICS RESEARCH Section A
www.elsevier.com/locate/nima

Energy dependence in dental imaging with Medipix2

Börje Norlin*, Christer Fröjdh

Department of Information Technology and Media, Mid-Sweden University, SE-85170 Sundsvall, Sweden

Available online 7 April 2005

Abstract

The possibility of achieving better contrast in dental images by selecting specific X-ray energies is investigated. By applying both the low- and the high-photon counting energy threshold of the Medipix2 chip, only a narrow interval of the spectrum of a 60 keV standard dental source used is selected. The relative contrast between the parts of the tooth with the highest and lowest absorption increases 18% when the energy spread of the X-rays is narrowed from the full spectrum to a 4 keV window centred around 30 keV. The small tail of high-energy photons from the full source spectrum lowers the achieved relative contrast significantly. This result can be used in the development of X-ray sources or in consideration of energy weighting.

PACS: 07.07.Df; 07.85.−m; 07.85.Nc; 87.50.Gi; 87.57−s; 87.57.Ce; 87.59.−e; 87.62.+n; 87.64.Bx

Keywords: Dental diagnosis; X-ray; Image quality; Pixel detector; Medipix; Energy weighting

1. Introduction

To improve the image quality and thereby be able to reduce the necessary dose in medical imaging is one of the driving forces behind the Medipix collaboration [1]. The dose delivered to patients by different types of medical examinations seems to be constantly increasing, therefore the possibility of decreasing the dose delivered in, for example, dental imaging [2] and mammography imaging [3] is important. One way to reduce the dose delivered in medical X-ray imaging is to optimize the energy range of sources for certain applications. As the detector technology improves, it is likely that demands on improvement of medical X-ray sources will be raised in the near future. This present work exemplifies how the Medipix2 system can be used to find guidelines for such X-ray source development. Medipix2 is a photon counting detector system with selectable lower and higher energy thresholds and 55 μm pixel size [4]. The results indicate that energy weighting of several images achieved at different energies is a possible way of improving medical X-ray images [5].

*Corresponding author. Tel.: +46 60 148594; fax: +46 60 148456.
E-mail address: borje.norlin@miun.se (B. Norlin).

0168-9002/$ - see front matter © 2005 Elsevier B.V. All rights reserved.
doi:10.1016/j.nima.2005.03.035

2. Measurements

Images of a lower jaw are taken using a setup similar to a dental X-ray imaging system. A Medipix chip with a 300 μm thick silicon detector is mounted inside the jaw. The dental source used is a PLANMECA PROSTYLE INTRA operated at 70 kV with 2.0 mm Al filtration. This source is DC operated with a short start-up transient that is stable after 100 ms (Fig. 1) and a spectrum with maximum X-ray intensity at 30 keV (Fig. 6).

If the detector thresholds are set to count only photons from an interval in one part of the spectrum, the count rate will be low and the contribution from photonic noise will be significant. To compensate for this the exposure time of the source is adjusted to get an equal "effective" dose for each energy interval setting. In this way the dose delivered to the patient should have been constant for all images, if the selection of energies had taken place in the source and not in the detector. For each energy interval setting a flood image (without object) is achieved. The flood image is used for flat field correction and is needed to compensate for variations in the response over the detector area. The flat field correction is unique for each chip and also varies with energy. It can be argued that a certain flat field correction is valid for a range of energy settings, which is not considered here [6]. The flat field correction can be improved by averaging over a large number of flat field images [7].

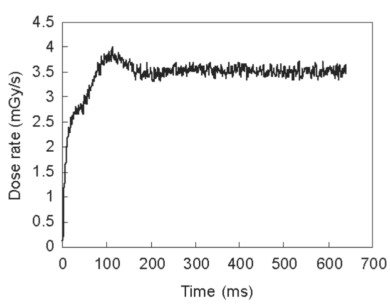

Fig. 1. Start up transient of the X-ray source taken with a Barracuda system from RTI Electronics.

To get a quantitative measurement of the image quality, one region with high photon absorption and one with low photon absorption are defined for the tooth (Fig. 2). The contrasts for these two regions relative to the part of the image above the tooth are extracted. Some bad pixels are excluded. The contrast is relevant to extract since it is dose independent. If the contrast is improved more noise can be tolerated in the image thereby decreasing the dose to the patient.

A photon counting system must always operate with a lower energy threshold set to exclude readout noise. A feature of the Medipix system is the ability to adjust the threshold for each individual pixel by defining a calibration mask for the pixel matrix. A calibration mask for the lower threshold can be achieved by letting the software equalize the noise edge for each pixel [8]. This mask is valid for lower settings of the low-energy threshold, for high-energy settings it would be preferable to generate the calibration mask using another method as described in Ref. [9].

The tooth is more transparent when the photon energy is higher so a decrease in contrast for high settings of the threshold is expected. In preliminary

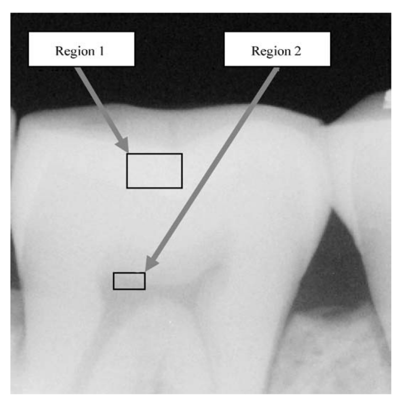

Fig. 2. Image of a tooth achieved with Medipix2. Two regions with high and low X-ray absorption are defined to study the contrast variation.

measurements without a threshold mask, the number of pixels affected by readout noise is significant for low threshold settings. Therefore the contrast degenerates for threshold settings close to the noise edge if no calibration mask is applied. Since the mask is most important for the lowest energy settings, a mask generated by equalizing the noise edge is sufficient for the measurements in this paper.

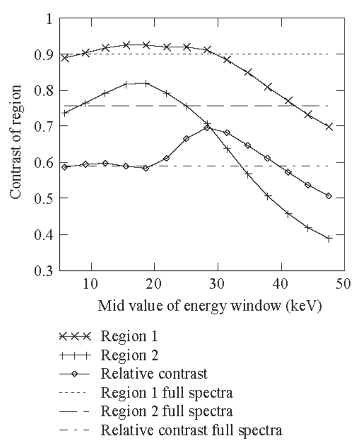

Fig. 3. Achieved contrast for the two defined regions of the tooth and the relative contrast between these regions for a serie of 4 keV wide energy windows. The measurements are compared to the value for a full spectrum.

To use the higher energy threshold in Medipix2, this threshold must also be calibrated for each pixel. The calibration determines how narrow the energy window can be set without introducing noise in the image from the high threshold [10]. For this work, a window of 4 keV was achieved for one of the detector chips available when the high threshold calibration mask was copied from the low threshold calibration mask. This window was used to sweep the available energy spectrum and achieve the energy dependence of the contrasts of the defined regions of the tooth (Fig. 3).

It can be concluded from Fig. 3 that the relative contrast can be improved from 0.59 for the full spectra to 0.70 when a narrow energy centred about 30 keV is applied. A maximum relative contrast near this energy is expected, since at this energy region 1 is still absorbing strongly while region 2 starts to get transparent [11]. In Fig. 4, three images are supplied to illustrate how the actual image varies with energy. The images show low energy, maximum relative contrast and high energy.

To simulate tissue, 10 mm of water is placed between the source and the teeth. The water will primarily absorb low-energy photons and thereby decrease the image quality both due to statistics and radiation hardening. The count rate above the tooth decreases 46% due to absorption in water. The decrease in contrast can be seen in Fig. 5, which is a repetition of the previous contrast measurement but with water between the source and the object.

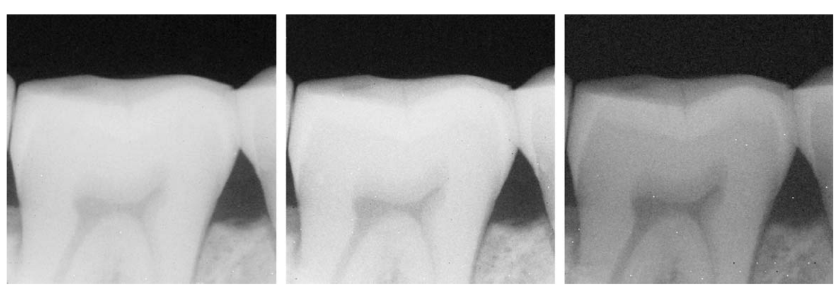

Fig. 4. Energy-dependent image quality variation in dental images. Window energies are 4–8 keV for the left image, 26–30 keV for the middle image and 45–49 keV for the right image.

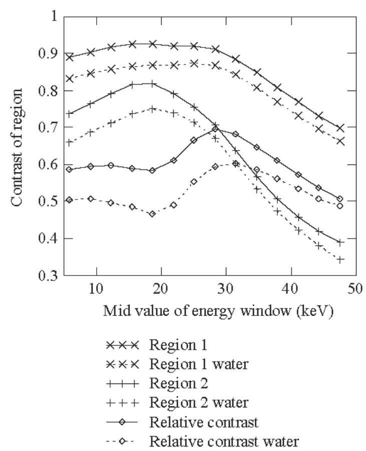

Fig. 5. Achieved contrast after water absorption for the two defined regions of the tooth for a series of 4 keV wide energy windows. The contrasts and the relative contrast between the regions are compared to the values in Fig. 5.

The energy scale of the Medipix2 system can be calculated by

$$E = (th + th_0)\Delta E$$

where E is the energy in keV and th is the daq value set for the energy threshold of the system. th_0 is the daq value corresponding to zero energy and ΔE is the energy step corresponding to a daq unit. For the particular detector chip the value of th_0 is 179 derived from noise measurements and the value of ΔE is 0.64 keV/setting derived from measurements of known line spectra.

When the results in this paper are interpreted, it must be considered that the energy spectrum is strongly degenerated due to charge sharing between pixels. In Fig. 6, a measured spectrum for Medipix2 is compared to a simulation from Ref. [12]. In the achieved spectrum, high-energy photons are redistributed to one or several low-energy counts.

Charge sharing can be slightly suppressed by increasing the bias voltage of the detector. Therefore all images are achieved at a bias voltage of 120 V. But the results for low energies still contain

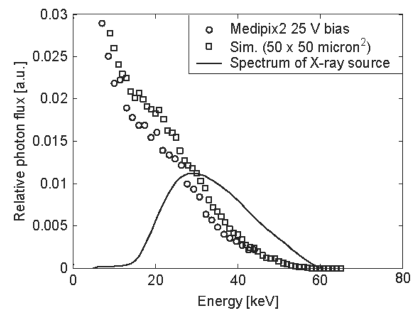

Fig. 6. Degenerated spectrum due to charge sharing. Simulated [12] and measured spectrum on Medipix2 at depletion voltage compare to the spectrum of the X-ray source.

contributions from high-energy photons. The real contrast variation due to X-ray energy is probably larger than the measurements presented in this paper, since the high energies negatively influences the achieved contrast.

3. Conclusions

It is possible to improve the contrast in dental images by selecting specific X-ray energies. The relative contrast between a high absorbing and a low absorbing region of a tooth is increased by 18%. It is possible to decrease the dose delivered to dental imaging patients by improving the energy profile of dental sources, and probably also by introducing energy weighting in a multichannel pixellated imaging system.

Acknowledgments

This work was done using detectors, software and readout system developed within the MEDIPIX2 collaboration.

References

[1] B. Mikulec, Ph.D. Thesis, University of Vienna, Austria, June 2000, CERN-THESIS-2000-021.

[2] J. Watt, D.W. Davidson, C. Johnston, C. Smith, L. Tlustos, B. Mikulec, K.M. Smith, M. Rahman, Nucl. Instr. and Meth. A 513 (2003) 65.
[3] G. Mettivier, M.C. Montesi, P. Russo, Phys. Med. Biol. 48 (2003) N173.
[4] X. Llopart, M. Campbell, R. Dinapoli, D. San Segundo, E. Pernigotti, IEEE Trans. Nucl. Sci. NS-49 (2002) 2279.
[5] J. Giersch, D. Niederlöhner, G. Anton, Nucl. Instr. and Meth. A, Corrected proof, 2004.
[6] D.W. Davidson, C. Fröjdh, V. Oshea, H.-E. Nilsson, M. Rahman, Nucl. Instr. and Meth. A 510 (2003) 13.
[7] B. Mikulec, Nucl. Instr. and Meth. A 509 (2003) 102.
[8] M. Conti, M. Maiorino, G. Mettivier, M.C. Montesi, P. Russo, IEEE Trans. Nucl. Sci. NS-50. (4) (2003) 869.
[9] A. Manuilskiy, B. Norlin, H.-E. Nilsson, C. Fröjdh, Nucl. Instr. and Meth. A, Corrected proof, 2004.
[10] J. Karg, D. Niederlöhner, J. Giersch, G. Anton, Presentation at Sixth IWORID, Glasgow, Scotland, July 2004, http://www.iworid2004.ph.gla.ac.uk/.
[11] J. Ludwig, A. Zwerger, K.W. Benz, M. Fiederle, H. Braml, A. Fauler, J.P. Konrath, Nucl. Instr. and Meth. A, Corrected proof, 2004.
[12] H.-E. Nilsson, et al., Nucl. Instr. and Meth. A 487 (2002) 151.

PAPER V

Spectral Response of Pixellated Semiconductor X-ray Detectors

P a p e r V

Spectral Response of Pixellated Semiconductor X-ray Detectors

Christer Fröjdh, *Member, IEEE*, Hans-Erik Nilsson, Börje Norlin,

***Abstract*— X-ray imaging with energy resolution can be performed using a detector matrix bonded to a photon counting CMOS readout circuit as the MEDIPIX2 chip [1]. In previous experiments it has been shown that charge sharing between neighboring pixels plays an important role in the formation of the image [2-4] and especially for the spectral information in the image. Charge sharing is caused both by the localization of the initial energy deposition and by diffusion during the transport of the charge to the readout electrode. In this work we have studied different factors that can effect the energy resolution in pixellated X-ray imaging detectors. Results are compared to experimental data.**

***Index Terms*—X-ray image sensors, semiconductor materials, X-ray fluorescence, charge transport**

I. Introduction

X-RAY imaging detectors with energy resolution are currently being developed by different research collaborations. One example of such a development is the MEDIPIX2 chip[1]. In order for these devices to give correct spectral information it is important that the signal from the capture of one X-photon is fully collected within the pixel where the original interaction occurred. The spectral information can be destroyed by effects as:

- Charge sharing or escape due to X-ray fluorescence
- Charge sharing due to Compton scattering
- Charge sharing due to charge diffusion
- Bad alignment of the detector in the beam
- Incomplete charge collection due to trapping of carriers

When an X-ray photon with an energy below a few hundred keV hits a detector the primary interaction is typically photoelectric absorption or Compton scattering. In both cases the primary interaction is followed by secondary events and energy is deposited at different locations in the detector. For detectors made from high-Z materials an important secondary event is X-ray fluorescence which can range over several pixels. The deposited energy releases electrons and holes which are then drifted towards the readout electrodes. During the drift the size of the charge cloud will increase due to diffusion and some of the charges might be trapped before they reach the electrode.

In addition, if the detector is not exactly perpendicular to the beam, photons originating form the same point but being captured at different depth in the detector might be allocated to different pixels.

In the following sections we discuss how these effects will affect the spectral response of a pixellated semiconductor X-ray detector.

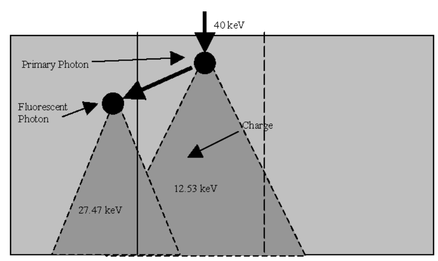

Fig. 1. A typical X-ray event in a detector. The primary photon is captured by a photoelectric event. A fluorescent photon is emitted and captured in the next pixel. The charge cloud from these two interactions widens by diffusion during drift towards the readout electrode. (only one type of carrier shown). It should be noted that most of the energy is deposited outside the pixel where the primary interaction occurred.

II. Photoelectric Absorption and Compton Scattering

In a photoelectric event the energy of the X-ray photon is transferred to a core electron of an atom. During de-excitation of the atom either an Auger electron or a fluorescent X-ray photon is released. The range of the electrons is typically a few micrometers. For heavy atoms the fluorescent photons have high energy and their range can be several hundred micrometers.

When a photon is Compton scattered some of its energy is transferred to an electron and the photon continues in a different direction. The range of the Compton electron is typically just a few micrometers. The scattered photon might undergo another interaction, photoelectric or Compton, or escape from the detector. Unless the photon escapes the detector the total energy will be captured in the detector, just as for a photoelectric event, but the energy distribution might be more complicated.

Manuscript received November 11, 2005. C. Fröjdh is with Mid Sweden University, SE-851 70 Sundsvall, Sweden(phone: +46 60 148733; fax: +46 60 148520; e-mail: christer.frojdh@miun.se).

H-E. Nilsson and B. Norlin are with Mid Sweden University, Sundsvall, Sweden

III. X-RAY FLUORESCENCE

A photoelectrical event removes a core electron from an atom in the detector leaving a vacancy which then has to be filled. The excess energy is typically released as a fluorescent X-ray photon. If the electron is a K-shell electron and the material is a high-Z material the fluorescent photon has high energy and might travel a significant distance before it is reabsorbed or even escapes the detector. The table below lists the energy and range of the fluorescent photons in some detector materials. The fraction of 90 keV photons absorbed in a 1 mm thick detector is included as an additional figure of merit. The range of the fluorescent photons can be several pixels in a small pixel detector.

TABLE I
ENERGY AND RANGE OF FLUORESCENT PHOTONS IN SOME DETECTOR MATERIALS

Atom and material	Fluorescence		Stopping 90keV 1 mm
	Kα (keV)	Range (um)	
Si	1.74	12	0.05
Ga in GaAs As in GaAs	9.25 10.54	40 16	0.32
Cd in CdTe Te in CdTe	23.17 27.47	112 59	0.75
Tl in TlBr Br in TlBr	72.86 11.93	621 20	0.98
Pb in PbI2 I in PbI2	74.96 28.61	450 78	0.95

The effect of X-ray fluorescence can be overcome by charge summing over a number of pixels provided that the range of the summing is sufficiently large. However if the energy of the incident photon is just above the K-edge of the detector material then the range of the fluorescent photon is larger than the range of the incident photon and a significant number of photons will escape the detector. Fig 2 shows the resulting spectrum from an exposure with a 10 um wide beam of 40 keV photons on different detector materials. It is evident that the amount of fluorescence causing escape peaks increases with increasing Z of the material. The exception is TlBr where the K-edge of Tl falls above the photon energy used in this case. The very low absorption in Si is also clearly seen in the figure.

To study the effect of charge summing a simulation was made for CdTe using larger pixel sizes, 150 um and 1 mm. Resulting spectra are shown in Fig. 3. The data for the pixel size of 1 mm could be regarded as a limiting case. The escape peaks are in this case caused by photons escaping the detector and can not be cured by charge summing or any other technique.

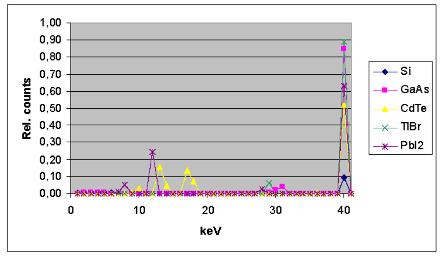

Fig. 2. Resulting spectrum from illuminating different detectors with a 10 um wide beam of 40 keV photons. Escape peaks in the various materials are clearly seen.

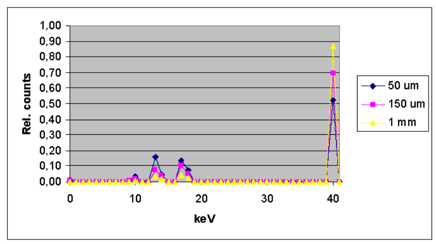

Fig. 3. Effects of charge summing can be simulated by using different pixel sizes. In this simulation charge summing over neighbors (150 um) and charge summing over a large area has been calculated for a detector with a pixel size of 50 x 50 um^2. Photons escaping the detector limits the height of the full energy peak even for large area summing.

An additional simulation was done using photons of 90 keV. In this case the photon energy is above the K-edge of all detector materials. This is also an energy where high-Z materials are necessary to get sufficient stopping. The absorption of 90 keV photons in GaAs is below 10% and the absorption in Si is almost negligible. From the simulation it is evident that charge summing or similar techniques are required to get any relevant spectral information.

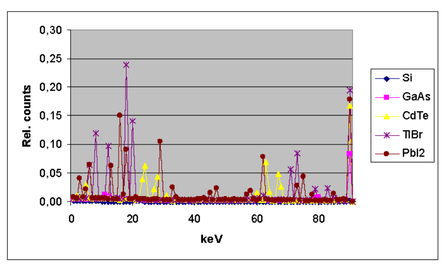

Fig. 4. Spectral response for 90 keV photons in a number of detector materials. The large number of escape peaks present for all materials with sufficient stopping should be noted.

IV. Charge Transport

During the transport through the detector the charge cloud is spreading by diffusion. This effect is essentially proportional to the electric field in the device and the drift distance. It is clear that for a thick detector with small pixels only a fraction of the charge will be detected in the right pixel.

Simulations were made for a 1 mm thick CdTe detector with 55 x 55 um^2 pixels biased at 300 V. Since the field inside the detector was unknown the simulation was made for the two limiting cases, constant field and linear field. In this specific case the same result was obtained for both cases. The charge collection efficiency in the central pixel was about 75%.

Effects of charge spreading can be reduced by increasing the electric field by overdepletion or increased doping. The limiting case is when the breakdown field is reached in the detector or when the leakage current becomes to high resulting in saturation of the readout electronics or excessive heating of the detector. Effects of charge diffusion can also be corrected by charge summing over neighboring pixels.

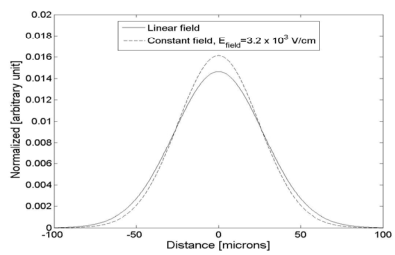

Fig. 5. Extension of the charge cloud at the pixel contact for 40 keV photons captured in a 1 mm thick CdTe detector biased at 300 V. Both constant field case (compensated material) and linear field case (diode like structure) give the same result for this specific case.

V. Charge Collection

The charge transport properties of many detector materials are far from ideal. One or both of the types of carriers are likely to be trapped before they reach the readout electrode. A well known example is the depth dependence of the pulse height in CdTe detectors originating from the short drift distance for holes in the material. A number of different electrode configurations have been proposed to overcome this problem. However these configurations might be difficult to implement in a detector with small pixels. In this case the situation is somewhat improved due to the small pixel effect [5,6].

VI. Detector Alignment

A 1 mm thick detector with a pixel size of 50 um has an aspect ratio of 20:1. An angular misalignment of only 1,4 degrees corresponds a difference of half of the pixel width over the depth of the detector. Alignment tends to be a crucial problem when using thick detectors with small pixels. In the above case visual alignment is not sufficient, Mechanical or optical alignment systems have to be introduced. A second problem is the parallax error introduced when a planar detector is illuminated with a point source. Possible solutions include segmenting of the detector and mounting the detector elements in a spherical shape. Misalignments of less than one pixel can be corrected by charge summing.

VII. Experimental Results

The response of a 1 mm thick CdTe detector illuminated with a narrow beam of 40 keV photons has been measured at the ESRF. A resulting spectrum is presented in Fig. 6. Complete results from the experiment are presented in [7]. The measurements confirm both the fluorescence and the charge diffusion. Due to the high stopping in CdTe no effects of alignment and depth of interaction were present. Biasing conditions were the same as presented in Fig. 5. Calculations of the energy scale confirms a charge collection of 75% for photons absorbed close to the centre of the pixel.

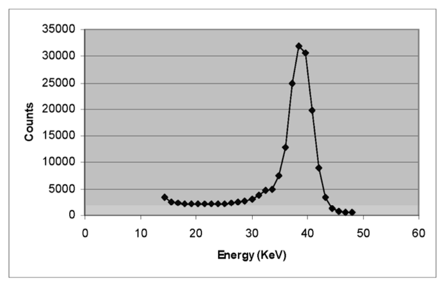

Fig. 6. Spectrum from a 1 mm thick CdTe detector with a pixel size of 55 x 55 um when illuminated with a narrow beam of 40 keV photons.

VIII. Conclusions

X-ray imaging detectors with pixel sizes in the range 50 – 150 um are being developed for a number of applications. In order to get sufficient sensitivity these detectors are made form thick layers of high-Z materials. The spectral response of such detectors is severely degraded by effects as X-ray fluorescence, charge spreading during charge transport, misalignment and charge trapping. The first three effects can be reduced by charge summing over neighboring pixels. Incomplete charge collection will need other methods to be corrected. Charge summing is an efficient tool to restore the spectral information but the spatial resolution might be affected if most of the energy is deposited in the wrong pixel, which can happen if the photon energy is close to the K-edge of the detector material.

REFERENCES

[1] X. Llopart, M.Campbell, R. Dinapoli, D. San Segundo, E. Pernigotti, "Medipix2, a 64k pixel readout chip with 55 µm square elements working in single photon counting mode ", *IEEE Transactions on Nuclear Science*, v 49, n 5, pt.1, Oct. 2002, p 2279-83.

[2] K. Mathieson, M. S. Passmore, P. Seller, M.L. Prydderch, V. O'Shea, R.L. Bates, K.M. Smith, M. Rahman, *Nuclear Instruments & Methods in Physics Research, Section A*, v 487, n 1-2, 11 July 2002, p 113-22

[3] M. Chmeissani, C. Frojdh, O. Gal, X. Llopart, J. Ludwig, M. Maiorino, E. Manach, G. Mettivier, M. C. Montesi, C. Ponchut, P. Russo, L. Tlustos, and A. Zwerger, "First Experimental Tests with a CdTe Photon Counting Pixel Detector Hybridized with a Medipix2 Readout Chip", *IEEE Transactions on Nuclear Scence.*, Vol. 51, No. 5, Oct 2004.

[4] M. Chmeissani, M. Maiorino, G. Blanchot, G. Pellegrini, J. Garcia, M. Lozano, R. Martinez, C. Puigdengoles, M. Ullan, "Charge Sharing Measurements of pixilated CdTe using Medipix-II chip", IMTC 2004 – *Instrumentation and Measurement Technology Conference Como, Italy, 18-20 May 2004*

[5] L.-A Hamel, S. Paquet, "Charge transport and signal generation in CdTe pixel detectors" *Nuclear Instruments & Methods in Physics Research, Section A*, v 380, 1996, p 238 - 240

[6] P. Sellin, "Modelling of the small pixel effect in gallium arsenide X-ray imaging detectors", *Nuclear Instruments & Methods in Physics Research, Section A*, v 434, 1999, p 75 - 81

[7] C. Fröjdh, H.Graafsma, B. Norlin, H. E. Nilsson, C. Ponchut, "Characterisation of a pixellated CdTe detector with Single Photon Processing Readout", *Nuclear Instruments & Methods in Physics Research, Section A, [IWORID 2005, Grenoble, July 2005],* submitted for publication.

PAPER VI

Characterization of a pixellated CdTe detector with single-photon processing readout

Paper VI

Available online at www.sciencedirect.com
SCIENCE DIRECT®
ELSEVIER
Nuclear Instruments and Methods in Physics Research A 563 (2006) 128–132
NUCLEAR INSTRUMENTS & METHODS IN PHYSICS RESEARCH Section A
www.elsevier.com/locate/nima

Characterization of a pixellated CdTe detector with single-photon processing readout

C. Fröjdh[a,*], H. Graafsma[b], B. Norlin[a], H.E. Nilsson[a], C. Ponchut[b]

[a]Mid Sweden University, SE-851 70 Sundsvall, Sweden
[b]ESRF, BP220, Avenue des Martyrs, 38043 Grenoble, Cedex, France

Available online 17 February 2006

Abstract

A 1 mm thick pixellated CdTe detector bonded to the MEDIPIX2 [X. Llopart, M.Campbell, R. Dinapole, D. San Segundo, E. Pemigotti, IEEE Trans. Nucl. Sci. NS-49 (5, Part 1) (2002) 2279] readout chip has been characterized using a monoenergetic microbeam at the ESRF. This is an extension of the tests previously reported in Chmeissani et al. [IEEE Trans. Nucl. Sci. NS-51(5) (2004)]. The results show that a full energy peak can be obtained when a narrow beam is focused in the center of the pixel. There is also evidence of significant charge diffusion and fluorescence. The results indicate that the charge sharing is the most important problem and will cause loss of the energy information in an imaging application. The second problem is the fluorescence which limits the number of counts in the full energy peak even for hits in the center of the pixel.

PACS: 72.20.−I; 78.70.Dm; 78.70.−g

Keywords: Pixel detector; CdTe; Medipix; Charge sharing; Photon counting

1. Background and experimental conditions

Pixel detectors using single-photon processing readout (see Refs. [1–3]) are interesting because of low noise operation and their ability to record the energy of each individual photon [3]. One such readout chip is the MEDIPIX2 chip[1] with a pixel size of $55 \times 55\,\mu m^2$. It has, however, been observed that significant charge sharing occurs for most detectors with small pixels [4]. For detectors made from heavy materials, the charge sharing can be caused both by charge diffusion and fluorescence in the detector.

In this experiment we have been using a 1 mm thick CdTe detector bonded to the MEDIPIX2 readout chip and measured its response to a narrow monoenergetic X-ray beam. Readout was done using the MUROS2 interface and the Medisoft4 program.

The measurements were performed at the ESRF, where previous versions of the MEDIPIX chip have been characterized [5], using a beam with a photon energy of 40 keV. A set of motor-driven slits, located about 10 cm from the detector were used to adjust the beam width to $10 \times 10\,\mu m^2$. The detector was mounted on an XY-translation stage to move between the pixels and a rotation stage to align the detector perpendicular to the beam. During the calibration phase a 300 μm silicon detector was used as a reference. After calibration the CdTe detector was inserted in the same position as the Si detector. The beam width was verified both by measuring the flux of X-ray photons through the slit and by scanning the beam across a pixel. Almost no scattered photons were visible in the neighboring pixels. The final beam intensity was around 65 000 photons/s.

The detector was operating in electron collection mode with positive bias on the pixel contact and negative bias on the uniform back contact. Radiation was entering from the backside.

2. Theoretical model

When a beam of 40 keV photons enter a CdTe detector most of the photons are absorbed close to the detector

*Corresponding author. Tel.: +46 60 148733; fax: +46 60 148520.
E-mail address: christer.frojdh@miun.se (C. Fröjdh).

0168-9002/$ - see front matter © 2006 Elsevier B.V. All rights reserved.
doi:10.1016/j.nima.2006.01.076

surface (Fig. 1). As a consequence the generated electrons have to be drifted through the full depth of the detector, to the pixel contact, while the holes only travel a short distance to the back contact. This is the best case in order to get full charge collection. Since we do not know the internal field structure in the detector we have used the simplified concept that the electrons contribute to the signal when they reach the pixel contact in our discussion.

In a thick CdTe detector charge can be lost either due to fluorescence, where secondary photons contribute in a different pixel, or due to charge diffusion where part of the charge cloud is detected in neighboring pixels [6].

The charge transport in the detector was simulated using MEDICI. Since the internal field structure in this detector is not very well known, the charge diffusion was simulated both for a diode-like structure (linear field case) and for a semi-insulating structure (constant field case) using the same bias voltage as in the experiment. The resulting charge distribution is shown in Fig. 2. It is clear that only 75% of the charge hits the pixel contact even if the photon is absorbed in the center of the pixel. This information was

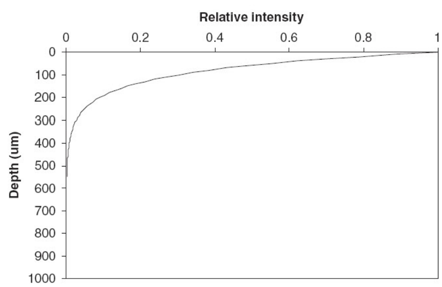

Fig. 1. Relative beam intensity as a function of the depth in the detector. More than 90% of the radiation is stopped within the first 200 μm.

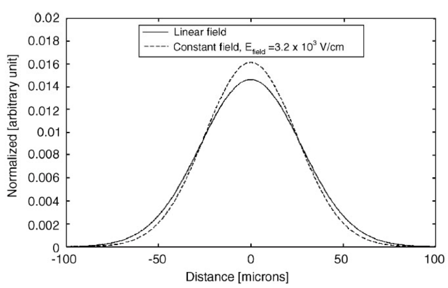

Fig. 2. Average extension of the charge cloud at the pixel contact for an X-ray photon captured in the detector under the bias condition in the experiment. Both linear field case and constant field case give similar results.

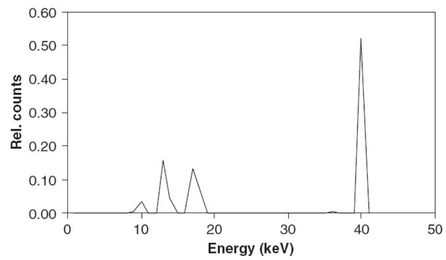

Fig. 3. Simulated response in the center pixel. Only 55% of the photons contribute in the full energy peak. The effect of fluorescence is seen as escape peaks.

then used in order to calculate the energy scale of the system. The energy scale was calculated starting from the position of the full energy peak of a hit on the silicon detector, taking into account the differences in the energy to create an electron–hole pair between Si and CdTe, the difference in gain in the readout electronics and the expected charge collection efficiency of the CdTe detector according to simulation. The resulting energy scale was 1.05 keV/ADC unit, which has been used in the following figures.

The effects of fluorescence were simulated using MCNP. The number of incident photons was 1×10^6. The absorbed energy was counted in 40 energy bins with a width of 1 keV corresponding to the built in energy cutoff in MCNP. The effect of fluorescence is seen as escape peaks in the central pixel and as peaks at the characteristic energies in the neighboring pixels. It should be noted that charge diffusion is not taken into account in this simulation (Fig. 3).

3. Experimental results

3.1. Operating point and bias

Initially a bias sweep was made to establish an operating point for the detector. The bias current was time-dependent and a diode-like behavior was observed as previously reported in Ref. [2]. The current started at a high value when power was turned on and then stabilized after a couple of minutes.

The X-ray response as a function of bias voltage for the detector was measured. There is almost no response at low voltages, then a sharp increase (Fig. 4). The response reaches a plateau at about 300 V. This behavior, together with the IV-curve indicates that the pixel contact is rectifying and that the electric field is penetrating from that contact since most photons are absorbed close to the back contact. The rise of the response is seen when the field reaches the back side of the detector. During measurements the bias voltage was kept at 320 V with a current of 60 μA.

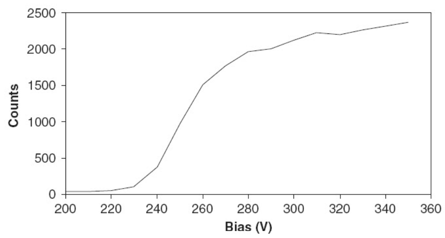

Fig. 4. Response of the detector as a function of bias. The operating point was chosen to be 320 V, in a region with flat response and reasonably low currents, 60 μA.

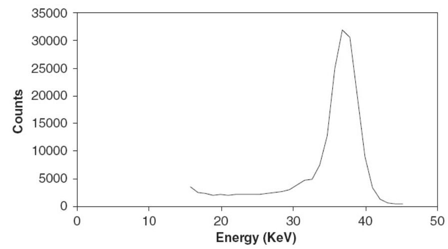

Fig. 6. Spectral response from a pixel with the beam centered in the pixel. The energy scale is adjusted for incomplete charge collection.

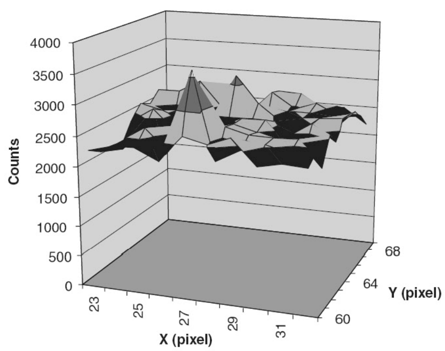

Fig. 5. Response from an area of 100 pixels. The beam was centered in each pixel. A low threshold energy was used.

3.2. Response uniformity

To get an indication of the uniformity of the central part of the detector the beam was scanned over a number of pixels. The response was measured using a low threshold of the readout circuit. The average number of counts per pixel was 2456 with a standard deviation of 229 counts (Fig. 5). It is hard to determine to what extent this variation is caused by the detector or by variations in the threshold of the readout circuit. Since the objective of this experiment was to measure the X-ray response in single pixels no threshold calibration was used. The conclusion is, however, that the response in the area of interest is reasonably uniform.

3.3. Response in the center pixel

The spectral response for a pixel was measured by positioning the beam in the center of the pixel scanning an energy window. Beam alignment was made by adjusting the beam position in small steps measuring the response in the neighboring pixels using a low threshold. The beam is assumed to be in the center when there is equal response in the surrounding pixels. A low threshold was selected to capture shared events.

During the experiment the exposure time was varied in the interval 100 ms–10 s to get a comparable number of counts for each energy interval. The resulting spectrum is shown in Fig. 6. A clear energy peak is observed with a FWHM of 4.9 keV and a peak to valley ratio of about 15. The energy scale used in the figure is calculated as described above.

A small number of hits were recorded with energies up to twice the beam energy. These are double hits which could easily be explained by the time properties of the synchrotron beam and the finite peaking time of the MEDIPIX chip [5].

3.4. Response in neighboring pixels

The response in a number of neighboring pixels was measured. This response is mainly caused by fluorescent photons recorded in these pixels. However, due to the random position where they are captured in the pixel and the strong charge diffusion they do not show up as peaks in the spectrum.

The response in a number of neighboring pixels, recorded at different threshold energies is shown in Fig. 7. In addition the simulated number of hits is included. Even if no charge diffusion was included in the simulation the numbers match. Contributions due to charge diffusion will have too low energy to be recorded.

3.5. Scanning the beam over the pixel

In order to get better understanding of the energy deposition and transport in the pixel the beam was scanned over the pixel area and the spectral response was measured using an automatic threshold scan and subtracting the response between the energy steps. The advantage of this

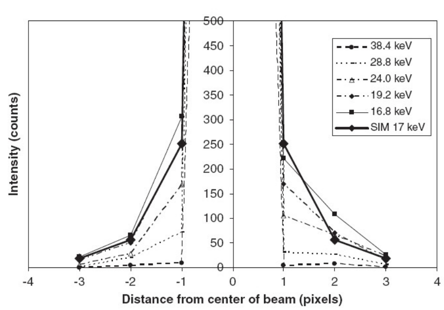

Fig. 7. Response in neighboring pixels as a function of the threshold energy. The bold line indicates results form a simulation at 17 keV without taking charge transport into account.

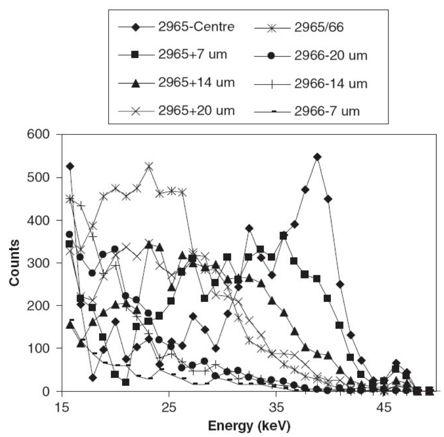

Fig. 8. Response from pixel 2965 when the beam is scanned from the center towards pixel 2966. Since the scan was made using only the low threshold and subtracting consecutive images the data is very noisy.

method is that it is fast but a major drawback is that the subtraction introduces significant noise.

Fig. 8 shows the spectral response in one pixel (2965) with the beam in the center of the pixel and for beam positions offset 7, 14, 20, 27, 31 and 38 μm from the center. It is evident that the peak position shifts to lower energies as the beam is offset from the center of the pixel. This effect is explained by the fact that the fraction of the charge cloud that falls outside the pixel increases as the beam moves from the center of the pixel.

Even if the data is very noisy an attempt was made to find the peak position of each spectrum, mainly using the leading edge of the peak. The results are presented as dots in Fig. 9, together with a line representing the theoretical peak position calculated from the size of the charge cloud. There is good agreement between calculations and experiment. It should be noted that the energy scale of Fig. 9 reflects the incomplete charge collection of the detector.

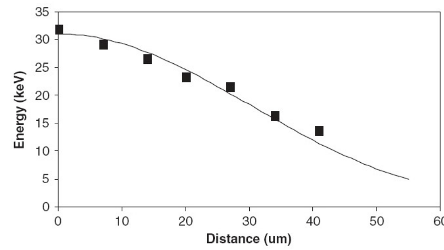

Fig. 9. Position of the energy peak as a function of beam distance form the center of the pixel. The line is simulation results. The dots represent experimental data without correction for incomplete charge collection.

It is evident that such a position-dependent energy deposition will destroy any energy information when the detector is uniformly illuminated. A good spectrum can only be obtained for a narrow beam.

4. Summary and conclusions

We have characterized a 1 mm thick CdTe detector with 55 μm pixels using a narrow monoenergetic beam. The results have been verified by simulations. An energy peak has been obtained in the center pixel. Effects of fluorescence are seen as counts in neighboring pixels, with a range of several pixels. However, due to the random distribution of the hits and the charge diffusion no energy peaks are observed in the fluorescence. The effects of fluorescence limits the height of the full energy peak and will cause escape peaks in the spectrum.

Due to the charge diffusion the contribution from a photon is strongly dependent on its position in the pixel indicating that no valid energy information can be recorded under flood illumination. It is clear that for a small pixel on a thick detector full charge collection will not be achieved without charge summing over several pixels. Charge summing will also, to some extent, limit the effects of fluorescence, but the range is probably too large to capture all events.

Acknowledgments

This work has been done within the framework of the MEDIPIX2-collaboration. The MEDIPIX2-chip is designed at CERN. The MUROS2 readout electronics is designed at NIKHEF and the MEDISOFT4 readout

software is developed at University of Napoli. The CdTe detectors are designed by IFAE, Barcelona.

References

[1] X. Llopart, M. Campbell, R. Dinapoli, D. San Segundo, E. Pernigotti, IEEE Trans. Nucl. Sci. NS-49 (5, Part 1) (2002) 2279.
[2] M. Chmeissani, C. Frojdh, O. Gal, X. Llopart, J. Ludwig, M. Maiorino, E. Manach, G. Mettivier, M. C. Montesi, C. Ponchut, P. Russo, L. Tlustos, A. Zwerger, IEEE Trans. Nucl. Sci. NS-51 (5) 2004.
[3] B. Mikulec, M. Campbell, E. Heijne, X. Llopart, L. Tlustos, Nucl. Instr.and Meth. A 511 (2003) 282.
[4] K. Mathieson, M.S. Passmore, P. Seller, M.L. Prydderch, V. O'Shea, R.L. Bates, K.M. Smith, M. Rahman, Nucl. Instr. and Meth. A 487 (1–2) (2002) 113.
[5] C. Ponchut, J.L. Visschers, A. Fornaini, H. Graafsma, M. Maiorino, G. Mettivier, D. Calvet, Nucl. Instr. and Meth. A 484 (1–3) (2002) 396.
[6] K. Mathieson, R.L. Bates, V. O'Shea, M.S. Passmore, M. Rahman, K.M. Smith, K. Valpas, IEEE Nuclear Science Symposium and Medical Imaging Conference, vol. 1, 2000, pp. 4/52–4/57.

PAPER VII

Characterisation of the charge sharing in pixellated Si detectors with single-photon processing readout

Paper VII

Available online at www.sciencedirect.com
SCIENCE DIRECT®
ELSEVIER
Nuclear Instruments and Methods in Physics Research A 563 (2006) 133–136
NUCLEAR INSTRUMENTS & METHODS IN PHYSICS RESEARCH Section A
www.elsevier.com/locate/nima

Characterisation of the charge sharing in pixellated Si detectors with single-photon processing readout

Börje Norlin[a,*], Christer Fröjdh[a], Hans-Erik Nilsson[a], Heinz Graafsma[b], Vedran Vonk[b], Cyril Ponchut[b]

[a]Department of Information Technology and Media, Mid-Sweden University, SE-85170 Sundsvall, Sweden
[b]Experimental Division, ESRF, BP2200 Avenue des Martyrs, 38043 Grenoble, Cedex, France

Available online 17 February 2006

Abstract

Pixellated silicon detectors with a thickness of 300 and 700 μm bonded to the MEDIPIX2 readout chip have been characterised using a monoenergetic microbeam at the ESRF. The spectral response when a $10 \times 10\,\mu m^2$ wide 40 keV beam is centred on a single pixel is achieved. When the beam is scanned over the pixel, the charge sharing will increase when the beam approaches the border of the pixel.

The experimental results have been verified by charge transport simulations and X-ray scattering simulations. Agreement between measurements and simulations can be achieved if a wider beam is assumed in the simulations. Widening of the absorption profile can to a large extent be explained by backscattering of lower-energy photons by the tin/led bump bounds below the detector. Widening of the detected beam is also an effect of angular alignment problems, especially on the 700 μm detector. Since the angel between the depth and a half-pixel is only 2.2°, alignment of thick pixellated silicon detectors will be a problem to consider when designing X-ray imaging setups.

PACS: 07.07.Df; 07.85.−m; 07.85.Nc; 07.85.Qe; 78.70.Ck; 78.70.Dm; 87.57.−s; 87.59.−e; 87.62.+n

Keywords: Charge sharing; X-ray; Medipix; Pixel detector; Monte Carlo simulation; Synchrotron radiation

1. Background and experimental conditions

Pixel detectors using single-photon processing readout are interesting because of low-noise operation and their ability to record the energy of each individual photon [1]. One such readout chip is the MEDIPIX2 chip [2] with a pixel size of $55 \times 55\,\mu m^2$. It has, however, been observed that significant charge sharing occurs for most detectors with small pixels [3]. The charge sharing strongly affects the energy information in the image. In this experiment we have been using a MEDIPIX2 chip bonded to silicon detectors with different thickness and measured the response when exposed with a narrow monoenergetic X-ray beam.

The measurements were performed at the ESRF using a monoenergetic beam with photon energy of 40 keV. A set of motor driven slits, located about 10 cm from the detector were used to adjust the beam width to $10 \times 10\,\mu m^2$. The slits were made of 2 mm thick tungsten with a slight angle. A second pair of slits where mounted closer to the detector to suppress scattered radiation from the first pair. A MEDIPIX detector was mounted on an XY-translation stage to move between the pixels and a rotation stage to align the detector perpendicular to the beam. During the calibration phase the 300 μm silicon detector was used as a reference. After calibration, data were taken with this detector and a 700 μm thick detector. The beam width was verified both by measuring the flux of X-ray photons through the slit and by scanning the beam across a pixel. Almost no scattered photons were visible in the neighbouring pixels. The final beam intensity was around 65,000 photons/s. The applied bias was 100 V for the 300 μm detector and 250 V for the 700 μm detector. The readout was controlled by MUROS2 and Medisoft4 [4].

*Corresponding author. Tel.: +46 60 148594; fax: +46 60 148456.
E-mail address: borje.norlin@miun.se (B. Norlin).

0168-9002/$ - see front matter © 2006 Published by Elsevier B.V.
doi:10.1016/j.nima.2006.01.077

2. Measurements

Spectra for a centred beam for both 300 (Fig. 1) and 700 μm (Fig. 2) thick detectors were achieved by automatic low threshold scans. The raw data from each threshold scan is a cumulative spectrum which is then differentiated. In the differential spectrum a distinct 40 keV peak appears. The width and the position of the peak are discussed in chapter 3.

A direct observation is that lower energies are present in the spectra, although the beam is monochrome and the charge sharing is strongly suppressed by the narrow centred beam. Simulations using MCNP [5] show that this presence of low-energy counts is due to X-ray fluorescence from the bump-bonding [6]. The slope in the cumulative spectrum can be reproduced if indium or tin/lead is present below the detector in the MCNP model, as shown in Fig. 3. The two Medipix chips in the measurements used tin/lead for bump bonding of the detector. The Kα energies for tin and lead are 25 and 75 keV, the 12 keV peak originates from the Pb L-shell. These energies are not expected to be seen as peaks in measurements or simulations, since the fluorescence is radiated spherically and therefore shared between pixels. The flourescence from the bump-bond is further on refered to as "backscattering".

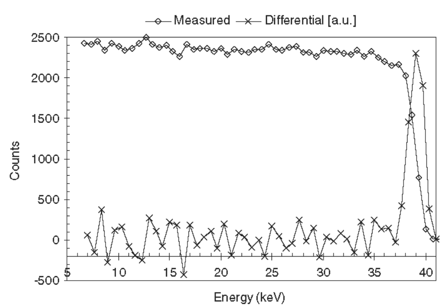

Fig. 1. Measured cumulative spectrum and differential spectrum for a 300 μm thick silicon detector with the beam centred on a pixel.

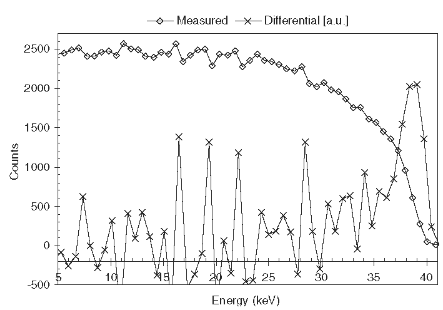

Fig. 2. Measured cumulative spectrum and differential spectrum for a 700 μm thick silicon detector with the beam centred on a pixel.

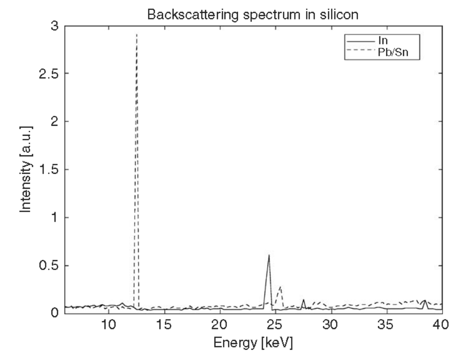

Fig. 3. Spectrum achieved from MCNP due to fluorescence and backscattering from a bump bond consisting of indium or tin/lead. The relative intensity of the 40 keV peak outside the figure is 100.

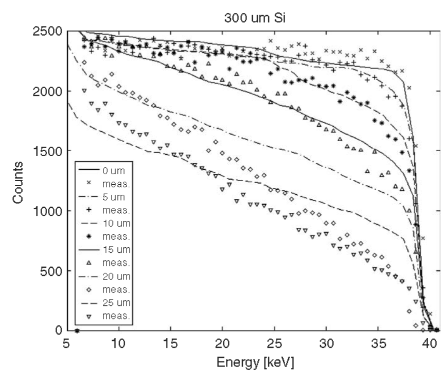

Fig. 4. Comparison of measured and simulated cumulative spectra for a 300 μm thick Si detector. Each spectrum corresponds to a specific beam position relative to the centre of the pixel. The assumed absorbed beam width is 32 μm.

2.1. Scanning the beam over the pixel

To be able to see how the charge sharing influences the spectrum, the beam was moved from the centred position towards the border of the pixel. The best spectrum should be achieved with the beam centred above a pixel (0 μm). The position on the border between two pixels (28 μm) should give mostly counts from photons with their charge

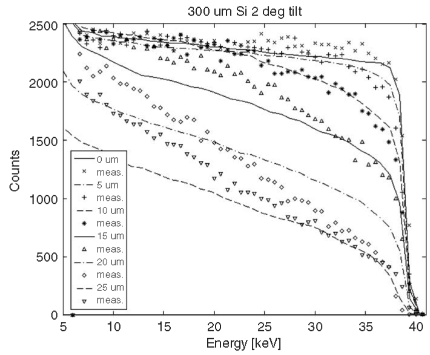

Fig. 5. Comparison of measured and simulated cumulative spectra for a 300 μm thick Si detector. The assumed beam absorption width is 26 μm and the tilt is 2°.

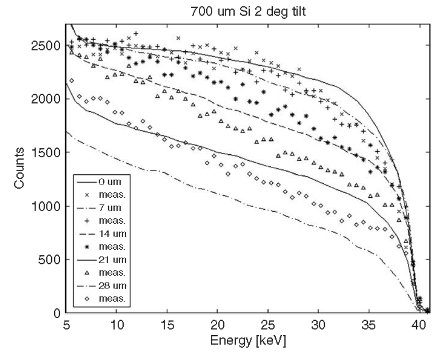

Fig. 7. Comparison of measured and simulated cumulative spectra for a 700 μm thick Si detector. The assumed beam absorption width is 32 μm and the tilt is 2°.

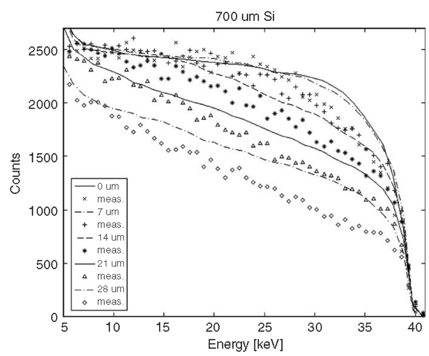

Fig. 6. Comparison of measured and simulated cumulative spectra for a 700 μm thick Si detector. The assumed beam absorption width is 38 μm without tilt.

cloud divided between the two pixels. The resulting cumulative spectra (Fig. 4 7) confirm this behaviour, the slope of the spectra between 10 and 35 keV increases when the beam is moved away from the centred position, indicating that the amount of shared counts increases.

3. Simulations

The experimental results have been verified by simulations. The effective beam detected by the readout chip appears to be wider than the actual beam due to scattering and charge drift. If the effective beam is almost as wide as the pixel, charge sharing will take place immediately when the beam is moved one step from the centre towards the border. On the contrary, for an extremely narrow effective beam only the border position will give an altered spectrum.

Due to X-ray scattering in Si the absorbed beam will be some microns wider than the actual beam, achieved from simulations with MCNP. Charge transport simulations are carried out using a full band self-consistent ensemble Monte Carlo device simulator (GEMS) [7]. A profile of absorbed energy is used as input to the charge transport simulation. The assumptions that are needed to get a reasonable agreement between the measured and the simulated spectra can be used to understand the experimental conditions and the charge sharing process in more detail.

3.1. Simulation of a 300 μm thick Si detector

Simulated spectra for a 300 μm thick detector are compared to measured spectra in Fig. 4. To reproduce the slope of the 40 keV edge in the spectra, a noise level of $80e^-$ from the readout must be added. This corresponds to the noise expected from the MEDIPIX chip [2] and corresponds to a peak width of approximately 0.7 keV. The contribution of the Fano-factor to the peak width is negligible for silicon. The additional widening of the peak in Fig. 3 and the slight shift to lower energy is due to the charge sharing process. This is indicated by the soft bending at about 38 keV in Fig. 4.

When the energy spectrum of backscattered photons (Fig. 3) is added to the model, the low-energy slope for the centred position will correspond to the measurements. The backscattered photons are assumed to come from a point source located where the beam hits the bump-bond.

To get reasonable position sensitivity for the simulated spectra, the absorbed beam width used in the charge transport simulation must be about 30 μm. With this beam width the peak width and peak shift in Fig. 3 is also reproduced. This beam width is significantly wider than the absorbed beam width expected from MCNP.

One explanation for the widening of the beam is alignment problems in the setup. The alignment error is assumed to be up to 2° in the direction perpendicular to the axis of the rotation stage. If the beam is tilted, charges created close to the detector surface will reach the readout on a shifted position compared to charges created close to the readout. Charge clouds created close to the surface has a long drift path and will result in wider clouds reaching the readout. A tilted beam will result in more complex position sensitivity for the spectrum. If a 2° tilt is included in the simulations a smaller beam can be assumed and the agreement with measurements is improved (Fig. 5). Note that the peak shift for the border position is reproduced in the simulation when the beam is tilted, but not if the beam is aligned. In the measurements this peak shift is stronger for the 20 μm position than for the 25 μm position, indicating an uncertainty in the beam position or imperfections in the detector material.

3.2. Simulation of a 700 μm thick Si detector

The comparisons between simulated and measured spectra were carried out for the 700 μm thick detector also. To reproduce the bended curvature between 30 and 40 keV in the spectra the beam width has to be about 40 μm without tilt (Fig. 6) and about 30 μm with 2° tilt (Fig. 7). The agreement is reasonable, but the simulated peak shift for the 28 μm position in Fig. 7 can not be observed in the measurements. This might be the case if the border position was located about 10 μm from the border.

The measurement of the 7 μm position actually shows a more distinct energy edge than the centred position. This indicates a misalignment of the centring for this detector. Simulations show that centring of a tilted beam is a complex problem for the 700 μm detector. Cases when the 7 μm position has a higher intensity than the centred position can even occur. The spectrum for the neighbour pixel is also measured (although not shown in the figures). Comparison of these two border positions also indicates a misalignment; since the energy edge of the neighbour is shifted down to 34 keV.

3.3. Considerations about simulation accuracy

A uniform absorption depth profile along the beam was assumed in the charge transport simulation. This simplification is valid since silicon is a low absorbing material. The backscattered photons were assumed to be absorbed uniformly in the last 5 μm of the beam, close the bump bond. This distance was estimated from MCNP simulations were the spherical profile of the backscattered radiation is verified. The actual range of the radiation is of course much longer in silicon. The absorption profile orthogonal to the beam was assumed to be a uniform square with sharp edges. Test with a soft Gaussian profile gave less agreement with measurements, so it is reasonable to assume that the actual orthogonal absorption profile in fact was sharp. These assumptions about the absorption profile gave a reasonable accuracy to reproduce the conditions of this experiment.

4. Conclusions

Position-dependent spectra from a narrow monochrome source at ESRF are achieved with Medipix2 with 300 and 700 μm thick silicon detectors. It is possible to reproduce the measurements using charge transport simulations and X-ray scattering simulations. The peak width of the simulations fits the measurements if $80e^-$ readout noise is assumed. Therefore it is likely that the readout noise for the Medipix2 chip is not higher than $80e^-$ specified in Ref. [2]. The presence of backscattered X-rays from the bump bonds [6] is verified since the low-energy slope of the simulations fits the measurements when backscattering is considered. The size of the absorbed beam was, however, wider than expected from the experimental conditions. It is concluded that the beam must have been tilted in the experimental setup. This angular misalignment has strong influence on the measurements on the 700 μm thick detector, since it also affects the centring of the beam. An important conclusion is that angular detector alignment will be a problem in the design of high resolution X-ray imaging systems containing thick silicon detectors.

Acknowledgments

This work was done using detectors, software and readout system developed within the MEDIPIX2 collaboration. The MEDIPIX2-chip is designed at CERN. The MUROS2 readout electronics is designed at NIKHEF and the MEDISOFT4 readout software is developed at University of Napoli.

References

[1] B. Mikulec, M. Campbell, E. Heijne, X. Llopart, L. Tlustos, Nucl. Instr. and Meth. A 511 (2003) 282.
[2] X. Llopart, M. Campbell, R. Dinapoli, D. San Segundo, E. Pernigotti, IEEE Trans Nucl. Sci. NS-49 (2002) 2279.
[3] K. Mathieson, M.S. Passmore, P. Seller, M.L. Prydderch, V. O'Shea, R.L. Bates, K.M. Smith, M. Rahman, Nucl. Instr. and Meth. A 487 (2002) 113.
[4] M. Conti, M. Maiorino, G. Mettivier, M.C. Montesi, P. Russo, IEEE Trans Nucl Sci. NS-50 (2003) 2869.
[5] J.F. Briesmeister (Ed.), MCNP—A General Monte Carlo N—Particle Transport Code, version 4C, Manual, 2000.
[6] M. Hoheisel, A. Korn, J. Giersch, Nucl. Instr. and Meth. A 546 (2005) 252.
[7] H.-E. Nilsson, et al., Nucl. Instr. and Meth. A 487 (2002) 151.

PAPER VIII

Spectral performance of a pixellated X-ray imaging detector with suppressed charge sharing

Paper VIII

Available online at www.sciencedirect.com
ScienceDirect
Nuclear Instruments and Methods in Physics Research A ∎ (∎∎∎∎) ∎∎∎–∎∎∎
NUCLEAR INSTRUMENTS & METHODS IN PHYSICS RESEARCH Section A
www.elsevier.com/locate/nima

Spectral performance of a pixellated X-ray imaging detector with suppressed charge sharing

Börje Norlin*, Christer Fröjdh, Hans-Erik Nilsson

Department of Information Technology and Media, Mid-Sweden University, SE-85170 Sundsvall, Sweden

Abstract

The ability to perform X-ray imaging with energy resolution on a small pixel detector is severely limited by the charge sharing in the detector. Different schemes have been proposed in order to overcome the problem. Previous studies using synchrotron radiation have shown that, for a 300-μm-thick Si detector with 55 μm pixel size, almost no charge sharing occurs for photons hitting the centre of each pixel. In this study, we have used slits to focus the beam from a standard X-ray unit onto the centre of a pixel for a MEDIPIX detector. The attenuation of the spectrum was measured for a number of samples of different materials with K-edge energy in the range of 30–50 keV. The measurements were performed by scanning an energy window through the spectrum. Requirements for new X-ray imaging systems with true energy resolution, based on these measurements, are discussed.

PACS: 02.70.Hm; 07.07.Df; 07.85.−m; 07.85.Nc; 29.30.Kv; 32.30.Rj; 78.70.Dm; 81.70.−q; 87.59.−e; 87.62.+n; 87.64.Gb

Keywords: X-ray spectroscopy; Pixel detector; Medipix; Charge sharing; Material recognition

1. Introduction

When a test sample is irradiated using a wide-range energy X-ray source, the energy dependence of the attenuation for X-ray photons will differ between different materials [1]. The absorption cross-section in a specific material will be significantly larger for photons with energy just above the K-edge energy of that material than for those with slightly lower energy. Hence, energy resolved X-ray imaging can be used to achieve colour images revealing the material content of a test sample. The MEDIPIX2 chip [2] with a pixel size of $55 \times 55\,\mu m^2$ is an example of a single photon processing readout chip suitable for energy resolved imaging. However, energy resolved X-ray imaging with such a small pixel size can only be achieved if charge sharing between the pixels is corrected for [3]. An alternative solution would be to read out each analog signal separately and process it outside the chip, but this is inconvenient for high photon flux applications such as for example medical imaging. A promising design strategy to overcome the problem with charge sharing in the MEDIPIX systems has been proposed in Ref. [4]. This study investigates the performance of the MEDIPIX system, if the addition of a correcting scheme for charge sharing is made. The charge sharing is suppressed by centring a narrow collimated X-ray beam onto a pixel. Almost no charge sharing occurs for photons that hit the centre of a $55 \times 55\,\mu m$ pixel when the detector thickness is 300 μm [5]. The main focus of this work is to demonstrate the identification of some materials by finding the K-edge of X-ray absorption. Hence, it is possible to argue that future versions of the MEDIPIX system will be capable of material resolving X-ray imaging in the 55 μm scale. For larger pixel sizes, the influence of charge sharing is less critical, so material recognition can be demonstrated without correction [6].

2. Experimental setup

The measurements were performed using a standard dental X-ray tube operated at 70 kV. The source is a PLANMECA PROSTYLE INTRA with 2.0 mm Al

*Corresponding author. Tel.: +46 60 148594; fax: +46 60 148456.
E-mail address: borje.norlin@miun.se (B. Norlin).

0168-9002/$ - see front matter
doi:10.1016/j.nima.2007.01.095

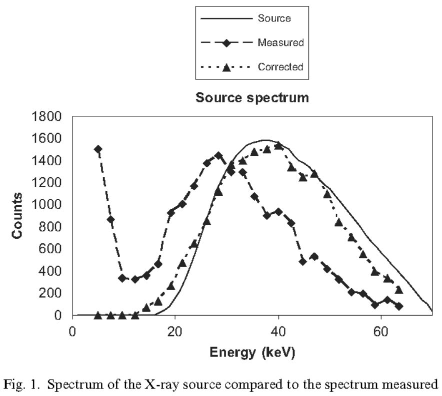

Fig. 1. Spectrum of the X-ray source compared to the spectrum measured with Medipix and a corrected measured spectrum where absorption in 300 μm silicon is considered.

filtration that gives a photon spectrum of the shape shown in Fig. 1. Two crossed 10 μm slits were used to collimate the X-ray beam to the size of 10 × 10 μm. The slits were made of 1.5-mm-thick tungsten, with relief angles of 4° and the lower slit was located approximately 1 mm above the MEDIPIX2 detector. The divergence of the beam is assumed to be negligible as the distance of 350 mm from the focal spot point (width 100 μm) to the slit is much longer than that between the slit and the detector. The MEDIPIX chipboard was mounted on an XY-translation stage, so that adjustments of the position were possible in order to ensure that the beam is centred on one pixel. The beam is centred by maximizing the signal on the pixel and by comparing this position to border positions when the signal equals the neighbour pixel signal.

The readout was controlled by MUROS2.1 and Pixelman version 1.2.1 [7]. The window spectra of the irradiated pixel could be achieved using the DACs scan tool in Pixelman through the application of a mask containing only one active pixel. The detector bias of 100 V was supplied by means of a Keithley 4210 sourcemeter.

3. Measurements

The measurements were performed by scanning an energy window of 2.3 keV through the spectrum. In the absence of an object, a spectrum corresponding to the X-ray source spectrum will be captured. The achieved spectrum is different to that of the source spectrum due to the energy variation of X-ray absorption in silicon, as shown in Fig. 1. If a correction is made for the absorption in 300 μm silicon, the measured spectrum fits the expected tube spectrum.

Table 1
Test sample description

Element	Atom	K_{ab} (keV)	Test sample
Sn	50	29.190	Soldering tin with 3% silver
I	53	33.164	Iodine powder
Gd	64	50.229	Gd_2O_2S:Tb scintillator powder

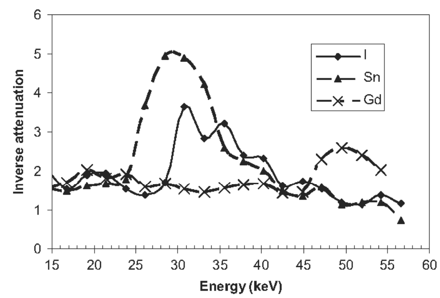

Fig. 2. Inverse attenuation spectra for test samples of tin, iodine and gadolinium. The inverse attenuation is the number of counts without object divided by the number of counts achieved with a test sample in the beam line.

4. Results

The reference spectrum achieved without an object is compared to that of the spectra in which test samples of different materials are placed in the beam line before the slits. Transmission measurements for the three different test samples are provided; tin, iodine and gadolinium (Table 1).

The absorption coefficient for X-ray photons is strongly dependent on the atomic number of the material, but also on the photon energy. The absorption increases if the photon energy is high enough to cause excitation within the K-shell. The attenuation spectra is defined as the ratio between the achieved spectra and the source spectra ($I(E)/I_0(E)$). The spectra shown in Fig. 2 will increase rapidly at the K-edge energy and hence reveal this energy for the irradiated material sample.

5. Conclusions

It is possible to correctly measure the spectrum of an X-ray tube using the MEDIPIX2 system, if the beam is centred on one pixel in order to suppress charge sharing and if a correction is made to compensate for the absorption in silicon. The MEDIPIX3 system is designed to correct the energy information by adding the collected charge between neighbouring pixels. The main conclusion of this study is that the MEDIPIX3 system makes it possible for energy resolved X-ray imaging to reveal the material content of a sample.

Acknowledgements

This work was performed using detectors, software and readout system developed within the MEDIPIX collaboration. The MEDIPIX2-chip was designed at CERN. The MUROS2 readout electronics was designed at NIKHEF and the Pixelman readout software was developed at IEAP.

References

[1] G.F. Knoll, Radiation Detection and Measurement, third ed, Wiley, New York, ISBN 0-471-07338-5, 2000, p. 49.
[2] X. Llopart, M. Campbell, R. Dinapoli, D. San Segundo, E. Pernigotti, IEEE Trans. Nucl. Sci. NS-49 (2002) 2279.
[3] H.-E. Nilsson, et al., Nucl. Instr. and Meth. A 487 (2002) 151.
[4] H.-E. Nilsson, B. Norlin, C. Fröjdh, L. Tlustos, Simulation study of charge sharing suppression in photon counting X-ray imaging systems by different charge summing schemes, in: Presentation at Eight IWORID, Pisa, Italy, July 2006.
[5] B. Norlin, et al., Nucl. Instr. and Meth. A 563 (2006) 133.
[6] B. Norlin, et al., Nucl. Instr. and Meth. A 531 (2004) 265.
[7] Pixelman webpage http://www.utef.cvut.cz/medipix/⟨http://www.utef.cvut.cz/medipix/⟩.

PAPER IX

Charge sharing suppression using pixel to pixel communication in photon counting X-ray imaging systems

Paper IX

Available online at www.sciencedirect.com
ScienceDirect
Nuclear Instruments and Methods in Physics Research A ▮ (▮▮▮▮) ▮▮▮–▮▮▮
NUCLEAR INSTRUMENTS & METHODS IN PHYSICS RESEARCH Section A
www.elsevier.com/locate/nima

Charge sharing suppression using pixel-to-pixel communication in photon counting X-ray imaging systems

H.-E. Nilsson[a,*], B. Norlin[a], C. Fröjdh[a], L. Tlustos[b]

[a] Mid-Sweden University, Department of Information Technology and Media, 851 70 Sundsvall, Sweden
[b] CERN, ETT/TT, 1211 Geneva 23, Switzerland

Abstract

In planar silicon detector structures, the charge sharing between pixels is one limiting factor for colour X-ray imaging using integrated photon counting pixel detectors. 3D detector structures have been proposed as one solution to this problem. However, there are also readout system solutions to the problem, i.e., introducing pixel-to-pixel communication and distributed charge summing in the readout electronics. In this work, different charge summing schemes are evaluated using Monte Carlo simulation techniques. The increase in electronic noise introduced by the charge summing is one of the most severe problems. A proper selection of summing scheme is necessary to obtain an efficient system.

PACS: 07.07.Df; 07.05.Tp; 07.85.Fv; 85.60.Gz

Keywords: Monte Carlo simulation; X-ray imaging; Photon counting

1. Introduction

Charge sharing limits the energy resolution in integrated photon counting pixel detectors such as the MEDIPIX2 system [1]. This problem becomes severe in silicon detectors as pixel dimensions reach below 100 μm. Charge from a single-photon absorption event that is shared between pixels will show up in the spectrum as several photon absorptions with lower energy than the true event. Thus, it provides a distortion of the energy spectra. Fig. 1 compares the energy spectrum of a standard dental X-ray source with that recorded by a MEDIPIX2 [1] pixel detector (55 μm × 55 μm pixel size and a 300 μm thick silicon detector). The difference between the true spectrum of the X-ray source and the recorded spectrum is very large due to charge sharing.

One way to overcome the charge sharing problem, using pixel signal processing, was presented by Llopart et al. [1] in 2002. The suggested method requires additional signal processing electronics in each pixel. The additional signal-processing unit should determine in which pixel all the charge from an absorption event should be summed. The summation should be done with as little additional noise contribution as possible. Summing of charges will always provide additional noise according to a square root relation (noise increases as the square root of the number of contributions summed). In order to understand better how this type of signal processing (distributed decision-making) will affect the detector system, a system level Monte Carlo simulation of the MEDIPIX2 system [1] has been developed. This simulation tool has been used to compare different signal-processing schemes and how these will affect the energy resolution of the system.

2. Numerical model

The numerical model is based on detailed charge transport modelling of the charge diffusion in the detector. The charge transport simulations were made using our in-house full band self-consistent ensemble Monte Carlo device simulator (GEMS) [2], where the trajectory of each electron and hole has been recorded for a large set of absorption events. Cylindrical coordinates were used in

*Corresponding author.
E-mail address: Hans-Erik.Nilsson@miun.se (H.-E. Nilsson).

0168-9002/$ - see front matter © 2007 Elsevier B.V. All rights reserved.
doi:10.1016/j.nima.2007.01.160

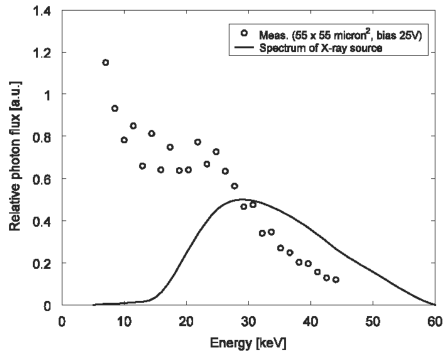

Fig. 1. Comparison of the measured energy spectrum extracted from threshold scans on the MEDIPIX2 system and the actual spectrum of the dental X-ray tube used.

accounting for 3D electrostatic effects in the 2D charge transport simulations. The charge transport simulations were used to extract the charge spread at the surface of the detector as a function of the position of the absorption. The data for the charge spread is then used in a system level Monte Carlo simulator to simulate the imaging performance of the detector system.

In Fig. 2, the planar detector structure studied in this work is presented. For a more detailed description regarding the simulation technique, see Ref. [2].

Over-depletion of the detector has been modelled using a scaling rule developed from the charge spread expression derived in Ref. [3]:

$$\Delta x = 4\sqrt{\frac{\varepsilon k_{\mathrm{B}} T}{q^2 N} \ln\left(\frac{W}{W - y_0}\right)} \tag{1}$$

where T is the temperature, N the doping level, W the depletion width, q the elementary charge, ε is the dielectric constant, k_{B} is Planck's constant and y_0 is the position from the surface at which the photon was absorbed. The scaling of the charge cloud needed to compensate for the over-depletion can be written as

$$\frac{\Delta x_{\mathrm{over}}}{\Delta x_{\mathrm{norm}}} = \sqrt{\frac{\ln(1 - (y_0/W_{\mathrm{over}}))}{\ln(1 - (y_0/W_{\mathrm{norm}})}} \tag{2}$$

where W_{norm} is the depletion width without over-depletion and W_{over} is what the depletion width would be for a thicker detector for the higher voltage. In Figs. 3 and 4, we have compared simulated and measured energy spectra for 25 and 100 V bias, respectively. The results demonstrate the accuracy of the model and show that the simulation model can be used to estimate the effect of different charge summing algorithms on the energy resolution.

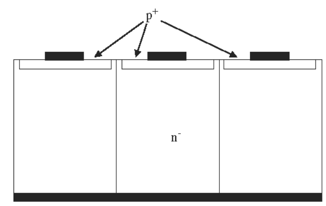

Fig. 2. Structure used in the simulation.

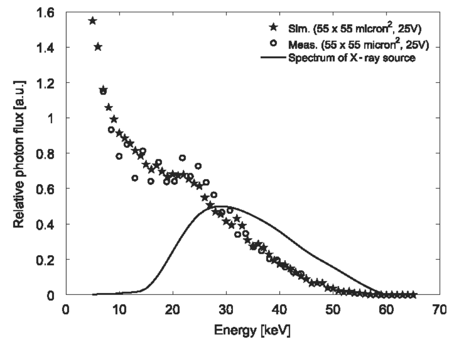

Fig. 3. Comparison between simulation model and measurement (MEDIPIX2 system, 25 V bias, dental X-ray source).

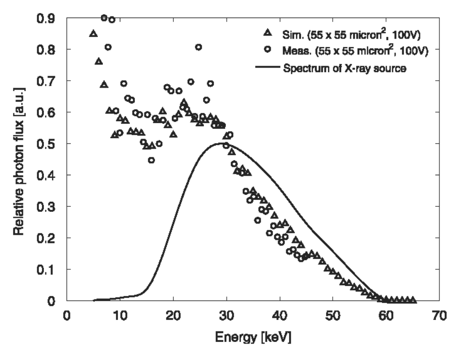

Fig. 4. Comparison between simulation model and measurement (MEDIPIX2 system, 100 V bias, dental X-ray source).

3. Charge assignment schemes

In Figs. 5 8, we present the charge assignment schemes studied in this work. The pictures include a schematic

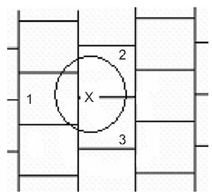

Fig. 5. Three pixel summing configuration (3PS).

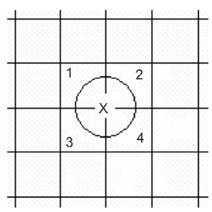

Fig. 6. Four pixel summing configuration (4PS).

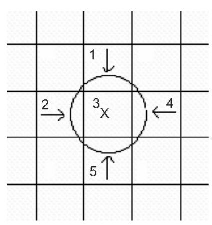

Fig. 7. Five pixel summing configuration (5PS).

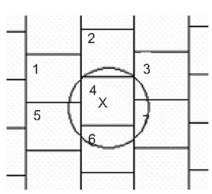

Fig. 8. Seven pixel summing configuration (7PS).

picture of charge assignment for an absorption event in the centre of the pixel cluster configured to record the event.

The pixel layout is based on two different designs of the pixel matrix; the normal 2D pixel layout (Figs. 6 and 7) and a 2D Odd Column Shifted Matrix, OCSM (shift of half a pixel height see Figs. 5 and 8). Note that the OCSM layout requires a simple interpolation transformation in order to be transferred to a standard image format.

Table 1 presents the equivalent area and radius as well as the theoretical limit for the increase in noise due to the charge summing.

The charge assignment algorithm starts by determining the pixel with the highest signal value (centre pixel). In the case of non-symmetric configurations such as the three pixel summing (3PS) and the four pixel summing (4PS) an additional logic step is needed to determine which set of neighbours should be summed. The 3PS has six possible summing configurations (see Fig. 9) and the 4PS has four possible summing configurations (see Fig. 10).

Note that the 4PS configuration shown in Fig. 10 is the only configuration that for all possible absorption positions covers the entire charge cloud (radius of approximately 40 μm) at 30 keV in a 300 μm thick silicon detector.

Table 1
Increase in noise and equivalent pixel area (55 μm × 55 μm pixels) due to charge summing

Configuration	Increase in noise	Summed area (μm^2)	Covered area (μm^2)
1 pixel	1.0	3025	3025
3 pixel summing	1.73	9075	21,175
4 pixel summing	2.0	12,100	27,225
5 pixel summing	2.24	15,125	15,125
7 pixel summing	2.65	21,175	21,175

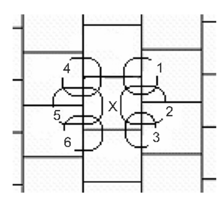

Fig. 9. Different possibilities for the charge assignment in the 3PS configuration.

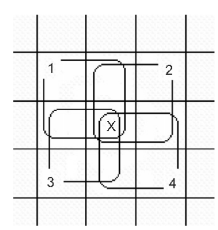

Fig. 10. Different possibilities for the charge assignment in the 4PS configuration.

In the case of the 3PS schemes presented in Fig. 9, a cloud radius of only 27 μm is completely covered by the scheme. In both of these statements, the pixel size has been assumed to be 55 μm × 55 μm.

4. Simulation results

All the assignment schemes have advantages and disadvantages. The lower the number of neighbours, the better from a noise perspective. However, the scheme with the smallest number of neighbours also has the largest loss of carriers, which results in the largest energy tail towards low energies. A larger number of summing neighbours provide a more complicated charge assignment algorithm and suffers from the largest electronic noise distortion. In order to understand the trade off that is needed, we have simulated each scheme for a mono-energetic source of 30 keV. The bias condition is the worst case with no over-depletion (25 V bias). In Figs. 11 and 12, the simulated energy spectrum is presented for an assumed electronic noise of 10 and 100 EHP, respectively. The 4PS algorithm is the best in terms of suppressing charge sharing and still providing reasonable noise levels. The main reason for the better performance is that the configuration covers a larger area than all the other configurations, while in the summation only four pixels are included (see Table 1).

All the proposed summing configurations provide significantly better peak amplitude. The width of the peak is directly linked to the amount of noise added in the summation. The best performance is given by the 4PS algorithm due to the largest sensing area (9 pixels, see Fig. 10) and at the same time, the reasonably low number of pixels used in the summation (4 pixels). A possible drawback with the 4 pixel summation is that it demands more logic to sense all 9 pixels in order to select the 4 pixels with the highest signal contribution. The standard configuration shows a very pronounced charge sharing tail towards lower energies.

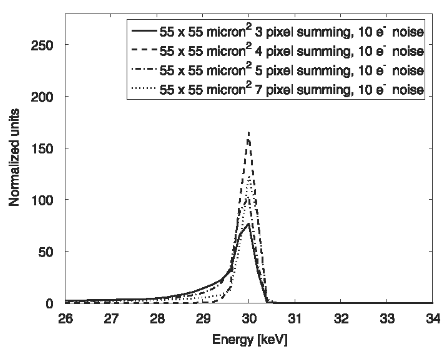

Fig. 11. Simulated energy spectra for different charge assignment schemes assuming a mono-energetic 30 keV X-ray source. The assumed electronic noise-level is 10 electrons.

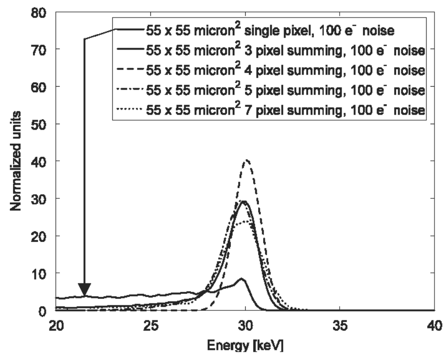

Fig. 12. Simulated energy spectra for different charge assignment schemes assuming a mono-energetic 30 keV X-ray source. The assumed electronic noise-level is 100 electrons.

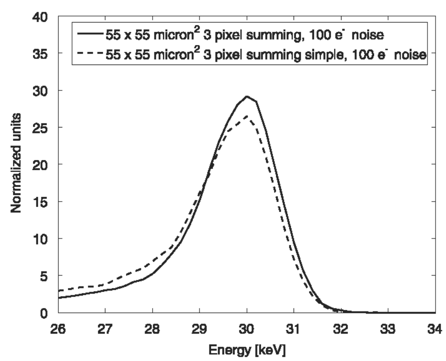

Fig. 13. Simulated energy spectra for the two proposed summing strategies for the 3PS configuration. A mono-energetic 30 keV X-ray source and an electronic noise-level 100 EHP are assumed.

The electronic noise-level in each pixel of the MEDIPIX2 system is approximately 100 electrons. The same noise level has been applied in the simulation to the signal recorded in each pixel by summing a normally distributed elementary charge contribution with a standard deviation of 100. According to theory [4], the full-width of the peak at half-maximum (FWHM) should then be 851 eV. Our simulations show good agreement with this theory. For example, the 4PS scheme FWHM is 1700 eV, which divided by the square root of 4 yields a contribution of 850 eV from each pixel. Thus, the energy resolution is no longer limited by charge sharing but rather limited by the electronic noise in the pixels. Another important noise source adding to the electronic noise in the pixels results from threshold variations, which can seriously degrade the system in energy-sensitive imaging configurations. This has not been considered in the simulations since this noise will affect all pixel summing schemes in the same way.

An alternative simplification is to use the 3PS configuration with the same summing strategy as for the 4PS configuration. In this case, the summing is done according to the 1, 3, 4, 6 cluster shown in Fig. 9. Thus, we deliberately neglect the case when the charge in clusters 2 and 5 is the largest. In Fig. 13, the result of this approximation is compared to the result for the full solution of the 3PS algorithm.

5. Conclusions

Different readout system solutions to the problem of charge sharing in photon counting X-ray imaging detectors have been studied. The solutions are all based on different schemes for pixel-to-pixel communication and distributed charge summing in the readout electronics. Five different charge summing schemes have been evaluated; two versions of a 3PS solution, one 4PS solution, one 5 pixel summing solution and one 7 pixel summing solution.

The scheme covering the largest search area combined with a minimized pixel summation over 4 pixels shows the best characteristics. For 30 keV, approximately 100% of the charge cloud is collected within a radius of 40 μm from the surface projection of the absorption position (for a 300 μm thick silicon detector). Thus, the charge summing configuration that covers this area for all possible cases will be the best solution. The only scheme providing this area coverage in a $55\,\mu m \times 55\,\mu m$ pixel system is the 4PS configuration.

References

[1] X. Llopart, M. Campbell, R. Dinapoli, D. San Segundo, E. Pernigotti, IEEE Trans. Nucl. Sci. NS-49 (2002) 2279.
[2] H.-E. Nilsson, E. Dubaric, M. Hjelm, K. Bertilsson, Nucl. Instr. and Meth. A 487 (2002) 151.
[3] H.-E. Nilsson, C. Fröjdh, E. Dubaric, IEEE Trans. Nucl. Sci. NS-51 (2004) 1636.
[4] G.K. Knoll, Radiation Detection and Measurement, third ed, Wiley, New York, 1999, p. 630.